The Dissertation Committee for Hyo-Jin Kim Certifies that this is the approved version of the following dissertation:

A NEW APPOACH TO THE DETERMINATION OF A MEAN SEA SURFACE MODEL USING MULTI-SATELLITE ALTIMETER DATA

Committee:

Byron D. Tapley, Supervisor

Wallace T. Fowler

Ryan P. Russell

Clark R. Wilson

John C. Ries

Timothy J. Urban

A NEW APPROACH TO THE DETERMINATION OF A MEAN SEA SURFACE MODEL USING MULTI-SATELLITE ALTIMETER DATA

by

Hyo-Jin Kim, B.S.;M.S.E.

Dissertation

Presented to the Faculty of the Graduate School of

The University of Texas at Austin

in Partial Fulfillment

of the Requirements

for the Degree of

Doctor of Philosophy

The University of Texas at Austin

May 2015

Dedication

To my parents,

my husband and my children Christina and Nathan

and

the glory of God

Acknowledgements

I would like to express my gratitude to my advisor, Dr.Tapley, who has supported me all these years with tremendous patience and enduring trust. It is an honor for me to be one of his last students before his retirement. I would like to thank Dr.Ries and Dr.Urban for offering me unending guidance for my research since I was a graduate student here. I would like to thank my other committee members, Dr. Fowler, Dr. Wilson and Dr. Russell. I also would like to acknowledge Dr. Chambers, who has helped me tremendously with background knowledge about my dissertation research.

I would like to thank my parents, parent in law, my husband, Ung-Dai Ko, and my lovely children, Christina and Nathan. Also, I would like to thank my sisters and brother and my friends.

A NEW APPROACH TO THE DETERMINATION OF A MEAN SEA SURFACE MODEL USING MULTI-SATELLITE ALTIMETER DATA

Hyo-Jin Kim, Ph.D.

The University of Texas at Austin, 2015

Supervisor: Byron D. Tapley

Models for the mean sea surface (MSS) are created by combining and interpolating on a specified spatial grid inhomogenous data sets from different satellites with different ground track coverage. There are various approaches in which the sea surface height (SSH) data from different satellites can be combined to create an accurate reference surface. The orbit errors (especially from the early missions) need to be reduced, and systematic biases between different satellites can be decreased by re-processing them using the improved models and geophysical corrections. In this research, a new method for the data adjustment (or error reduction), which attempts to compensate for both long-wavelength orbit errors and systematic biases, simultaneously and efficiently. The approach is based on using an accurate sea surface profile as a reference surface for the integration process.

The new data adjustment technique is based on along-track SSH gradients computed for each satellite, which are integrated along-track with initial values obtained by dual crossover computation with respect to an accurate set of sea surface heights. The

accurate Jason-1 SSH data were used to determine the reference surface, and a total of 5 different satellites (Geosat ERM, ERS-2, T/P, Envisat and ERS-1 geodetic mission) data were adjusted to the Jason-1 SSH data. After editing, the new homogeneous SSH datasets were averaged into mean SSH profiles. Then, they were gridded into a 5-minute resolution mean sea surface over the global ocean within ±60º latitudes, as defined by the Jason-1 mean profile, using a 2-D spline interpolation in tension with Green's function approach.

The new gridded mean sea surface, named CSRMSS14 was validated by three comparisons. First, it was compared with two accurate altimeter data sets: 7-year Jason-1 and 8-year Envisat mean profiles. Second, two recent MSS models, DNSC08 and DTU10, were compared to investigate the accuracy of CSRMSS14. Third, a somewhat independent test is obtained by comparing a 2-year Jason-2 mean profile with the three MSS models (CSRMSS14, DTU10 and DNSC08), since Jason-2 data were not used in their construction. These three validations demonstrated that CSRMSS14 mean sea surface model obtained with this new approach is comparable in accuracy to DNSC08 and DTU10.

Table of Contents

List of Tables

List of Figures

Chapter 1: Introduction

The Mean Sea Surface (MSS), which is an essential feature for geodesy, geophysics and oceanography, has important applications beyond just a reference surface [Kim, 2002]. The altimeter-measured MSS is composed of the geoid (±100 m), which represents the shape of the geopotential field due to the Earth's gravity field [Louis et al., 2010], and the mean ocean dynamic topography, which reflects the ocean currents and mean inverted barometric effects on the ocean surface [Tapley and Kim, 2001]. The MSS can be used to derive the ocean circulation, by subtracting the geoid, as a test of the geoid model accuracy. Moreover, the marine geoid reflects the ocean bottom topography, revealing the seafloor features such as ocean ridges and seamounts, which are easily seen in high accuracy MSS models [e.g., Sandwell and Smith, 2001].

Previous studies developed mean sea surface models by gridding the average sea surface height (SSH) measurements from multiple satellites and utilizing different gridding methods and different combinations of altimeters. However, the problems of inconsistency among different altimeter datasets occurs prior to the gridding process. In particular, the inaccuracy of old radar data, which are contaminated by a host of errors, is problematic. The altimeter SSH data from different missions have initial differences resulting from systematic biases, residual orbit errors, and instrument and geophysical correction errors. The systematic differences among different altimeter datasets, caused by these various error sources, and different reference frame offsets, should be reduced when these datasets

are used for the MSS [Le Traon et al., 1995; Andersen and Knudsen, 2009]. In addition, some of the residual biases and errors from orbit and geophysical corrections remain in the SSH data set from the early satellite missions because the correction models are not perfect enough to remove them completely.

There are long-wavelength errors such as orbit errors, residual tidal correction, or inverse barometer errors [Le Traon et al., 1998], and other instrumental and environmental effects. Although the orbit error has been reduced with more accurate geoid models, it still has both time-varying and time-invariant errors, or biases. Others, such as sea state bias and troposphere errors, are short-wavelength errors. These also contain time-varying and bias errors. Time-varying errors can be averaged out by using data from repeat tracks, but the systematic errors in the total systematic differences remain. These affect the MSS as a local bias. The problem is even worse in the case of non-repeating tracks, such as from the Geosat or ERS-1 geodetic mission.

In order to develop a high quality mean sea surface, the precise method to make multi-altimeter SSH data consistent and homogeneous with each other by reducing their systematic differences and other remaining errors and biases are essential before the gridding process. For this consistency process, a reference surface, which is believed to be the most accurate, is chosen and used for fitting the SSH from the different missions to them. The ultimate goal of fitting is to increase the accuracy of the other SSH dataset to the reference field and reduce the systematic differences between datasets.

One way to enhance the accuracy of the early missions and make them homogeneous with respect to the reference field is to re-process all of the old altimeter orbits using a new modern gravity model, such as GGM03C [Tapley et al., 2007], and update the altimeter data with the same modern models of the geophysical corrections, which are applied to the chosen reference field: Sea State Bias (SSB), tides, ocean pole tide, troposphere, ionosphere, etc. However, this requires an enormous level of time and computation effort, and could require perpetual reprocessing as future improvements are made. Another way is to take gradients of the SSH data of each altimeter mission, then integrate the data relative to a fixed reference track. This method works well when the wavelength of the error is larger than approximately 100 km, as is typical of orbit and geophysical correction errors.

One of the objectives in this research is to investigate and apply this second approach of error reduction to enhance the quality of altimeter mission datasets. Ultimately, this method will ensure that the SSH dataset of each satellite is adjusted well to a chosen reference surface, the Jason-1 mean profile, and also provide homogeneous datasets for the satellites. The final goal is to derive a new gridded mean sea surface using improved multi-satellite radar altimeter datasets, including Jason-1 SSH data, and validate the results by several comparisons. The new mean sea surface derived in this research is named CSRMSS14.

Chapter 1 presents a brief description of Jason-1, Jason-2 and Envisat satellites, which are the modern altimeter missions. The major measurements instruments, orbital

parameters, and important scientific findings or contributions are described. Then, an overview of altimeter measurements errors and their corrections follows. There are four categories of corrections: atmosphere, instruments, geophysical and sea-state bias corrections [Chelton el al., 2001]. Finally, the histories of mean sea surface determinations are presented in the following sub-section. Mean sea surface studies have been published since Seasat altimeter data in the 1970s [Marsh and Williamson, 1980; Marsh and Martin, 1982], and they have been updated gradually through the increasing number of satellite missions available, along with improved range and correction models.

Chapter 2 explains the datasets used for this research. Then, it discusses in detail the methodology and computational algorithms to improve the quality of the each altimeter SSH data that uses Jason-1 SSH mean profiles for the integrating process. The main strategy for this process is to compute along-track SSH gradients from existing SSH databases, then integrate them to a new SSH constrained by fixed points on a reference ground track. Jason-1 SSH data at dual crossovers are chosen as reference points or constraints for integration due to the high accuracy of the along track measurement.

In Chapter 3, the computation and validation of the new mean SSH profiles are described. The new mean SSH profiles are obtained by averaging and editing the adjusted SSH data computed through the processes presented in Chapter 2. For validation, the mean profiles of the original SSH dataset and updated SSH dataset are each compared with respect to two accurate mean sea surfaces, DNSC08 and DTU10.

In Chapter 4, the gridding technique of the new MSS, CSRMSS14, is presented. In the final step, the new MSS is determined by gridding the mean profiles of homogeneous SSH data, including ERS-1 geodetic mission data, into a regular surface bin. It is computed on a 5-minute grid oceanwide between ±60º latitudes. 2-dimensional spline interpolation in tension using the Green's function approach for the gridding technique [Wessel and Bercovici, 1998]. The computation algorithms are shown, and the tension factor for this research is examined.

Chapter 5 evaluates the newly gridded mean sea surface, CSRMSS14 through several comparisons. First, in order to analyze how accurate outputs are extracted with respect to inputs, CSRMSS14 is compared with the mean SSH profiles of Jason-1 and Envisat satellites, which are used as inputs in the gridding process. Second, CSRMSS14 is validated through comparison with two recent high-accuracy mean sea surfaces, DNSC08 and DTU10 MSS from DTU space (Technical University of Denmark) [Andersen and Knudsen, 2008; Andersen, 2010]. Finally, the Jason-2 mean SSH profiles are compared with three MSS models: CSRMSS14, DNSC08 and DTU10. Jason-2 SSH data are not used in any of these three MSS determination, so the comparison can provide an independent assessment.

In the last chapter, all of the processes and results of validations for the new mean sea surface are summarized. In addition, topics for additional investigation and recommendations for improvements of the quality and resolution of CSRMSS14 are discussed.

1-1. MODERN ALTIMETER SATELLITE MISSIONS

1-1-1. Brief History of Satellite Mission

The oceans cover three-quarters of the Earth and form a critical component of Earth's climate system. Satellite altimetry has revolutionized our capability to measure the oceans, and led to a greater understanding of the current state of the oceans and their changes. The Geodynamic Experimental Ocean Satellite (GEOS-3) and Seasat in the 1970's demonstrated the use of radar altimetry for oceanography on a global basis. The Geodetic satellite (Geosat) data from 1983 to 1989 improved our knowledge of the marine geoid.

The two European Remote Sensing Satellites, ERS-1 and ERS-2 from the European Space Agency monitored the ocean's surface successfully and improved the resolution of the marine geoid until they were retired in 2000 and 2011, respectively. They were designed as sun-synchronous polar orbiting satellites for the purpose of observing the ocean and land, including ice and atmosphere.

Whereas ERS-2 has a repeat cycle of 35-days, ERS-1 was designed to have multiple phases with repeat cycles of 3-days, 35-days, and as a Geodetic Mission (GM), 168-days. Radar altimeter data from the ERS-1 GM provide very dense coverage spatially, which is essential for determining the short wavelength signals for Earth sciences applications. Their successor, the Environmental Satellite (Envisat), was launched into an altitude of 790 km on March 2002. As can be determined from the name of the satellite, Envisat was designed to observe the Earth from space to assist in studies of Earth's environment such

as ozone depletion and hydrology. The details of the mission will be explained in the sub-section later.

Launched on August 1992, TOPEX/POSEIDON (T/P) provided ocean altimeter data with unprecedented accuracy for 12 years until it was shut down in 2005. It was an international collaboration mission between the United States National Aeronautics and Space Administration (NASA) and the French space agency, Centre Nationale d'Etudes Spatiales (CNES). The two countries built two different kinds of radar altimeters to measure the sea surface heights. The U.S. built the dual frequency TOPEX altimeter, which used C band (5.3 GHz) and Ku band (13.6 GHz), and France built the POSEIDON altimeter, which used Ku band (13.6 GHz). T/P led to invaluable improvements in the studies of physical oceanography and climate changes. In particular, the results from observing global ocean circulations and eddies, establishing the record of global sea level measurements and monitoring El-Nino phenomena are highly successful achievements in the history of ocean remote sensing from satellite. Jason-1 and Jason-2 satellites extended the T/P mission to obtain a series of ocean surface topography missions. The following sub-sections will concentrate on Jason-1, Jason-2 and Envisat missions, which are more recent follow-up missions of the highly successful series of Earth surface observing altimeter satellites, T/P and ERS satellites.

1-1-2. Jason-1 and Jason-2 Missions

As a successor of T/P, Jason-1 was launched on the Delta 2 rocket on December 7, 2001, and it began collecting data on January 15, 2002. Its orbital parameters were designed

to be identical to the T/P mission. Its repeat cycle, about 10 days, enabled it to observe the same area of the ocean for over a decade. The main scientific objectives were to continue to map the ocean topography every 10 days to improve the knowledge of global ocean circulations, observe global sea-level changes, and study global climate variations, to which T/P mission made very successful contributions.

The Jason-1 satellite carried the Poseidon-2 radar altimeter for the measurements of satellite altitude, and the JASON microwave radiometer (JMR) for correction of path delay due to atmospheric water vapor. DORIS (Doppler Orbitography and Radio positioning Integrated by Satellite), TRSR (Turbo Rogue GPS Space Receiver), and LRA (Laser Retro-reflector Array) were onboard for satellite positioning. For scientific purposes, the Jet Propulsion Laboratory (JPL) distributed the altimeter data products called Jason-1 Geophysical Data Records (GDR) [AVISO and PODAAC, 2008]. The GDR contains the modified measurement data applied by corrections algorithms and models from the original observation data. These data have so far produced valuable results, including improved ocean related models and studies of climate and weather prediction.

Before Jason-1 was officially retired, the Jason-2 mission launched on June 20, 2008. The Jason-2 mission was designed to continue and improve the original purposes of its predecessors, T/P and Jason-1 missions, so it shared the orbital parameters and used the updated instruments. The main instrument, Poseidon-3 radar altimeter, sent 2 frequency pulses, at 13.6 GHz and 5.3 GHz, to measure range from the satellite to the surface. To measure water vapor in the atmosphere, which affected the path time of radar

altimeter, the Advanced Microwave Radiometer (AMR) was added aboard. AMR is an upgraded version of the Jason-1 Microwave Radiometer (JMR) used for Jason-1 mission, and its measurements determine how much water vapor is contained in the atmosphere. The Jason-2 satellite is still in orbit and faithfully providing continuous measurements of the oceans and land surface. A Jason-3 mission is scheduled to launch in 2015 to continue to observe the ocean and land.

The Figure 1.1 depicts the 5 instruments aboard Jason-1; Jason-2 payloads are the same, except the JMR radiometer and Poseidon-2 altimeter have been replaced with an AMR radiometer and Poseidon-3 altimeter, respectively.

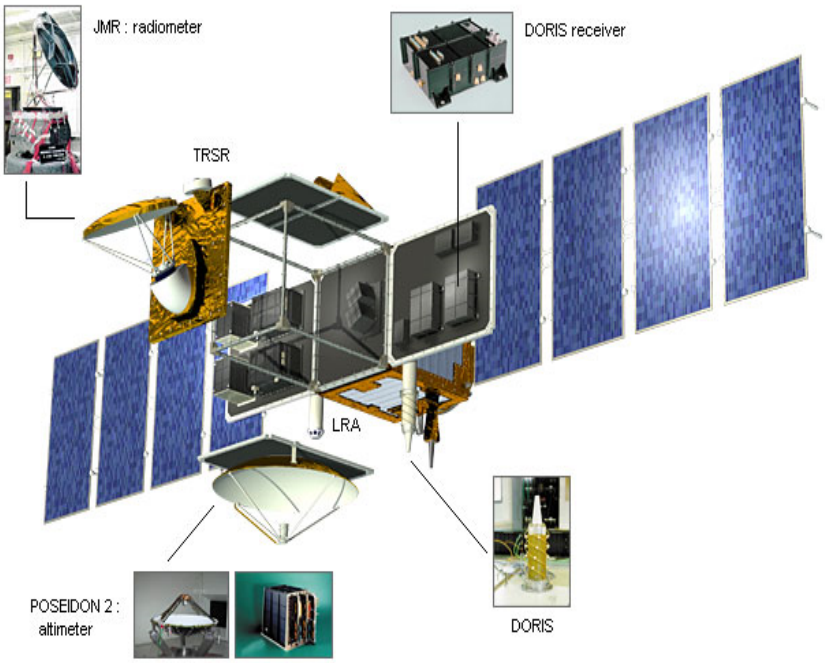

Figure 1.1: Jason-1 Payloads
[http://www.altimetry.info/html/missions/jason1/instruments]

1-1-3. Envisat Satellite

On March 1, 2002, the Envisat satellite was launched on an Arian 5 rocket from the Guinea Space center in Kourou, French Guyana. It was designed to have a sun-synchronous polar orbit at an inclination of 98.4 degrees, allowing it to monitor the Earth's surface more densely and covers high latitude areas. The primary objective of the Envisat mission is to observe and monitor the ocean, land, and atmosphere. In addition, it is used to monitor regional environments such as ice and snow, hydrology, and agriculture.

Envisat is the world's largest Earth-observing satellites in space, carrying 10 satellite instruments. One of the 10 instruments, RA-2 (Radar Altimeter 2), sends and receives radar pulses to and from the Earth's surface, enabling a highly precise measurement of range. In addition, the Microwave radiometer (MWR) was used to measure atmospheric water vapor, providing the information on ice sheets and soil moisture. The Advanced Synthetic Aperture Radar (ASAR), Advanced Along-Track Scanning Radiometer (AATSR), Michelson Interferometer for Passive Atmospheric Sounding (MIPAS), and Doppler Orbitography and Radio-positioning Integrated by Satellite instrument (DORIS) operated to calculate the image mode, sea surface temperatures (SST), emission features in the atmosphere, and precise position measurement, respectively [Gardini el al., 1995].

For 10 years, it provided data successfully until it lost contact suddenly and was declared to be dead on May 9, 2012. It made tremendous contributions to studies of Earth

and its environment during its lifetime. Table 1.1 shows the summary of the main characteristics of T/P, Jason-1, Jason-2 and Envisat orbit parameters.

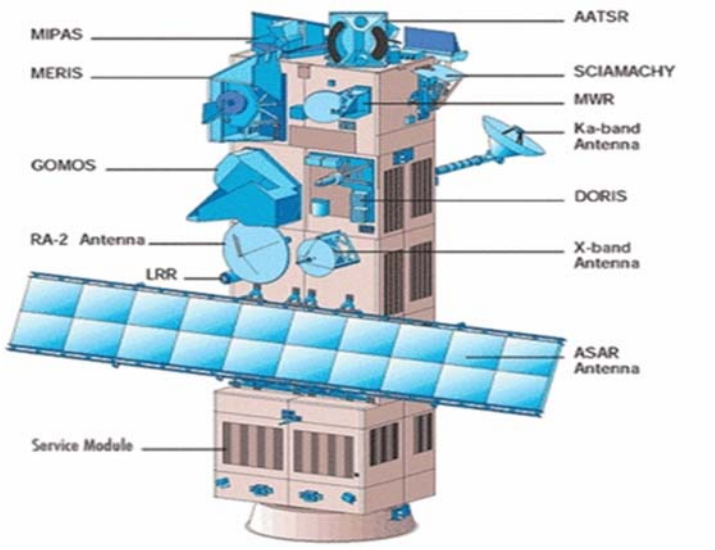

Figure 1.2: Envisat Payloads
[http://www.altimetry.info/html/missions/envisat/instrument].

	T/P	**Jason-1**	**Jason-2**	**Envisat**
Semi-major axis	7714.4 km	7714.4 km	7714.4 km	7159.5 km
Inclination	66 degrees	66 degrees	66 degrees	98.4 degrees
Equatorial Altitude	1336 km	1336 km	1336 km	799.8 km
Repeat Interval	9.9156 days	9.9156 days	9.9156 days	35 days
Ground track separation at equator	315 km	315 km	315 km	80 km
Number of passes per cycle	254	254	254	1002
Time span (month/year)	8/1992-1/2006	12/2001-7/2013	06/2008- current	3/2002-4/2012

Table 1.1: T/P, Jason-1, Jason-2 and Envisat orbit parameters.

1-2. Errors and Corrections of Sea Surface Height Measurements

The altimeter range measurement is computed by measuring the elapsed time, t, between the satellite and the surface. The sea surface height (SSH) is calculated by subtracting the range from the orbit height. For an accurate SSH, accurate orbit precision and accurate range measurements are necessary. The initial range measurement has errors and biases caused by several factors, so corrections must be applied to improve the accuracy of the sea surface height.

There are three groups that cause these errors and biases to altimeter range estimation. First, the environmental effects, such as dry and wet troposphere and ionosphere, result in a delayed radar signal due to content in the atmosphere [Urban, 2000]. The neutral atmosphere effects can be corrected by models such as the European Centre for Medium-Range Weather Forecasts (ECMWF) and National Center for Environmental Prediction (NCEP). Second, the geophysical corrections, which contain the inverted barometer and the tide corrections, should be applied to the sea surface height measurements. Finally, the instrument corrections include tracker bias correction, Doppler shift correction, oscillator drift correction, AGC attenuation corrections, etc. [Chelton et al., 2001]. Aside from these categories, sea-state bias correction should also be considered. For more details about errors and corrections for the range, see Chelton et al. [2001]. Table 1.2 explains the correction models that were applied to the Jason-1 Geophysical Data Record (GDR) data, which are used as a reference surface for this research [AVISO and PODAAC, 2008].

Contents	Model or Algorithm
Orbit	JGM3 gravity field
Wet tropospheric range	Radiometer
Dry tropospheric range	ECMWF
Inverted barometer correction	ECMWF
Tide	GOT99
Geoid	EGM 96

Table 1.2: Main range and error correction models for Jason-1 GDR data.

1-3. REVIEW OF MEAN SEA SURFACE DETERMINATIONS

Scientists have made efforts to create more accurate mean sea surface (MSS) models for oceanographic and geophysical applications. Marsh et al. [1992] created a mean sea surface called MSS-9012, based on GEOS-3 and SEASAT altimeter data in $\frac{1}{8}° \times \frac{1}{8}°$ regular grid. This study demonstrated that combining two different altimeter datasets for MSS provided more information and better results than using single satellite data. Since high quality SSH have been continuously provided, several mean sea surface models were derived based on longer-span altimeter data, and better corrections and mapping techniques by different research centers in the U.S. and Europe. In particular, recent MSS models were updated to a level of unprecedented accuracy following the usage of the very precise Topex/Poseidon (T/P) SSH as a reference surface, and improved to higher resolution after short-wavelength data, GM (Geodetic Mission) data, were carefully included.

The most important process of MSS determination is making homogenous datasets from different satellite missions. In particular, orbit errors of historical missions are relatively higher than those of recent altimeter data, so they should be corrected before merging. The technique of crossover adjustment, which is a common method, has been used directly to remove orbit errors and other biases, enabling the old mission altimeter data to be homogeneous to reference field such as T/P.

Gridding, which interpolates multiple kinds of SSH with various accuracies to the regular geographic locations from the scattered positioned data, is another important process to obtain the final results of MSS. Several MSS models used the least square collocation method for gridding, which is a similar to weighted least square objective analysis [Tapley and Kim, 2001]. In the following sub-sections, the several mean sea surface models published in 2000's are introduced.

1-3-1. CLS01 and GSFC00 MSS Models

Hernandez and Schaeffer at the CLS (Collecte Localisation Satellites) presented their updated MSS model, called CLS01 [Hernandez and Schaeffer, 2001]. The model is derived using 2-years of Geosat mean profiles, 5-years of ERS-1 and ERS-2 mean profiles, 7-years of T/P mean profiles and ERS-1 geodetic mission data. It was updated to a more accurate surface from its previous MSS models, CLS_SHOM98.2 and CLS_SHOM99. CLS01 used T/P mean profiles to reduce orbit, and range errors and biases of the other altimeter datasets, including geodetic SSH data, through the adjustment method [Le Traon and Ogor, 1998]. They performed the process to reduce the ocean variability, and CLS01

is gridded into 2-minute spatial resolution using local least square collocation. For least square collocation, refer to Bretherton et al. [1976].

The GSFC00 mean sea surface model, which was developed in Goddard Space Flight Center (GSFC) in the U.S., was updated from the GSFC98 model [Wang, 2000; Wang, 2001]. In order to reduce long wavelength orbit errors, the crossover adjustment technique, with 6-years of T/P mean tracks, was applied to adjust ERS-1/2 and Geosat ERM mean profiles. For ocean variability and other time varying errors in non-repeating Geosat GM and ERS-1 GM data, which cannot be reduced by time averaging, SSH gradients instead of SSH are used for MSS determination. Finally, the mean sea surface, GSFC00, was computed by gridding into 2-minute resolution nodes between latitude ±80º, using the least square collocation technique based on 2-D Fourier series in 2º by 2° cells [Hernandez and Schaeffer, 2000]. Even though CLS01 and GSFC00 are over a decade old, they have been used worldwide for oceanographic, geodetic and geophysical oceanography up to the present due to their good accuracy.

1-3-2. DNSC08 and DTU10 MSS Models

DTU (Denmark Technical University) space in Denmark of Europe, whose previous name was the Danish National Space Center (DNSC), has put effort into deriving its own mean sea surface models by using a longer time series of altimeter mission data and better processing methods. DNSC08 mean sea surface was determined using a combination of 12-years of T/P and Jason-1 mean tracks as a reference field, including multiple altimeter data from 8 different missions [Andersen and Knudsen, 2009]. It was

gridded into 1-minute resolution and, for the first time, it was expanded to the entire Artic Ocean by using ICESat laser altimeter data. The systematic biases between its reference surface and the other ERM altimeter data from different missions, were reduced by fitting to T/P+Jason-1 mean profile, using the crossover adjustment method. Figure 1.3 represents the DNSC08 mean sea surface [Andersen and Knudsen, 2008].

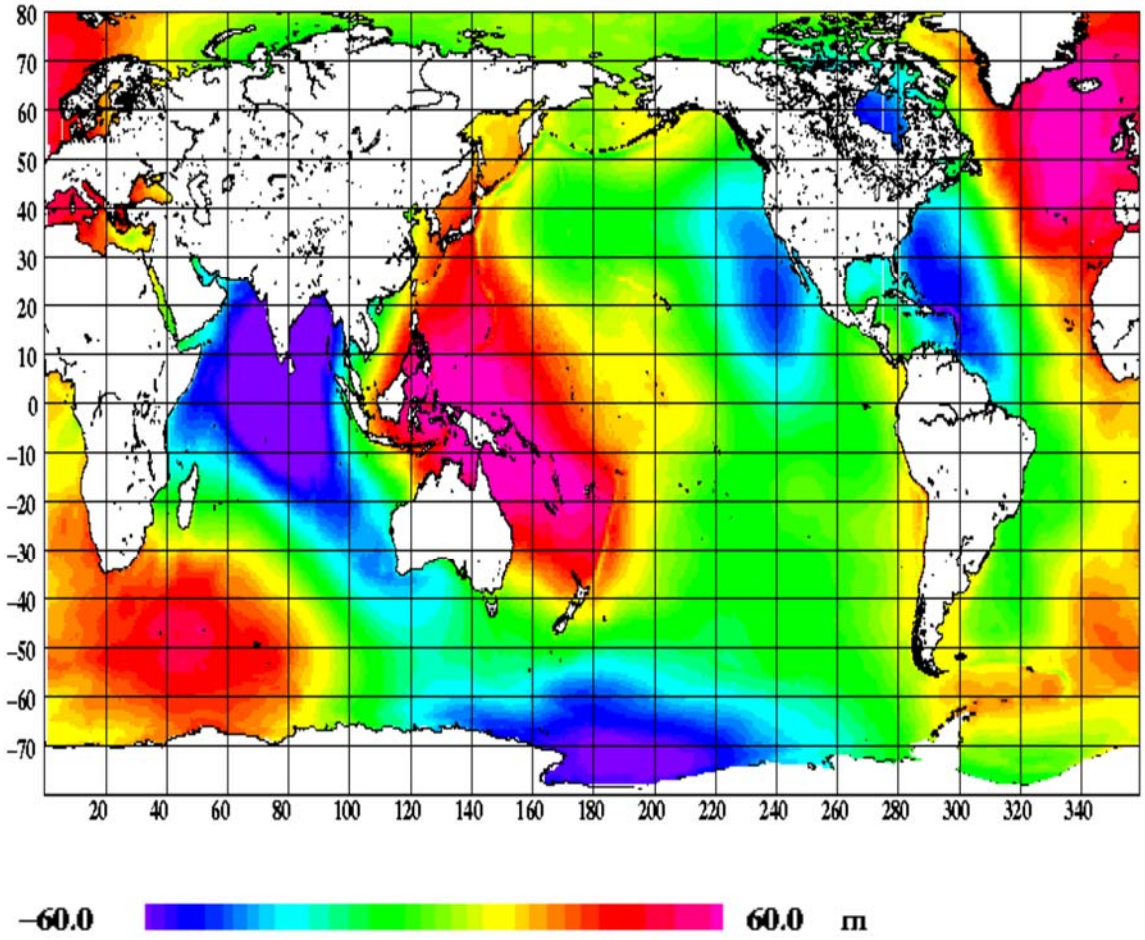

Figure 1.3: DNSC08 Mean Sea Surface.

DNSC08 was updated slightly to DTU10 mean sea surface in 2010, including longer Jason-1 data, up to 2009, for a reference surface. DTU10 was derived with the same methods for adjustments and gridding as DNSC08, except with slightly more corrected SSH datasets, which were processed with improved editing, and better range and geophysical corrections [Andersen, 2010]. Table 1.3 compares the models for range and geophysical corrections used in DNSC08 and DTU10 mean sea surface determination [Andersen, 2010].

	DNSC08	**DTU10**
Orbit	GGM02/ITRF2000	EIGEN-GL04C
Wet troposphere	ECMWF	Radiometer/ECMWF
Dry troposphere	ECMWF	ECMWF
Ionosphere	Altimeter	Altimeter
Sea State Bias	BM4	Non-PARAM
Ocean Tides	GOT 00.2	GOT4.7

Table 1.3: Models of range and geophysical corrections used for DNSC08 and DTU10.

DNSC08 and DTU10 are currently considered as very accurate and highest resolution surfaces, covering the entire Earth, from -90 degrees to +90 degrees of latitudes. Therefore, those two MSS were used for comparisons in several validations for this research due to their high accuracies. Table 1.4 represents the summary of four recent mean

sea surfaces, which are described above, and new MSS (CSRMSS14) developed in this research is also included for a reference.

Name	**CLS01**	**GSFC00**	**DNSC08**	**DTU10**	**CSRMSS14**
Reference surface (period)	T/P (1993-1999)	T/P (1993-1998)	T/P +Jason-1 (1993-2004)	T/P +Jason-1 (1993-2009)	Jason-1 (2002-2008)
Data Set used from non-reference surface	Geosat ERM ERS-1 ERM ERS-1 GM ERS-2	Geosat ERM Geosat GM ERS-1 ERM ERS-1 GM ERS-2	Geosat GM ERS-1 GM ERS-2 GFO Envisat ICESat	Geosat GM ERS-1 GM ERS-2 GFO Envisat ICESat	Geosat ERM ERS-1 GM ERS-2 T/P Envisat
Processing for data improvement	Orbit error reduction by crossover analysis	Orbit error reduction by crossover adjustment	Fitting to the reference field by expanding to spherical harmonic degree and order 2-4.	Re-tracking the entire ERS-2 and Envisat	Adjustment procedure using integrating process
Gridding Technique	Least squares collocation	Least squares collocation	Least square collocation	Least square collocation	2-D spline interpolation in tension using Green's function
Spatial gridding Resolution	2 min	2 min	1 min	1 min	5 min
Coverage	80 ºS to 82 ºN	80 ºS to 80 ºN	90 ºS to 90 ºN	90 ºS to 90 ºN	60 ºS to 60 ºN

Table 1.4: Summary of recent mean sea surface models; CSRMSS14 is included for a reference.

Chapter 2: Computation to Enhance Sea Surface Height Data

2-1. INTRODUCTION

The previous chapter explained the objective of this research, the histories of satellite missions and mean sea surface models, including the errors and corrections of the sea surface heights measured from the satellite altimeter. In this chapter, a method to enhance the quality of SSH data more efficiently, especially for historic data, whose orbit errors are generally larger than those of the recent missions, will be derived and performed. For this research, Jason-1 altimeter data are chosen as the most accurate and precise reference surface. The results of this method include the reduction of systematic differences, and errors and biases among multiple SSH data from different missions, especially, different databases. Ultimately, through this method, it is expected that the multi-satellite SSH data from the different satellite missions will be well adjusted to the chosen reference surface, Jason-1 mean SSH data, and become consistent with each other.

In this research, the data adjustment procedure is derived based on an integrating approach, and the computational algorithm is designed to be performed in three steps using a bin-by-bin format. The first step of the computation is to calculate the along-track SSH gradients of each satellite bin-by-bin. Next, we compute dual crossovers between the mean ground track of Jason-1 satellite and the other satellite's ground track. Finally, the new SSH values of each satellite are obtained by integrating the SSH gradients bin-by-bin with

the mean sea surface values of Jason-1 at crossovers used as the initial starting point. Through this process, the improved SSH dataset are obtained for each in the individual satellite data sets. These three steps are described in details in the following sections 2.3, 2.4 and 2.5.

In Section 2.2, the datasets used for this research will be explained. The satellite datasets used for this research are extracted from two kinds of existing altimeter databases from different research centers: the Center for Space Research (CSR) at the University of Texas at Austin and the Delft Institute for Earth-Oriented Space research (DEOS) in Netherland. Since the format of dataset from these two altimeter database are different, the altimeter data obtained from DEOS are pre-processed by reformatting the data into a similar format as those of the CSR altimeter database. In the last section, 2.6, the whole process for the improved SSH datasets of satellites is summarized.

2-2. DATA USED

Research centers or space agency data centers receive the original data from the satellite, then process and distribute the scientific data to users. The scientific centers that receive the information make their own altimeter databases by re-processing and editing the original data in order to prepare them useful for scientific analysis. The Center for Space Research at the University of Texas at Austin (UT-CSR) developed an easily accessible database for the altimeter data of the exact-repeated missions (ERM), referred to in the following as a Stackfile. Delft University of Technology in Netherland also has

such a database for altimeter radar data, called Radar Altimeter Database System (DEOS-RADS), which is referred to as RADS in the following discussion.

The CSR-Stackfiles are binned along the satellite ground track, and stores 1-Hz measurements of radar altimeter satellite. The bin-by bin structure of the Stackfile allows easy access, computing, comparing and combining the several altimeter datasets. Moreover, it allows us to compute the SSH gradients, mean values, and crossovers in a more straightforward way. For this research, most radar data of altimeter satellites are utilized from the Stackfile, and only datasets missing from the Stackfiles are received and used from RADS.

Envisat satellite data, which were never created in the Stackfile, and ERS-1 geodetic mission (Phase E and F) data (whose database became corrupted), were obtained from the altimeter database from DEOS. The locations and their associated SSH values by passes in each cycle, orbit parameters and other necessary information derived from those satellites were provided. The RADS data are not provided in the bin format of Stackfile, so a process to re-format the data into a bin-by-bin structure is performed as a part of the pre-processing.

In summary, the data used for this research are Geosat ERM, ERS-2, T/P, and Jason-1 data from Stackfile, and ERS-1 Geodetic data (Phase E and Phase F) and Envisat radar data from RADS. The following sub-sections will explain the structure of Stackfile data and the pre-processing of RADS data.

2-2-1. CSR-Stackfile Data

In order to allow efficient access to the altimeter data, CSR-Stackfiles were developed and upgraded by researchers at UT-CSR from the Geosat ERM altimeter mission to the Jason-2 mission. Stackfiles store 1Hz SSH measurements as a three dimensional array, called column-row-slot. Data information is contained in a finite sized bin, which is an approximate area of the 1-second observation. Columns are organized by pass numbers of the orbit in eastward order of equator-crossing longitude. Thus, column number 1 means that the longitude passing across the equator is $0° E$. The row is indexed as northward or southward along the track, by order across the equator crossing. The position nearest to the equator is indexed row number 0. The positive row numbers are assigned to northern areas of the equator, and the negative row numbers are determined as south of the equator. For the repeated orbits satellites, slots as the third dimension are indexed. In addition, the data for ascending and descending passes of the ground track are stored separately.

Each bin has all useful information about the altimeter radar data. The main parameters of a bin are ocean sea surface height data and positions of measurements (latitude and longitude). In fact, the positions are stored in slots by the displacements of latitudes and longitudes from the bin center by cycles in order to save the storage size. Thus, each slot includes information regarding SSH of each repeat cycle, atmospheric pressure, ocean depth (bathymetry), geographic corrections and editing criteria. As

mentioned earlier, the bin-by-bin format of the Stackfile is very useful to access and apply data to the computations more directly.

For this research, data used from the Stackfile are Geosat ERM, ERS-2 and T/P, and they will be adjusted to be homogeneous datasets later. Jason-1 data from Stackfile are used to reference the surfaces. Table 2.1 shows the ranges of the columns, rows, and slots for these four satellites in Stackfile.

	Columns Range	**Rows range**	**Slots range (Repeat cycles)**
Geosat ERM	1-244	-1550 ~ 1550	1-68
ERS-2	1-501	-1550 ~ 1550	1-65
T/P	1-127	-1570 ~ 1570	1-364
Jason-1	1-127	-1570 ~ 1570	1-256

Table 2.1: Information of three components in CSR-Stackfile structure.

2-2-2. Pre-Processing of DEOS-RADS Data

DEOS-RADS is an internet based database [http://rads.tudelft.nl/rads/rads.shtml]. The altimeter radar data are stored continuously in it and updated with recent corrections. For this research, two different datasets of Envisat phase 2 and ERS-1 SSH data in phase E and phase F were obtained from RADS. Upon request, we can choose the cycles and phases of data selection, geographical selection criteria, sea level anomaly construction, and correction options. The parameters requested from RADS database are the sea level anomalies (i.e., sea surface height) from the TOPEX ellipsoid as a reference field, within

longitude from 0º to 360º and latitude from -65º and +65º. The equator passing time, equator passing longitude, and time relative to equator passage by pass numbers in each cycle number are stored in the files.

The correction options are chosen by RADS recommendations because they are usually up-to-date models. The orbits for ERS-1 geodetic missions in RADS were corrected with the model based on the DGM-E04 gravity model, while the Envisat orbits came from CNES based on the EIGEN-GL04S gravity model. For dry and wet troposphere corrections, ECMWF (European Center for Medium Range Weather Forecasting) and MWF models for both satellite missions were applied [Scharroo et al, 2013]. For ionosphere correction, NIC09 (New Ionosphere Climatology 2009) climatology [Scharroo and Smith, 2010] was applied to both satellites, and a high-resolution version of the MOG2D dynamic atmospheric correction [Carrère and Lyard, 2003] was applied for the inverse barometer correction. A summary of range and geophysical corrections applied two radar datasets from RADS are described in Table 2.2. For more information of each model, see the user manual and format specification written by Scharroo [Scharroo, 2012].

For this research, in order to match the format of RADS dataset with that of the Stackfile, RADS data were re-formatted into the bin structure such as the column-row-slot form. They were processed from the pass numbers into column numbers, and from time differences relative to the time across equator passage to row numbers in order. After that, they were stored by cycle numbers in ascending and descending passes separately. For the

Envisat data, repeat cycles between 9 and 94 whose time spans are from 2002 to 2010 (8 years long) are computed for reformatting into bin-by-bin form.

After reformatting, the total column numbers for Envisat radar data in each ascending and descending passes are 501, and the row numbers are from -1550 to 1550. They are identical with column and row numbers of ERS-2 data in the Stackfile. 168-days of ERS-1 geodetic mission data (phase E and F) are non-exact repeating missions, but instantaneous SSH data. They were also obtained from RADS, reformatted and stored into row-column structure with a single cycle number. Through this pre-processing, Envisat and ERS-1 geodetic mission data from RADS are re-arranged into a bin-by-bin format: column-row-slot structure. Finally, they are ready to share the same computation programs as the satellite data from the Stackfile.

	ERS-1 (GM data)	**Envisat**
Orbit	DGM-E04	CNES EIGEN-GL04S
Dry tropospheric correction	ECMWF	ECMWF
Wet tropospheric correction	MWR	MWR
Ionospheric correction	NIC09	NIC09
IB (Inverse Barometer) correction	MOG2D	MOG2D
Ocean tide	GOT4.7	GOT4.7
Load tide	GOT4.7	GOT4.7
Sea State Bias	BM3 sea state bias	CLS sea state bias

Table 2.2: Correction models used for ERS-1 GM and Envisat data from DEOS-RADS.

2-2-3: Summary of Data Used

A total of 6 different satellite radar data from two different databases of altimeter satellite missions are used for this research: Geosat ERM, ERS-2, T/P and Jason-1 altimeter data from CSR-Stackfile, and ERS-1 GM (Phase E and F) and Envisat data from DEOS-RADS. Table 2.3 lists the time periods, inclinations, and database source of all the satellite datasets used for this research; Jason-2 data are used for a validation in Chapter 5 later, so included in the table.

These radar altimeter data used for the new MSS model (CSRMSS14) cover a 24-year time span from 1986 to 2010. Data from RADS are pre-processed for reformatting into bin-by-bin form consistent with the format of the Stackfile. The new method for data adjustments, which are described in the next sections, are designed to benefit from the bin-by-bin format.

Satellite	**Cycles**	**Dates (Mon/Year)**	**Inclination (unit: degrees)**	**Database source**
ERS-1 Phase E	139-140	4/1994-9/1994	98.5	DEOS-RADS
ERS-1 Phase F	141-143	9/1994-3/1995	98.5	DEOS-RADS
Envisat	9-94	8/2002-10/2010	98.5	DEOS-RADS
Geosat ERM	1-62	11/1986-7/1988	108	CSR-Stackfile
ERS-2	1-67	5/1995-10/2001	98.5	CSR-Stackfile
T/P	10-364	9/1992-8/2002	66	CSR-Stackfile
Jason-1	1-256	1/2002-12/2008	66	CSR-Stackfile
Jason-2	1-62	7/2008-3/2010	66	CSR-Stackfile

Table 2.3: Summary of all the datasets used for this research.

2-3. Computing Along-Track Gradients of Sea Surface Heights

A high accuracy mean sea surface model depends on the quality of multi-altimeter datasets from multiple missions. Before being combined, multi-satellite data must undergo a process to make them homogeneous with each other and to improve the data quality within a reliable accuracy level. In particular, the early mission data are required in order to reduce relatively higher orbit and range errors than those of recent missions. For such an adjustment procedure, 5 different satellites (Geosat ERM, ERS-2, ERS-1 GM, T/P, and Envisat) are processed into the new SSH dataset through an integrating method using along-track SSH data, and the final results are expected to have an improved data quality similar to the level of the reference surface, Jason-1 SSH. As the first step of the integration method, the description of the computation of along-track SSH of each satellite is followed.

2-3-1. Method

In general, the mathematical equation for a SSH gradient is written in a straightforward way:

$$G_i = \frac{SSH(x_{i+1}) - SSH(x_i)}{x_{i+1} - x_i} \tag{2.1}$$

where,

SSH is a sea surface height of a bin,

$x_{i+1} - x_i$ is an interval of two consecutive bin centers,

G_i is a SSH gradient in i^{th} bin.

The interval of two consecutive bin centers $(x_{i+1} - x_i)$ depends on the distance of the 1 Hz measurements. It changes with the satellite's ground-track, but within a limited range, which is approximately from 6000 m to 7000 m. Figure 2.1 shows the variation of the distance between two successive measurements for portions of cycle 10 for the Geosat ERM.

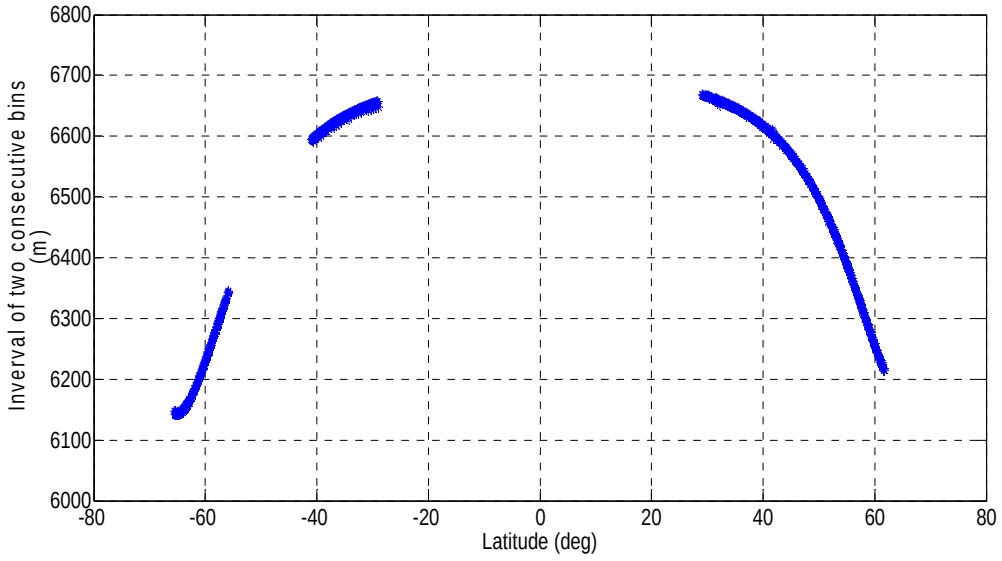

Figure 2.1: Example of interval of two consecutive bins $(x_{i+1} - x_i)$ in a portion of representative of Geosat ERM.

However, the SSH gradients obtained by the equation (2.1) are from two SSH data bins in ahead and current positions, so they are very sensitive to the accuracies of instantaneous SSH data in two consecutive bins. In the long run, SSH gradients affect the results of the new SSH values obtained through integrating SSH gradients in use. If a SSH at a certain time is inaccurate for some reason, it will result in a higher or lower gradient in

a bin than the true value and ultimately yield incorrect integrated results. Moreover, it would influence the results of the subsequent points along the same track during the integration process.

To reduce the risk of erroneous gradients due to inaccurate or highly variant points, three SSH data are considered for computing along-track SSH gradients. The three SSH data are an ahead, current, and behind data of SSH at a current position. First, the along-track gradients between the ahead and current bins of SSH data are computed ($G_{i\_forward}$). Then, the along-track SSH gradients from the current and behind bins of the current position are calculated ($G_{i\_backward}$). Finally, the along-track SSH gradients computed from forwarding ($G_{i\_forward}$), and backwarding ($G_{i\_backward}$) are combined using distance-weighting factors. Therefore, the mathematical equations of along-track SSH gradients using the three SSH data are:

$$G_{i\_forward} = \frac{SSH(x_{i+1}) - SSH(x_i)}{x_{i+1} - x_i} \tag{2.2}$$

$$G_{i\_backward} = \frac{SSH(x_i) - SSH(x_{i-1})}{x_i - x_{i-1}} \tag{2.3}$$

$$G_{i\_combined} = \frac{w_1 \times G_{i\_forward} + w_2 \times G_{i\_backward}}{w_1 + w_2} \tag{2.4}$$

where, w_1 and w_2 are distance-weighting factors.

Figure 2.2 shows the effects of gradients using three SSH data. The along-track SSH gradients in certain part of the first column of cycle 10 for Geosat ERM are computed. The blue stars and lines represent the results of the along-track SSH gradients computed using 2 consecutive SSH data, while red symbols mean usage of 3 consecutive SSH data. The figure indicates that the results of gradients using 3 SSH data yield smoother results, and can reduce the possible risk of producing inaccurate SSH gradients from inaccurate SSH points.

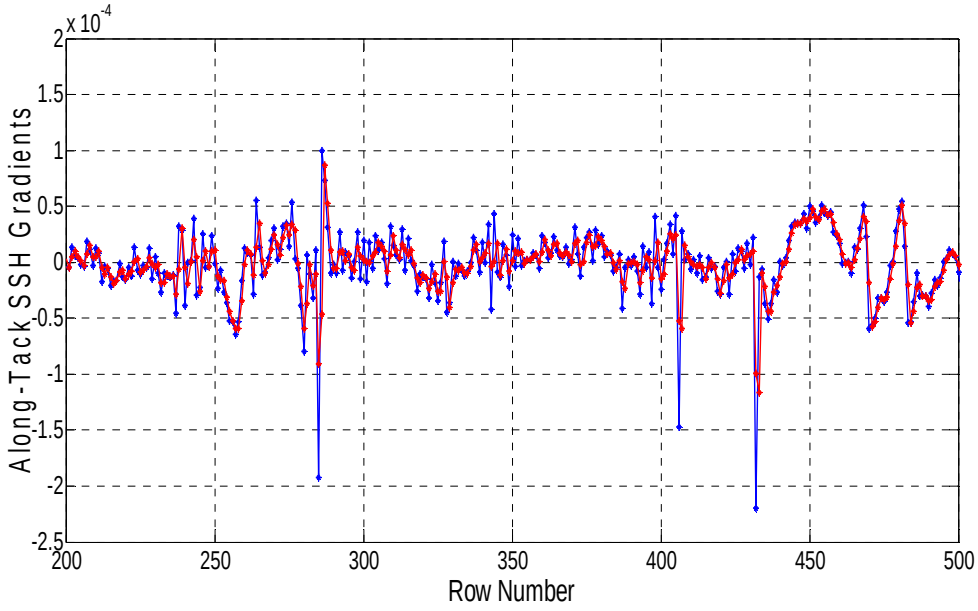

Figure 2.2: Example of comparing the effects of using 2 consecutive SSH data (blue stars) and 3 consecutive SSH data (red stars) of along-track SSH gradients.

From this process, we have a dataset of along-track SSH gradients by each cycle in each satellite, and finally, a total of 5 databases of the along-track SSH gradients for Geosat ERM, ERS-1 GM, ERS-2, Envisat, and T/P are obtained.

2-4. COMPUTING CROSSOVERS BETWEEN JASON-1 AND THE OTHER SATELLITE

2-4-1. Introduction

Dual crossovers refer to the intersections of two different satellites, whose techniques have been used to compute the precision orbit determination (POD) [Kozel, 1995] and sea level related applications. For mean sea surface (MSS) determination, the crossover adjustment method plays an important role in reducing orbit errors of relatively old SSH data. The main results from the dual crossover determination technique are the intersection positions by longitude and latitude, and two SSH data interpolated at crossover locations.

In this research, dual crossover computation is used as the second step of the integrating method of deriving the new SSH dataset. The process is performed with a reference ground track and the other satellite's ground track. The Jason-1 mean ground track is chosen as a reference arc, and the associated mean SSH data of Jason-1 at crossovers are used as initial points or constraints for integration due to their high accuracy. New studies have shown that T/P has been contaminated by very large hemispherical biases due to the tracker used, so Jason-1 is chosen instead of T/P as a reference surface [Don Chambers, personal communication, 2007]. The Jason-1 mean SSH values are obtained by averaging the SSH from cycle 1 to 256 (data span from 01/2002 to 12/2008).

Through the dual crossover procedures, the exact locations of two intersecting ground tracks, such as Jason-1 mean ground track and the other satellite ground track, and the two associated SSH are derived. The following sub-section, 2-4-2 provides the

computational algorithm for dual crossover computation. The analysis of dual crossovers determinations is discussed in sub-section 2-4-3. Height differences of two derived SSH at dual crossovers represent an indication of systematic biases between two satellites, which were caused from inconsistencies of applied orbit, range and geophysical correction models, reference frame offsets and time averaging periods and epochs [Chelton et al., 2001; Andersen and Scharroo, 2009; Andersen and Knudsen, 2009]. They yield insight into the initial differences between two satellite data sets and future changes after the integrating process. Thus, SSH differences between Jason-1 and the other satellite at crossover locations are taken into account for evaluation. In addition, as an analysis by statistics, the mean and standard deviation of height differences between Jason-1 mean SSH and the SSH of the other satellite at crossover locations are computed.

2-4-2. Algorithm for Dual Crossovers Computation

Based on the collinear interpolation method [Kruizinga, 1997], the crossover computation is repeated to obtain the exact results of the dual crossover locations, the associated time tags, and the interpolated SSH data between two satellites' ground tracks from the approximate values [Kozel, 1995]. The program software designed to process from altimeter data of Stackfile format, which consists of bins by columns and row numbers in each cycle, is used in this research. The computational algorithm is composed of nonlinear prediction and interpolation technique. More detailed information of dual crossover analysis and applications can be found in the doctoral dissertations written by

Kozel [1995] and Kruizinga [1997]. In this sub-section, important steps for computations are focused as follows.

First, given inputs of the longitudes and times of equator crossings in two passes, the equator longitude differences, ΔL_{equ}, between two passes (or arcs) are determined through the nonlinear prediction using spherical trigonometry. The two arcs are defined so that one arc is a pass of Jason-1 mean ground track, and the other arc is a pass of the other satellite ground track. For interpolated altimeter values, 7-years of Jason-1 mean SSH values, computed by averaging the Jason-1 SSH of cycles from 1 to 256, and the instantaneous SSH data of the other satellite by each cycle are used for computation.

Next, two relative arguments of latitude to the crossover location, with respect to equator crossing (u_j and u_{sat}), are computed given the determined equator longitude differences (ΔL_{equ}), inclinations ($i_j \; and \; i_{sat}$), and directions ($d_j \; and \; d_{sat}$) of two passes from Jason-1 and the other satellite. Note that directions mean ascending or descending passes of the ground tracks of the satellites, and index +1 or -1. In addition, u_j is the argument of latitude of a Jason-1 mean ground track, and u_{sat} is the argument of latitude of a pass of the other satellite. Figure 2.3 represents the spherical trigonometry of the equator longitude difference, two relative arguments of latitude to the crossover location of Jason-1 and the other satellites.

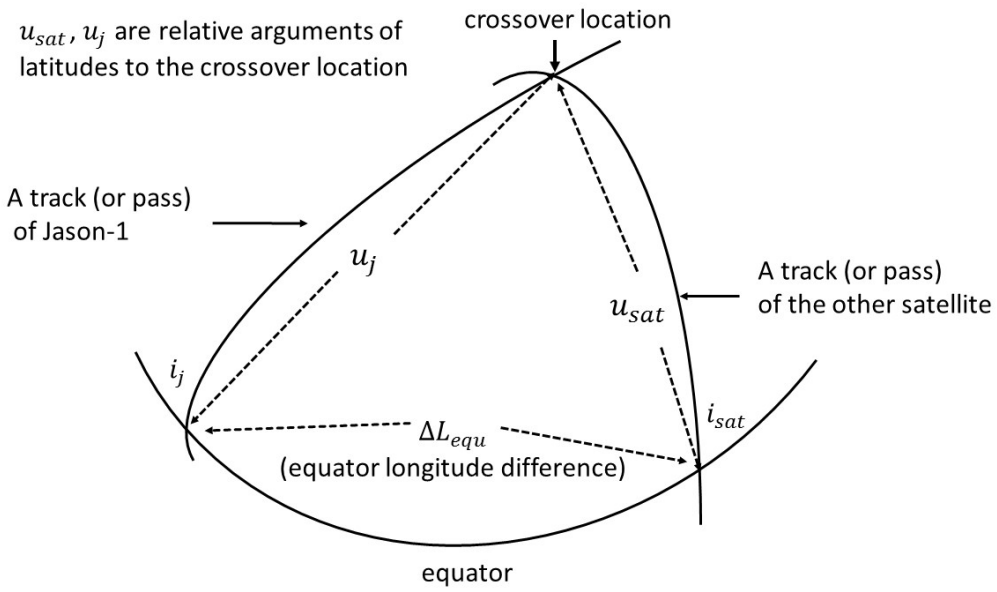

Figure 2.3: Spherical trigonometry of two intersection passes: Jason-1 and the other satellite.

As the next step, the approximate crossover locations in terms of row numbers of Stackfile format are found through an iteration process with inputs of the determined two relative arguments of latitudes to the crossover location (u_j and u_{sat}) and time tags of two passes. Finally, an exact crossover location and associated SSH data of Jason-1 and the other satellite, including row numbers, are computed through iterations until they are found.

In one computation, the results are produced from a pass (or arc or column in Stackfile format) of the other satellite and all passes of Jason-1 mean ground track in both ascending and descending passes. Then, it repeats through all passes in one cycle, then through all assigned cycles of the other satellite. Figure 2.4 represents the geographical

distributions of dual crossover locations between Jason-1 mean ground track and the Geosat ground track of cycle 5 in ascending pass.

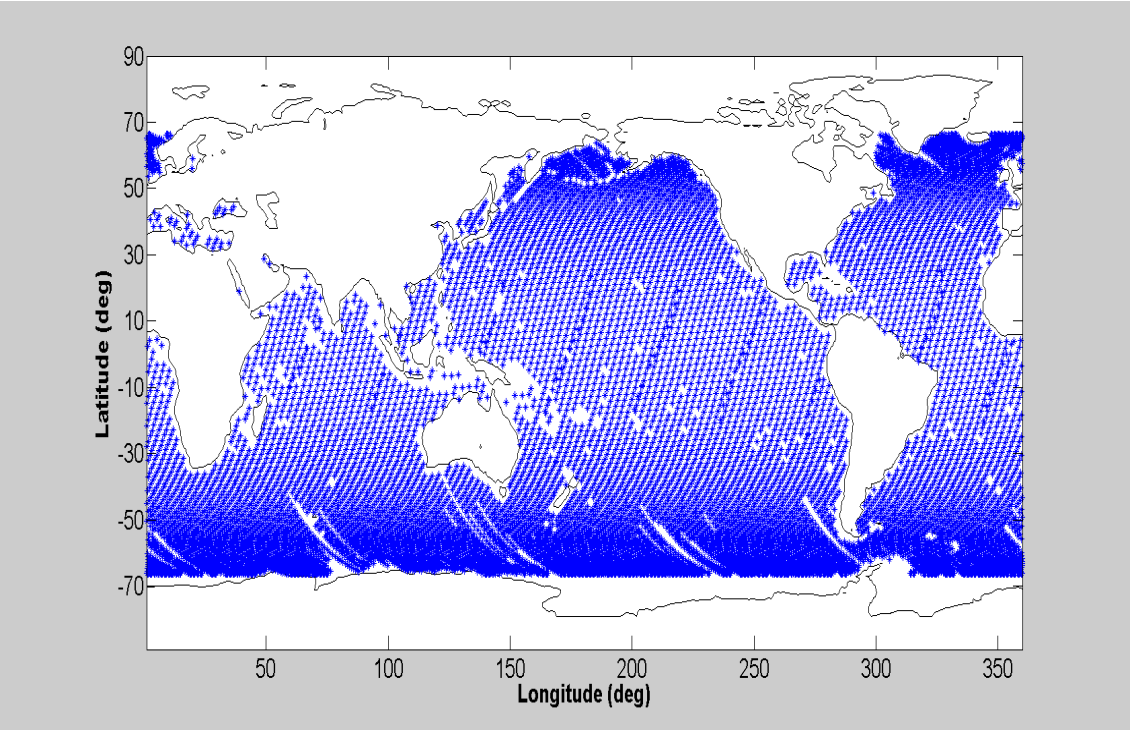

Figure 2.4: Geographical distribution of dual crossover locations between Jason-1 mean ground track in ascending and descending passes and Geosat ground track of cycle 5 in ascending pass.

The other satellites, Geosat ERM, ERS-2, Envisat, and T/P, including ERS-1 geodetic mission, are performed through the crossover process. The results for cycles 118, 174, 180, 186, 209, 216, 224, 234, and 246 were not determined, due to a lack of data in Stackfile, during the computation for T/P, so the final new SSH dataset of these repeated cycle numbers for T/P are not calculated as well. Note that Envisat and ERS-1 geodetic

data from RADS database were reformatted into Stackfile format as described before, so that computations were compatible with Geosat ERM, ERS-2 and T/P from Stackfile database.

Through this process, the results of the exact crossover locations (in degrees), their associated row numbers, and interpolated SSH data of Jason-1 mean track and the other satellite track are computed. Since the inclination of the Jason-1 satellite is 66º, the outputs are restricted to within these latitude ranges. As previously mentioned, these outputs will be used as constraints and initial values in the integrating process, which will be described in the next section, 2-5. Because of the limitation of latitudes of the reference field, the new SSH datasets are obtained within ±60º latitudes, and the new mean sea surface, which is the ultimate goal of this research, is derived within the same latitudes range.

The summary of the dual crossover computational algorithm for this research is shown in Figure 2.5. The next sub-section 2-4-3 discusses the analysis of the two interpolated SSH data at crossovers computed between Jason-1 and the other satellite ground track by statistics.

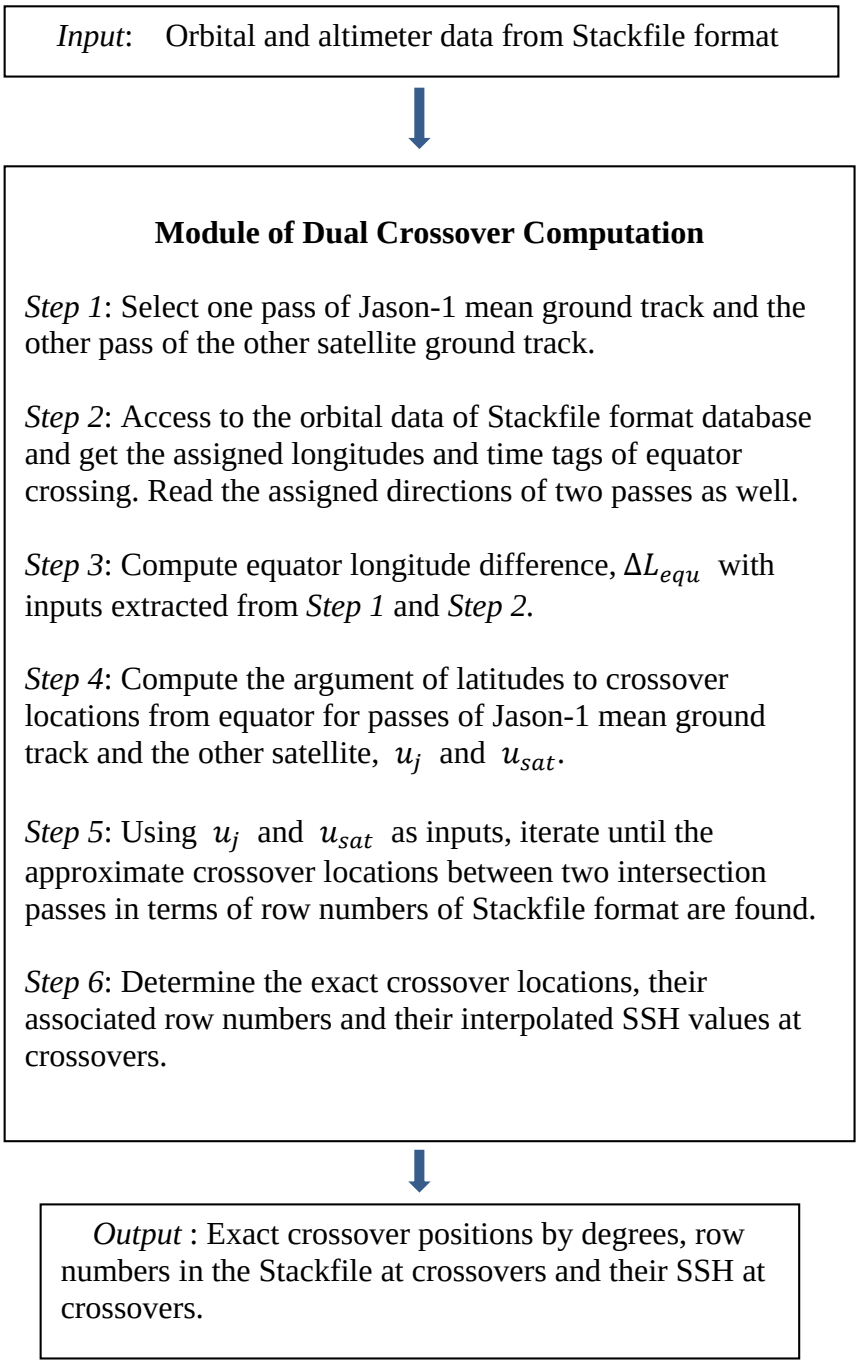

Figure 2.5: Process of dual crossovers computation with Jason-1 mean SSH values.

2-4-3. Analysis of Dual Crossover Computation

Through the process detailed in Figure 2.5, the crossover locations and two associated SSH values of the Jason-1 mean SSH and the SSH of the other satellite, which are necessary for the integrating process, were computed in ascending and descending passes separately. The original SSH data of the other satellite at the dual crossover location will be substituted with the corresponding Jason-1 mean SSH for the integrating process, as initial values and constraints.

For an analysis of the dual crossover determination process, two interpolated SSH data between Jason-1 and the other satellite at crossover locations are compared in terms of mean and standard deviations. First, the SSH differences at the dual crossovers for each satellite are computed by subtraction. These height differences are caused by the systematic biases between two satellites, and SSH measurement errors of the satellite, including ocean variability effects. Then, the statistics in terms of the mean and standard deviations of the SSH differences at dual crossover locations by cycles of the other satellite are calculated. The mathematical equations for this evaluation are in a straightforward way:

$$Mean\ of\ differences\ (cyc)\ = \frac{\sum_{i=1}^{N}(MSS_{jason} - SSH_{sat})_i}{N} \tag{2.5}$$

$$STD\ of\ differences\ (cyc) = \sqrt{\frac{\sum_{i=1}^{N}(SSH_{sat} - Mean)_i^2}{N-1}} \tag{2.6}$$

where,

i is a crossover location,

N is a total number of dual crossovers by cycle,

MSS_{jason} is the mean SSH value of Jason-1 at crossover location i,

SSH_{sat} is the SSH value of the other satellite at crossover location i,

Mean is a mean value of the differences by cycle.

This analysis gives us insight of how much (approximately) will be corrected in the SSH of the other satellite with respect to Jason-1 mean SSH data after the adjustment method. The SSH differences at dual crossovers represent the quantity of adjustments in the factors of systematic biases between two satellites and measurement errors of the other satellite. In other words, this test shows the approximate magnitude of the adjustments to the new SSH dataset over the cycles in order to improve the data characteristics of the satellite.

For a GM mission data such as ERS-1 phase E and F, there are a large number of crossover locations generated, 189447 and 210783, respectively. The height differences between Jason-1 and ERS-1 phase E at dual crossovers are computed and plotted in Figure 2.6. Table 2.4 represents that the mean and standard deviation (STD) of SSH differences between Jason-1 and ERS-1 GM data (phase E and F) at crossover locations.

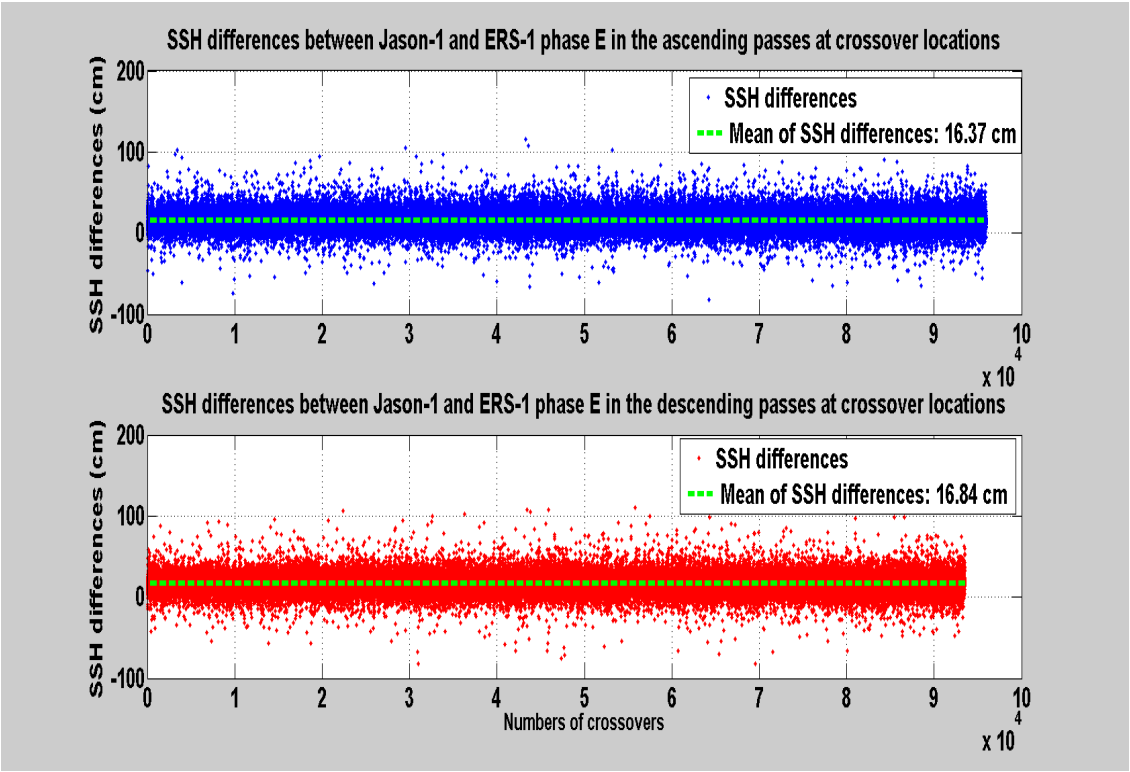

Figure 2.6: SSH differences between Jason-1 and ERS-1 phase E at the dual crossover locations: in the ascending passes (upper panel) and descending passes (lower panel).

	ERS-1 phase E		**ERS-1 phase F**	
	Ascending pass	Descending pass	Ascending pass	Descending pass
Numbers of generated crossovers	95949	93498	106651	104132
Mean of SSH differences (cm)	16.4	16.8	15.9	16.5
STD of SSH differences (cm)	10.7	10.6	10.7	10.7

Table 2.4: Statistics of dual crossover differences between Jason-1 and ERS-1 GM data.

For the Geosat ERM mission data, the SSH differences at crossovers are computed, same as for the GM data, and their mean and standard deviation (STD) of height differences over cycles are obtained. For the Geosat ERM, approximately 10000 dual crossovers are generated in each cycle, and the statistics are calculated by cycle from 1 to 62 in both ascending and descending passes separately, as shown in Figure 2.7. The upper two panels in Figure 2.7 represent the mean and standard deviation of SSH at dual crossovers computed between Jason-1 mean values and Geosat ERM data by cycles in ascending passes, and the lower two panels represent the same data in descending passes (Jason-1-Geosat ERM dual crossover differences). Blue dots show the mean, and red dots indicate the standard deviation of Jason-1-Geosat ERM dual crossover differences; units are in cm.

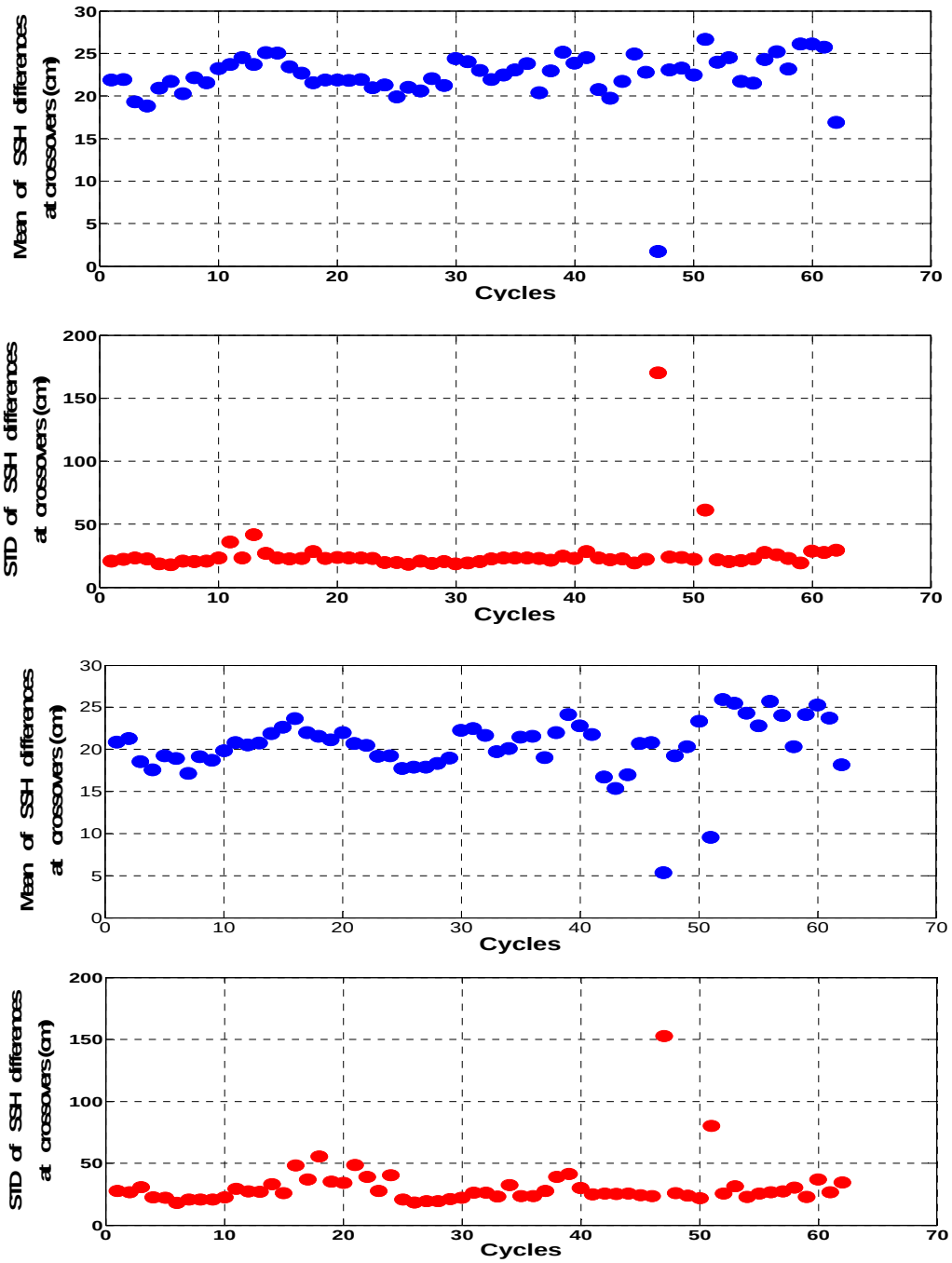

Figure 2.7: Mean and STD of Jason-1-Geosat ERM crossover differences in ascending passes (upper 2 panels) and descending passes (lower 2 panels) by Geosat cycles.

Figure 2.7 shows that results are relatively irregular and variable over cycles. The mean of the SSH differences range from approximately 17 cm to 27 cm for ascending passes, and from 10 cm to 26 cm for the descending passes, except cycle 47. The standard deviations of SSH differences are variable from 20 cm to 40 cm by cycles in ascending passes, and from 20 cm to 60 cm in the descending passes, except cycle 47 (over 150 cm) and cycle 52. The statistics of cycle 47 show relatively higher standard deviation of SSH difference than those of other cycles, because it was influenced by altimeter data of certain tracks in cycle 47, which are noisier SSH data relative to the neighboring sea surface height data. Such highly inaccurate data, especially from old missions, are expected to be corrected through an adjustment process by integrating the bin-by-bin technique later, and could be a major improvement.

The statistics of Jason-1-ERS-2 dual crossover differences computed from cycle 1 to 67 of ERS-2 are shown in Figure 2.8. Approximately, a total number of 25000 dual crossovers by cycle in each ascending or descending pass are generated, and the mean and standard deviations using those crossovers are computed by cycle. The results for mean of SSH differences (blue dots) indicate that they vary from 2 cm to 10 cm, excluding a few points, and the figure for standard deviation (red dots) shows that results vary from 10 cm to 15 cm. Since the altimetric noise of the ERS-2 data is much smaller than Geosat ERM, the results of the statistics show less variation and a more regular pattern than the results from Jason-1-Geosat ERM crossover differences in Figure 2.7.

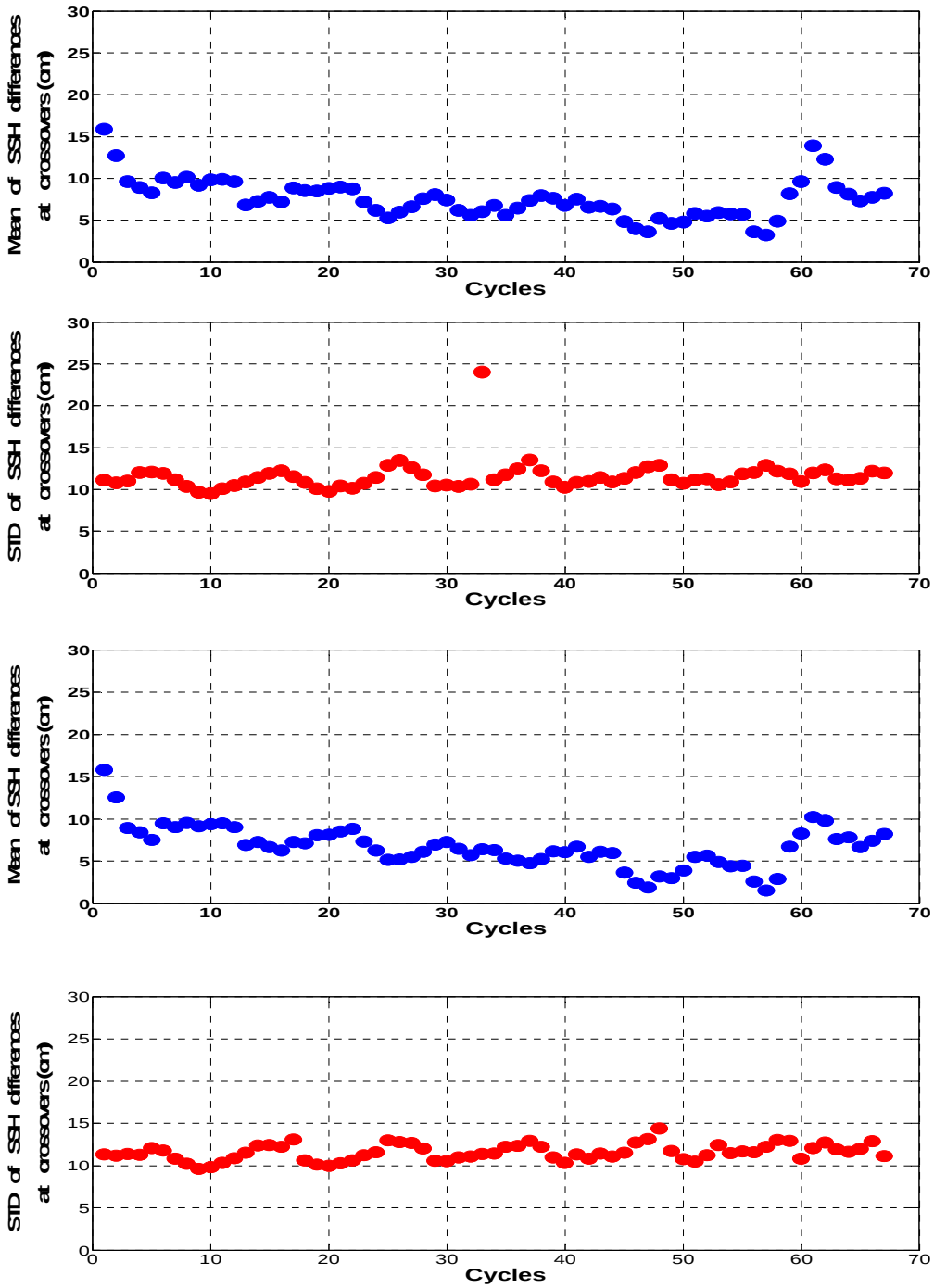

Figure 2.8: Mean and STD of Jason-1-ERS-2 crossover differences in ascending passes (upper 2 panels) and descending passes (lower 2 panels) by ERS-2 cycles.

The regular pattern shown in Figure 2.8 resembles a sinusoid, and is periodic approximately every 10 cycles. Since ERS-2 satellite has 35-day repeated cycles, and the patterns in the figure appear every 10 cycles, the period of the sinusoid signals is about 1 year. Therefore, the sinusoid pattern in the figure infers the signals of annual ocean variability in ERS-2 SSH data. The results of statistics for Jason-1-ERS-2 dual crossover differences demonstrated the possible degrees for improvement of ERS-2 original SSH data and for homogeneity with Jason-1 after adjustment technique. That is, the amounts for change to the adjusted ERS-2 SSH data will be much lower than those of Geosat ERM, because the original ERS-2 data are much more accurate than those of Geosat ERM.

The statistics for Jason-1-T/P at dual crossovers differences are computed and plotted from T/P cycle 10 to 364 in Figure 2.9. The figure shows that the mean varies from 14 cm to 18 cm, and the standard variations from 9 cm to 12 cm by cycles. It represents less variability, in terms of the mean and standard deviations by longest cycles, than those of other satellites from the Stackfile database due to the accuracy of T/P SSH data. In addition, more regular and consistent curves by cycles are observed in the figure. The fact that these sinusoidal signals repeat approximately every 36 cycles, and the repeat cycle of T/P is every 10 days, infers that the regular patterns are due to annual ocean variability. Their differences will be adjusted to the original T/P SSH data through an integrating process in order to obtain the new T/P SSH dataset. Figure 2.9, which represents the statistic results for Jason-1-T/P crossover differences, is following.

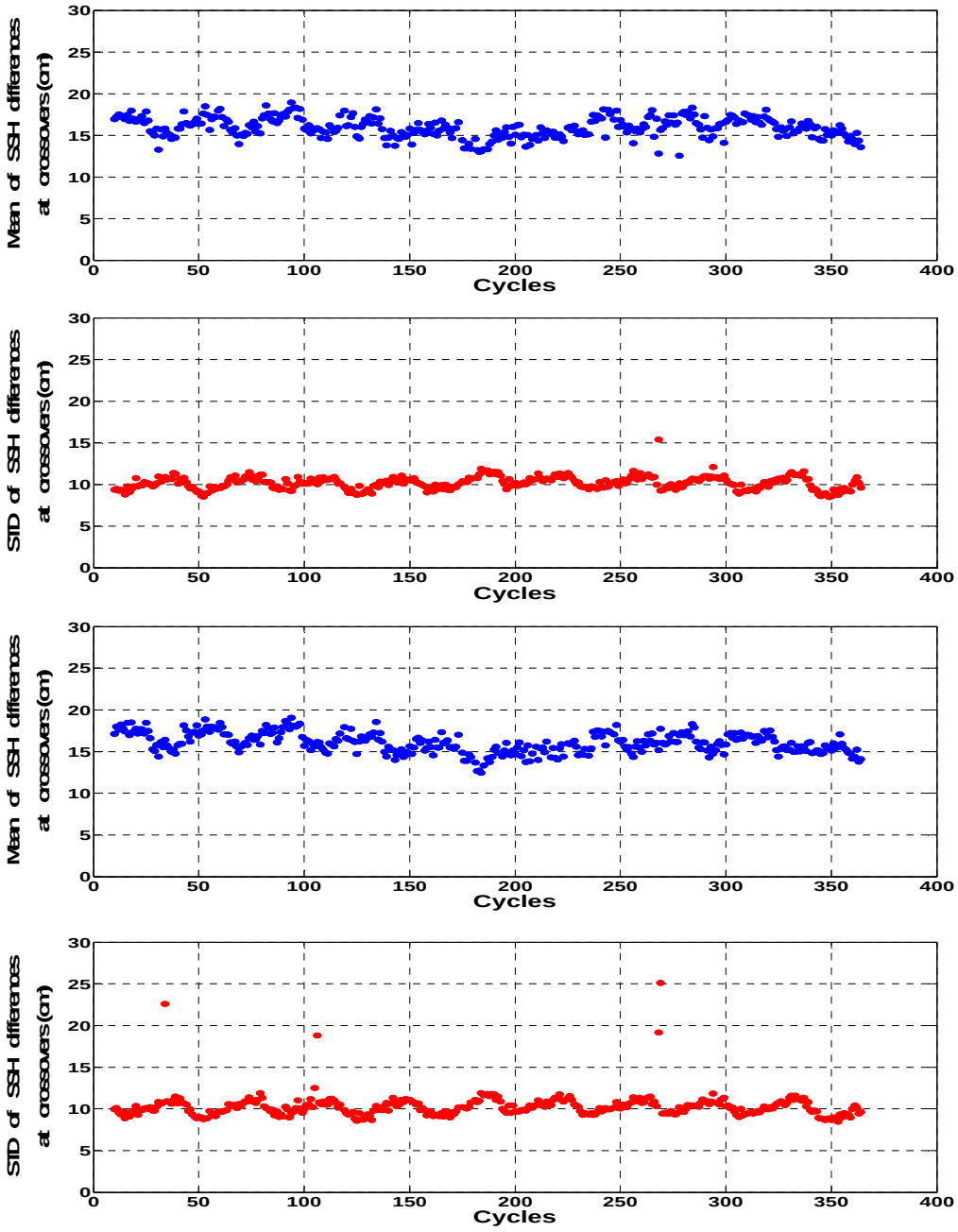

Figure 2.9: Mean and STD of Jason-1-T/P crossover differences in ascending passes (upper 2 panels) and descending passes (lower 2 panels) by T/P cycles.

The statistics of Jason-1-Envisat dual crossover differences by Envisat cycles are shown in Figure 2.10. The total number of dual crossovers between these two satellites is approximately 20000 by cycle, and the mean and standard deviation of the differences are computed from Envisat cycles 9 to 94. The figure shows that the variations of the mean and standard deviation of SSH differences at crossovers by cycle are very small and regular, except for those of cycle 51. The mean differences are variable from 10 cm to 14 cm, and the standard deviations vary from 8 cm to 12 cm, excluding those of cycle 51. In addition, a sine wave appears, as in the previously shown results of ERS-2 and T/P, indicating the annual ocean variability.

In cycle 51, the standard deviation at crossovers is over 2 m, so it is undeniably out of the boundary of data reliability. Thus, the Envisat SSH of every track in cycle 51 is examined through the crossover method, and it was found that outliers are due to the SSH measurements in track number 187 of Envisat. The associated SSH data at crossovers with Jason-1 and track number 187 of cycle 51 in Envisat are computed and plotted in the upper panel of Figure 2.11. For comparison as a reference, the dual crossovers between Jason-1 and the same track number of cycle 52 in Envisat are computed and plotted in the lower panel of Figure 2.11. The horizontal axis (x axis) indicates dual crossovers between the SSH data of track number 187 of Envisat and Jason-1 SSH data. The vertical axis (y axis) represents the sea surface height values. The unit is in meters (m). The red circle represents the Jason-1 SSH value, while the blue star represents the SSH of track number 187 of Envisat at dual crossovers.

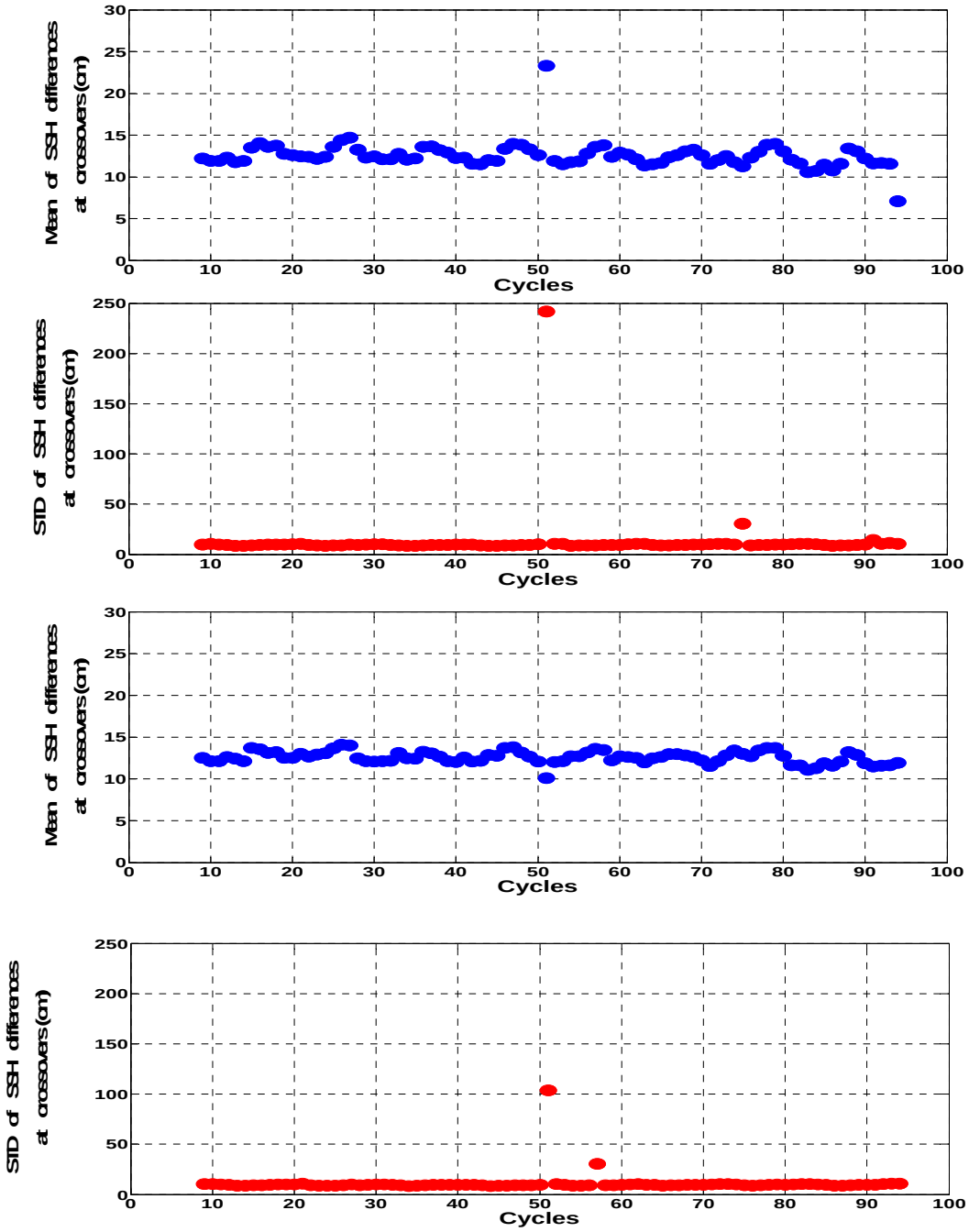

Figure 2.10: Mean and STD of Jason-1-Envisat crossover differences in ascending passes (upper 2 panels) and descending passes (lower 2 panels) by Envisat cycles.

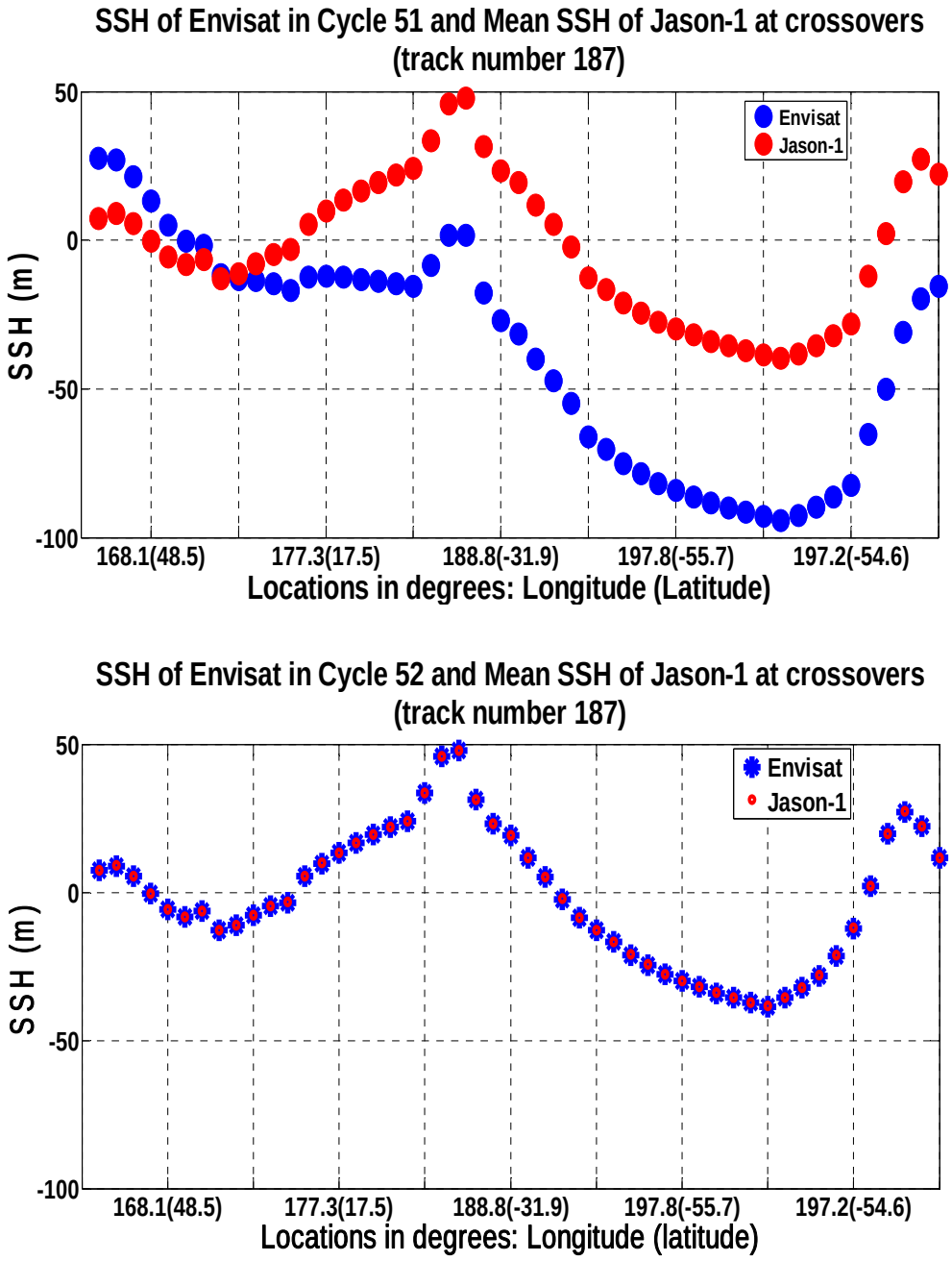

Figure 2.11: Jason-1-Envisat dual crossover differences for track 187 of cycle 51 (upper panel) and cycle 52 (lower panel).

By comparing the upper and lower panels by Figure 2.11, the Envisat SSH measurements of track 187 in cycle 51 are much lower than those of cycle 52 at the same dual crossover locations. The upper panel shows that the differences with Jason-1 are over 50 m, while, the lower panel, though almost identical in terms of meter level for cycle 52, displays expected results. Such high SSH differences at dual crossovers, shown in the upper panel, seem to be obviously abnormal. It is inferred that they might be measured or processed inaccurately for some reason. Therefore, this provided the unusually high standard deviations in cycle 51 shown in Figure 2.10. Since such inaccurate SSH affect all the points in the same track in the integrating process, Envisat data of track 187 in cycle 51 was excluded for the rest of process in this research.

2-4-4. Summary

The method and computational algorithm of dual crossover computation, for the initial values and constraints necessary for the integrating process are described in this section. In addition, the results from dual crossover determinations are analyzed by statistics in terms of mean and standard deviation of SSH differences by cycles. Statistics from Jason-1-each satellite dual crossover differences display the approximate amount of adjustments to be performed from the original SSH datasets to the new SSH datasets.

In particular, the statistics by cycles for satellites, except the old mission Geosat ERS, reveal the regular sinusoidal waves, which are due to signals of annual ocean variability of each satellite. The variability of ocean will be still preserved in the new SSH data processed through the integrating method, but reduced later while computing mean

profiles. By product, abnormally inaccurate Envisat SSH data of track 187 in cycle 51 are found from this analysis, and will be eliminated for the rest of processes for this research.

2-5. INTEGRATING PROCESS FOR NEW SSH DATASETS OF EACH SATELLITE

After the first and second steps, we obtain datasets of the along-track SSH gradients, crossover locations, and the interpolated mean SSH value of Jason-1 at the crossovers by each cycle in the satellites Geosat ERS, ERS-2, Envisat, and T/P, including ERS-1 geodetic mission data. As the final step, with the datasets described above, the new SSH datasets are obtained by integrating bin-by-bin using along-track SSH gradients from crossover locations. Through this computation, the new SSH datasets of each satellite, in ascending and descending passes separately, are obtained, and they are expected to be improved and close to the level of Jason-1 quality and, ultimately, become homogenous with each other enough to combine for new mean sea surface.

The key idea of this step is to integrate the along-track SSH gradient bin-by-bin with an initial value. An initial value is the MSS value of Jason-1 at dual crossover locations, which is computed through Figure 2.5. In general, multiple crossovers meet in one pass of the satellite track, so multiple new SSH data at a point can be computed by integrating from multiple crossover locations. A more optimal method to determine a single final result from several outputs could be used; but in this research, the new final SSH data is determined after selecting ‘two’ new SSH data computed from the nearest two dual crossovers: one is the nearest crossover point ahead (in backward direction), and the other is the nearest crossover point behind (in forward direction). There are some cases in which

the new SSH data is computed from crossovers in only one direction: either the forward direction or the backward direction. In this case, the new SSH data is computed considering only one nearest crossover.

Here are the mathematical expressions for integrating by the bin-by-bin method. If *F* is the nearest 'behind' crossover point for bin *i*, and the position of crossover *F* is the same as bin *x* of the pass, then the new SSH value of bin *i* in forward direction, $New\_SSH_i^F$, can be computed bin-by-bin starting from the Jason-1 MSS value of a dual crossover *F* (MSS_F^{Jason}):

$$New\_SSH_i^F = MSS_F^{Jason} + \sum_{k=x}^{i-1} G_k^{sf} \times d \tag{2.7}$$

where,

G_k^{sf} is the SSH gradients of *k th* row,

d is the distance between two consecutive bins.

Now, if *B* is the nearest 'ahead' crossover point for bin *i*, and the position of dual crossover is the same as bin *y* of the pass, then the new SSH value of bin *i* in backward direction, $New\_SSH_i^B$, can be computed bin-by-bin starting from the Jason-1 mean value of a crossover *B* (MSS_B^{Jason}):

$$New\_SSH_i^B = MSS_B^{Jason} - \sum_{k=i}^{y-1} G_k^{sf} \times d \tag{2.8}$$

In general, the crossover point does not meet exactly in a bin location, so the SSH gradient between an exact crossover location and a neighboring bin location, is included in the integrating process. From the process, one or two SSH datasets in a bin are generated through integrating bin-by-bin. If there is one bin that does not have an along-track gradient between the nearest crossover point and the target bin for computation, the integration process would be stopped because of the discontinuity of bin-by-bin flows. In this case, the flow of integration continues by integrating along-track gradients of two distant bins. However, if there are more than two consecutive bins that do not have SSH gradients data, the integrating would be stopped, so the new SSH in a target bin at this time is not obtained.

After combining the two new SSH datasets that are computed from two nearest crossovers (both in forward and backward directions or one direction), the new SSH (New_SSH_i) is determined considering the distance as weighting factors.

$$New\_SSH_i = \frac{w_1 \times New\_SSH_i^F + w_2 \times New\_SSH_i^B}{w_1 + w_2} \tag{2.9}$$

Since dual crossovers computed between Jason-1 and the other satellite are limited to ±66º latitudes, the final new SSH data are obtained within ±60º latitudes by cycles in each satellite for accuracy. Finally, through this step, the new SSH datasets of Geosat ERM, ERS-2, T/P, Envisat and ERS-1 geodetic data are obtained for each cycle.

As mentioned earlier, these new SSH datasets are expected that their accuracies and their homogeneity with the most accurate reference surface, Jason-1 mean SSH, are

improved. To evaluate the degree of improvement, the new SSH datasets of each satellite are analyzed in terms of mean profiles, which are obtained by averaging SSH data. The analysis will be described in the next chapter.

2-6. SUMMARY OF ADJUSTMENT METHOD

The new SSH dataset for each satellite is obtained, in order to enhance the SSH data quality from the original dataset, which contain different accuracies and initial systematic biases due to applied different models and algorithms. This adjustment was derived based on the integrating method, which is composed of three steps performed using the advantage of the bin-by-bin Stackfile format. First, the along-track SSH gradients of each satellite by available cycles are computed. Second, the interpolated Jason-1 mean SSH data at dual crossover locations are determined through dual crossover technique. This computation is also carried out by cycles of each satellite. Third, using two kinds of results obtained through first and second processes, the new SSH data are obtained by integrating the along-track SSH gradients with the Jason-1 mean values at dual crossovers as an initial values or constraints. Therefore, the improved SSH datasets by all available cycles in each satellite are obtained through the integrating method.

The computational algorithm for the three steps for adjustment are summarized in Figure 2.12. Through the integrating process, it is expected that some of the long wavelength and bias errors, residual errors due to correctional models, and systematic biases between Jason-1 mean SSH and each satellite will be reduced. Furthermore, it is

expected that their accuracies are improved, and they are made quite homogenous to each other, including Jason-1, which is considered as an accurate reference surface.

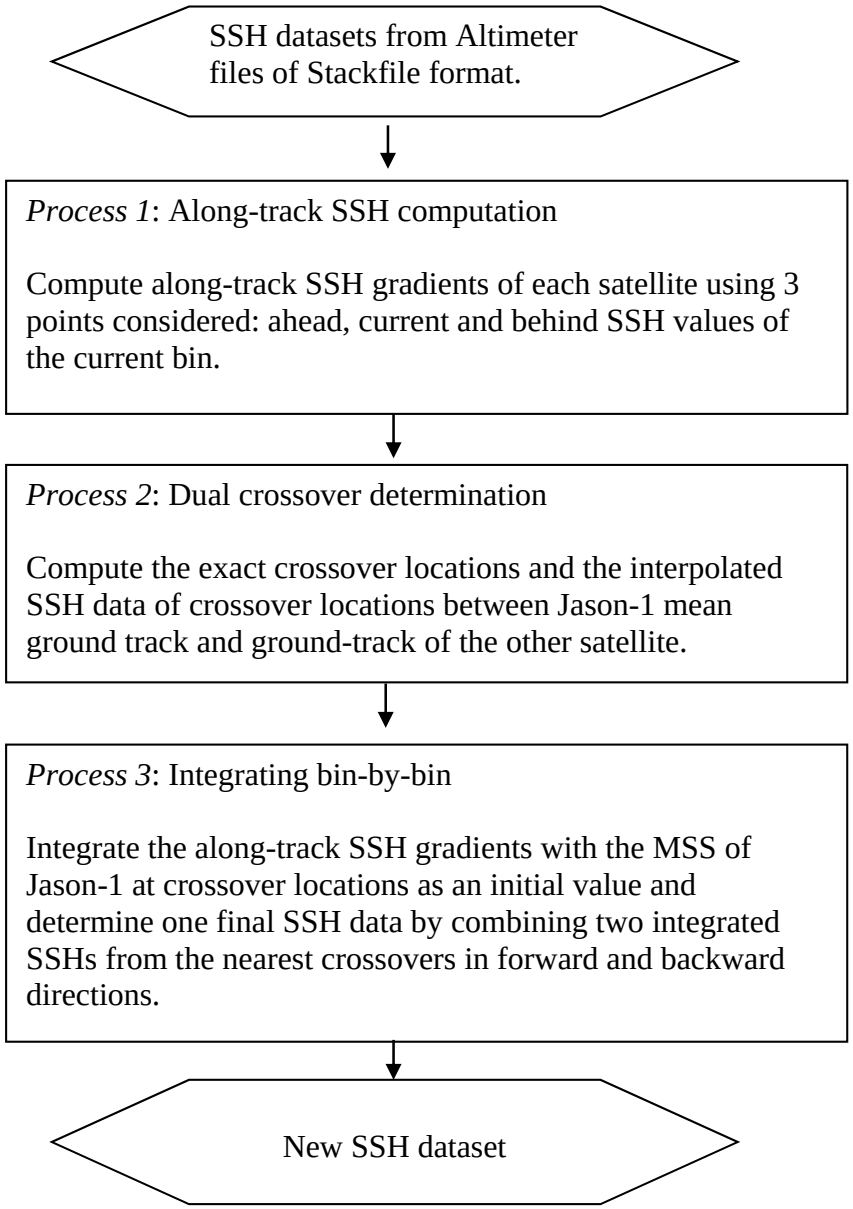

Figure 2.12: Adjustment procedure based on integrating method for improved SSH dataset.

Chapter 3: Computation of Accurate Mean SSH Profiles

3-1. INTRODUCTION

Through the three steps of the adjustment procedure described in the previous chapter, sea surface height datasets are computed by integrating along-track SSH gradients referenced to the mean SSH value of Jason-1 satellite. Then, they are improved and made more homogeneous with respect to the Jason-1 SSH data. These new SSH datasets are used for deriving a new accurate mean sea surface in this research by gridding them as inputs. In this case, the mean SSH profiles of each satellite, which are obtained by computing an averaged SSH data along the ground track of a satellite, are actually being utilized. Since some outliers of these adjusted SSH datasets remain, simply averaging the new SSH datasets by applied cycles is not enough to obtain the adequately accurate mean profiles. Therefore, more editing is required to remove these outliers prior to averaging.

In this chapter, the computation and evaluation of the accurate mean profile, with upgraded SSH of each satellite, are described. Section 3-2 will present how to compute the accurate mean SSH profile. As mentioned in the previous chapter, the new SSH datasets of each satellite contain the signals of annual and semi-annual ocean variability, which will introduce biases in the mean sea surface. Therefore, they are estimated and reduced before they are averaged into the mean SSH profiles of each satellite. In addition, more computations performed to increase the accuracy of the mean SSH profiles for the ERM and GM data are described, and the complete processing steps are summarized.

In Section 3-3, the Jason-1 mean SSH profile, which is chosen as a reference surface in this research, is evaluated by comparing it with two recent and accurate mean sea surfaces, DNSC08 and DTU10. Those two MSS are major references for comparisons of the results during this research. DTU10 is an upgraded version of DNSC08 MSS, using almost the same data and the same processing and gridding method, except the time span of data used as a reference field and the number of corrections used for the old data. Due to such differences, the initial systematic biases between them exist, which should be taken into account in analyzing the results in this research. In sub-sections, these systematic differences (or biases) between DNSC08 and DTU10 are discussed; then, the comparison of them with Jason-1 mean profile are described.

The mean profiles of the adjusted SSH datasets in each satellite are assessed in Section 3-4. Both the mean profiles of the original and new SSH datasets are compared with two reference surfaces, DNSC08 and DTU10 mean sea surfaces. The statistics of the differences are computed, and compared and figures are illustrated geographically by GMT (Genetic Mapping Tools).

3-2. COMPUTING MEAN PROFILES OF EACH SATELLITE

For this research, the mean profile of each satellite is computed by averaging new SSH datasets, whose qualities are enhanced closer to the level of Jason-1 data through the adjustment method. Note that some outliers still remain, although new SSH datasets are improved and more homogeneous, so several more processes to remove those outliers are performed. The new SSH datasets contain annual and semi-annual signals of ocean

variability, revealed in the test of the dual crossover computation described in sub-section 2-4-3. In addition, certain errors caused by the integrating process, outliers due to the less accurate SSH data in each satellite remain in the new SSH. Therefore, the processes to reduce such remaining outliers are carried out prior to the mean SSH profiles computation.

First, annual and semi-annual signals in the new SSH data are estimated and removed. Trend, annual and semi-annual signals in the SSH data are estimated by the following model:

$$SSH_k \approx Mean + trend \cdot \Delta t_k + Acos(w_1 \Delta t_k) + Bsin(w_1 \Delta t_k) + Ccos(w_2 \Delta t_k) + Dsin(w_2 \Delta t_k) \quad (3.1)$$

where,

Mean is an initial mean value of SSH in each bin,

trend is a secular trend,

Δt_k is time of observation – epoch (in days),

w_1 and w_2 are the annual and semi-annual frequencies,

A,B,C,D are the harmonic constants for the signals.

The coefficients of the model are estimated by minimizing the square of the residual signals using linear least squares. Then, the signals are removed from the new SSH data.

Second, the 3-sigma editing process is applied to each bin in order to exclude especially erroneous data or outliers. The average and standard deviations are computed

from the new SSH of all available cycles bin-by-bin. Then, the SSH data outside of three sigma of standard deviation are removed.

Third, the new SSH datasets are re-compared with the grid file of Jason-1 mean SSH, and data with high differences (more than 30 cm or less than -30 cm) are removed. Then, to fill the new SSH data in those edited bins, the new SSH are re-integrated from a new constraint from the grid of Jason-1 mean SSH values, using their original SSH gradients. This process helps to remove most of the outliers that occurred from integrating through a long distance, which causes an accumulation of integration errors.

Finally, the mean SSH profiles are computed by averaging the new SSH data by all applied cycles in each bin. These are considered as more accurate profiles than those that result by simply averaging due to these editing processes. Through the processes, 2-year Geosat ERM mean profiles, 6-year ERS-2 mean profiles, 8-year Envisat mean profiles, and 10-year T/P mean profiles of adjusted SSH data are obtained. Figure 3.1 shows the summary of steps to compute the accurate mean profiles of ERM satellite SSH data.

Input: New SSH data adjusted through integrating process.

Step 1: Estimate and remove annual, semi-annual and secular terms in new SSH.

Step 2: Perform 3-sigma editing.

Step 3: Compare with the grid file of Jason-1 mean SSH, remove data with high differences, and update by re-integrating.

Step 4: Average bin-by-bin.

Output: Accurate mean profiles of each satellite

Figure 3.1: Summary of editing and processing for accurate mean profiles.

The GM data of ERS-1 phase E and F (4/1994~3/1995) are not exactly repeated mission data, so an instantaneous SSH profile is generated instead of a mean SSH profile. The geodetic mission data have short wavelength spatial resolutions, and are very essential for high resolution MSS determination. The original GM data were processed to be adjusted relative to Jason-1 mean profile, through the integrating procedure. The adjusted GM data will help cover the vicinity of enclosed small seas, isolated seas and coastal areas, and empty spaces between the ERM data. As in ERM satellites, outliers will remain, but there will be even more remaining outliers for GM due to less accurate and noisier data in the original GM data.

For editing, the new instantaneous SSH data of ERS-1 phase E and F are compared with the grid file of Jason-1 mean profile, then the high differences, which ranges more than 30 cm or less than -30 cm are eliminated, the same as the editing of ERM satellite data. However, the new GM data for bins which are edited out, are re-integrated using the DTU10 MSS gradients. The use of existing MSS gradients, instead of using its original SSH gradients, is because more precise data are needed for the areas of the short wavelength features. Figure 3.2 shows the distributions of GM data between the mean profiles of ERM data. It clearly shows the GM data filling in the gaps between the ERM ground tracks.

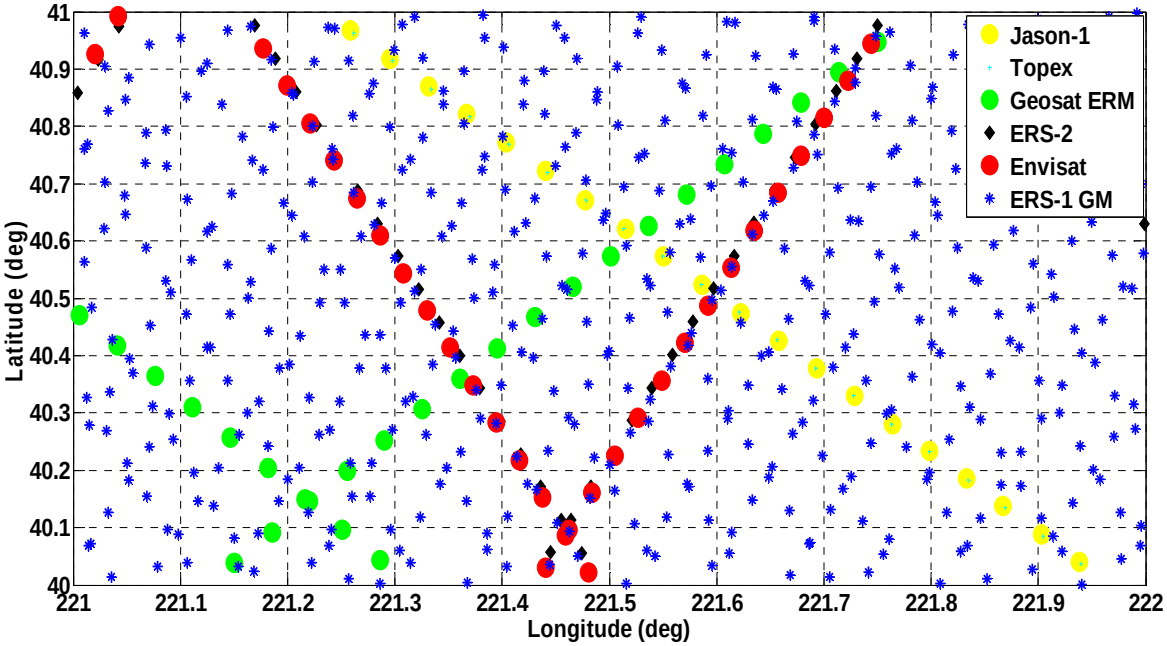

Figure 3.2: Distributions of 6 different satellites data in 1º×1º cell. Blue stars represent SSH data of ERS-1 GM satellite, while the other symbols show ERM data.

Finally, the mean SSH profiles and the instantaneous SSH profiles of the new SSH datasets are obtained after additional computations to improve their quality, and they are now ready to be gridded together for a new mean sea surface.

3-3. VALIDATION OF JASON-1 MEAN SSH PROFILES

Jason-1 mean SSH profiles are used as reference fields for adjusting other satellite data, and as the primary surface for gridding into the new MSS. Thus, they significantly affect the accuracy of the new MSS determination more than any other satellite data. In this section, Jason-1 mean SSH profile, which is computed by averaging data of from January 2002 to December 2008, is analyzed by comparing it with two recent reference fields, DNSC08 and DTU10.

DNSC08 and DTU10 are derived from the same research center (DTU Space), and the same scientific methods and computations for MSS determination. However, DTU10 used slightly more improved datasets with better range and geophysical corrections and a longer period of data by 5 years than that of DNSC08. Due to inconsistencies of applied corrections and time span of the dataset used as a reference field, the systematic differences between two MSS exist. In sub-section 3-3-1, such systematic biases between the two MSS, DTU10 and DNSC08, are explained in detail. Sub-section 3-3-2 represents an assessment by comparing Jason-1 mean SSH profile with the two MSS. For an evaluation, the statistics in terms of mean and standard deviation of height differences between Jason-1 mean SSH profile and two MSS are computed within ±60º latitudes.

3-3-1. Systematic differences between DNSC08 and DTU10

In general, the systematic differences or biases between two MSS occur due to different applied range and geophysical corrections, different orbits and different time averaging periods, etc. Both of DNSC08 and DTU10 MSS used T/P and Jason-1 combined mean profile as a reference surface. The primary difference between them is the time span of the referencing surface, for which that of DTU10 is longer by 5 years of Jason-1 data. Table 3.1 represents information about the reference surfaces, their referencing time spans, and database sourface for both MSS models [Anderson, 2010]. For comparison with our reference surface, facts regarding the Jason-1 mean profile used in CSRMSS14 are included in Table 3.1 as well.

	DNSC08	**DTU10**	**CSRMSS14**
Reference surface	T/P+Jason-1 mean profile	T/P+Jason-1 mean profile	Jason-1 mean profile
Period of reference surface	1993-2004	1993-2009	2002-2008
Database source	NASA Pathfinder V13.1	NASA Pathfinder V13.1	CSR Stackfile

Table 3.1: Information of reference surfaces of DNSC08, DTU10 and CSRMSS14.

DNSC08 and DTU10 are released with 1-minute resolution, and they are extracted into 5-minute resolution (consistent with CSRMSS14) and compared within ±60º latitudes for this research. For the test, the differences between DNSC08 and DTU10 are computed by subtracting directly. The mean of height differences between them is 5.7 cm, and the

standard deviation of height differences is 3.5 cm. Their differences will affect the evaluations of our new MSS, CSRMSS14, in comparing with these two MSS models later. The MSS differences between DNSC08 and DTU10 are illustrated geographically in Figure 3.3. The comparison shows both positive and negative differences, most likely caused by the inter-annual variabilities of the ocean between the time span of the Jason-1 mean profiles used for the MSS determination: 1993-2004 vs. 1993-2009 [Andersen, 2010].

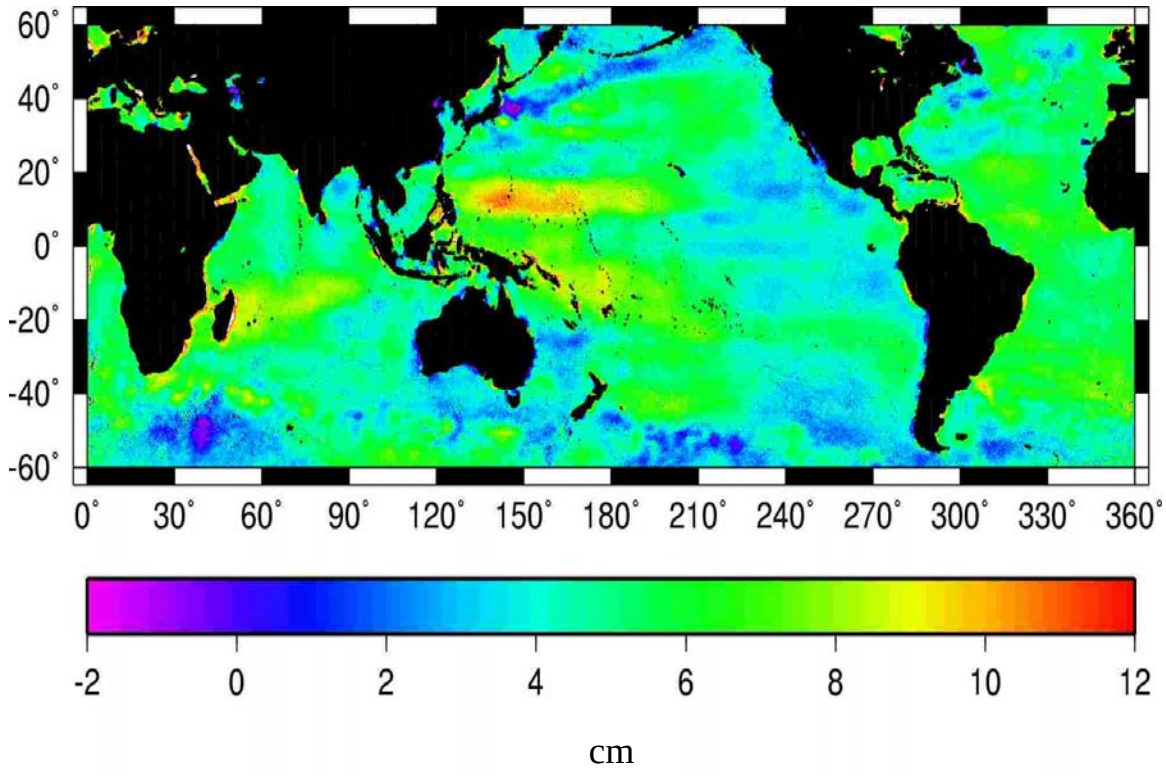

Figure 3.3: Map of the MSS height differences between DNSC08 and DTU10. The color scale range is in cm, and the latitudes are restricted to ±60º.

3-3-2. Comparision of Jason-1 Mean SSH profiles with DNSC08 and DTU10

In this sub-section, the 7-year Jason-1 mean SSH profiles are compared with two accurate MSS, DNSC08 and DTU10, respectively. Height differences between the Jason-1 mean SSH profile and the interpolated MSS along the Jason-1 mean SSH profile are computed within ±60 degrees latitudes, then the mean and standard deviation of height differences are calculated. Assuming that 7-year Jason-1 mean profiles are the most precise profile available, the mean of height differences show us the systematic biases between the 7-year Jason-1 mean profile and the two MSS. Moreover, the standard deviation represents the accuracy of the 7-year Jason-1 mean profile with respect to the two MSS.

The mean of the Jason-1 mean SSH profile with respect to DNSC08 is 17.2 cm and the standard deviation is 2.7 cm. The comparison with DTU10 shows that the mean of differences is 12.2 cm and the standard deviation of differences is 2.5 cm. The results from standard deviation of height differences (2.7 cm and 2.5 cm, respectively) shows that the 7-year Jason-1 mean profile is very close to the two reference surfaces, and is slightly smoother and closer to DTU10 than DNSC08. Assuming that the Jason-1 mean profile and the two MSS are comparable in accuracy, the statistics of mean indicate that our Jason-1 mean SSH profile has systematic biases between DNSC08 and DTU10, and that the biases could be approximately 17.2 cm and 12.2 cm, respectively.

To see the relative height differences geographically, the differences between the 7-year Jason-1 mean SSH profiles and DNSC08 are plotted in Figure 3.4 within ±60 degrees latitudes after subtracting the mean of the height differences (17.2 cm). The figure

shows that large positive/negative differences appear, and that they are associated with strong ocean variability areas, such as in the Tropics currents and parts of other major currents.

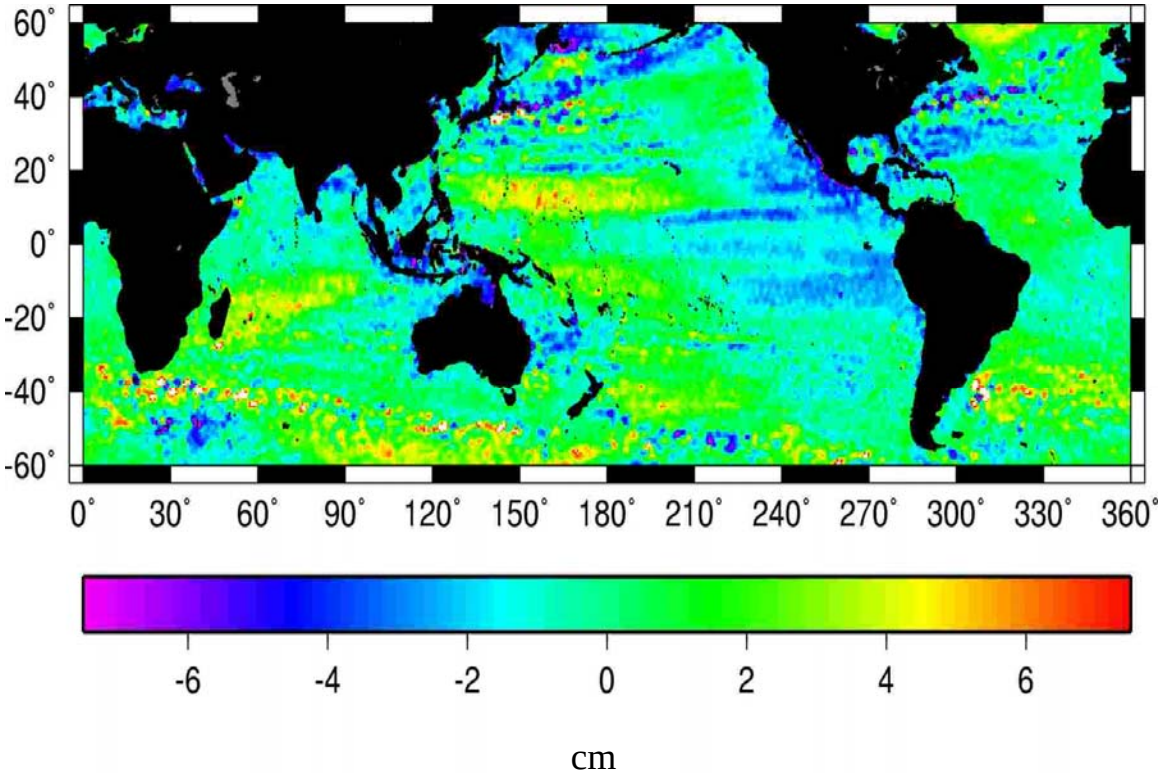

Figure 3.4: Height variations between Jason-1 mean profiles and DNSC08, after subtracting their systematic bias (17.2 cm).

For results of comparison with DTU10, 12.2 cm, which is the systematic bias between the 7-year Jason-1 mean profile and DTU10, is subtracted and plotted in Figure 3.5.

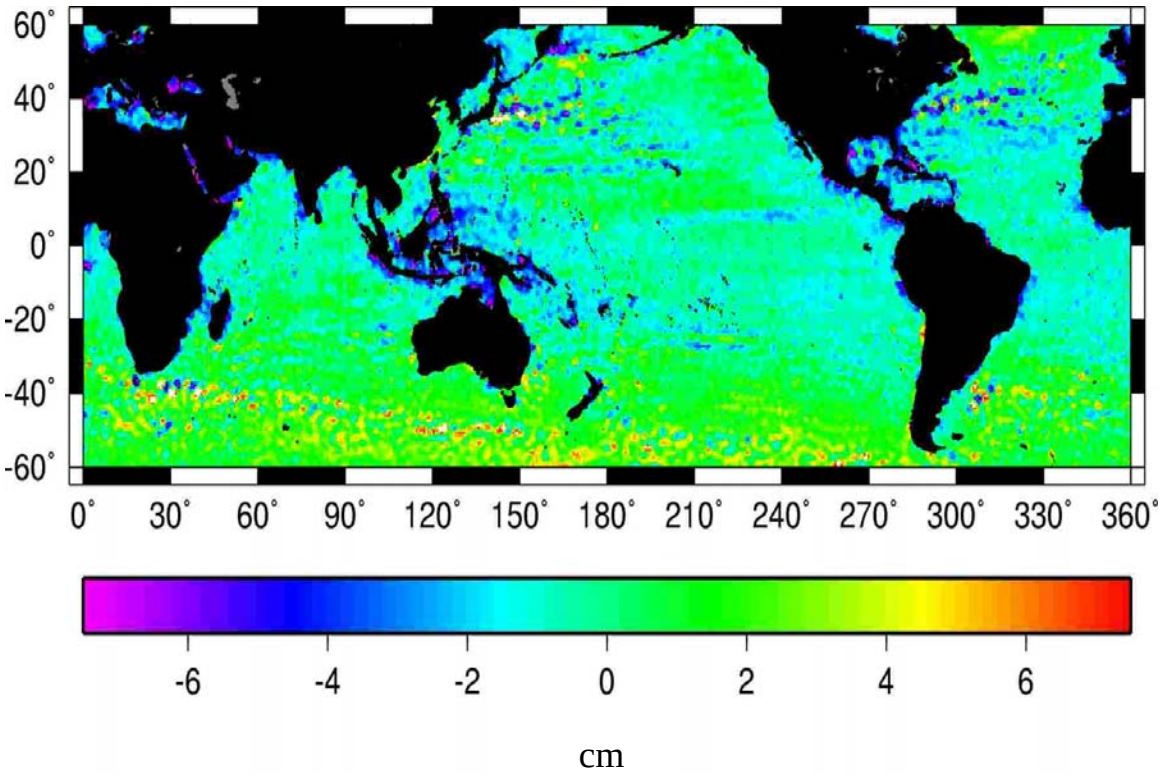

Figure 3.5: Height variations between Jason-1 mean profiles and DTU10, after subtracting their systematic bias (12.2 cm).

The figure shows significant reductions in areas of large differences present in Figure 3.4, especially the eastern Pacific Oceans of South Asia (open oceans area). The main differences between the two figures are due to the change of ocean variability between the time period of the reference surfaces of DNSC08 and DTU10. The time span of the 7-year Jason-1 mean profile (ending in 2008) is closer to that of DTU10 (ending in 2009) than that of DNSC08 (ending in 2004), so the differences shown in Figure 3.5 are lesser and smoother. The statistics of height differences obtained between the 7-year Jason-1

mean profile and the two MSS are used as reference data to investigate the accuracy of mean profiles of the other satellites, and new MSS, CSRMSS14, later.

3-4. VALIDATION OF THE MEAN SSH PROFILES OF OTHER SATELLITE MISSIONS

As described earlier, with SSH data adjusted into the Jason-1 mean SSH by the integrating method, a mean SSH profile for each satellite is computed by averaging after several editing iterations. In order to evaluate its accuracy, it is compared with the reference surfaces, DNSC08 and DTU10. The height differences between a mean SSH profile of each satellite and DNSC08 or DTU10 are computed, and the mean and standard deviation of the differences are obtained. Statistics of the mean of differences indicate the average of height differences, and the standard deviations represent the accuracy of the mean SSH profile with respect to the MSS. In addition, by comparing the results of Jason-1 mean SSH profile as described in Section 3-3, the statistics also indicate their homogeneity with respect to the Jason-1 SSH data, which was used for the data adjustment.

In sub-section 3-4-1, the results of the comparison with DNSC08 are described, and the evaluation by comparing with DTU10 are shown in the next sub-section, 3-4-2. The maps of comparisons for each satellite are plotted. The latitudes for the computation are limited between -60º and +60º.

3-4-1. Comparison with DNSC08 MSS

The original mean profiles derived by averaging the original SSH data and updated mean profiles, which are computed from the adjusted SSH datasets, are compared with

DNSC08. This analysis indicates the degree of change in the new mean SSH profiles from the mean profiles of the original dataset with respect to the MSS through the integrating method. Moreover, it also demonstrates their consistency and homogeneity with each other with respect to Jason-1 data.

First, the mean profile of the original dataset is obtained by averaging the SSH data in the database, without any editing process (from step 1 through step 3) in Figure 3.1. Then, the height differences between the mean profiles of original dataset and DNSC08 were computed by interpolating the DNSC08 at the mean profile positions. The mean and RMS of height differences were calculated, and the results are shown in Table 3.2; units are in cm. The statistics are computed by dividing in case of all different points, and points whose differences are within ±30 cm. The averaging takes away some of the ocean variability, but the large ocean variability signals remain. Thus, the statistics indicate that the mean profiles of the original SSH data for each satellite contain high variability signals relative to the global homogeneous surface, DNSC08.

Satellite	**All differences**		**-30 cm < Difference < +30 cm**	
	Number of points	Mean (RMS) (unit: cm)	Number of points	Mean (RMS) (unit: cm)
Geosat ERM	788432	-12.0 (35.2)	765072	-11.0 (15.0)
ERS-2	1515501	10.8 (19.8)	1508494	10.8 (11.3)
Envisat	1300070	5.4 (6.4)	1299128	5.4 (6.1)
T/P	453479	2.0 (3.2)	452492	1.8 (2.9)
ERS-1 Phase E	6351314	0.9 (10.7)	6247896	1.0 (9.3)
ERS-1 Phase F	6325180	1.6 (11.1)	6214320	1.5 (9.7)

Table 3.2: Statistics of the mean or SSH profiles of the original SSH datasets from Stackfile and RADS with respect to DNSC08, in terms of Mean and Root Mean Square (RMS).

The statistics of the height differences between the mean profiles of new SSH data sets and DNSC08 are represented in Table 3.3. With the same method, the mean and standard deviation of height differences were computed, excluding those with over 30 cm of height difference. For the GM data, ERS-1 phase E and F, the instantaneous SSH profiles which were obtained with the new SSH data sets and edited more rigorously, are compared with DNSC08 as well. By the statistics of Table 3.3, the mean of height differences of both ERM and GM satellites became much closer to the value of 17.2 cm, which is the systematic bias between the Jason-1 mean profile and DNSC08. The standard deviations of the height differences for the ERM data vary from a minimum of 2.6 cm and a maximum of 3.9 cm, and for the GM data, 4.8 cm.

Satellite	**Mean or SSH profiles of new SSH - DNSC08**		
	Number of compared points	Mean	STD
Geosat ERM	786894	17.0	3.9
ERS-2	1513549	17.0	3.6
Envisat	1299720	17.2	2.7
T/P	453163	17.2	2.6
ERS-1 Phase E	6351294	17.2	4.8
ERS-1 Phase F	6325161	17.2	4.7

Table 3.3: Statistics of height differences between mean or SSH profiles of new SSH and DNSC08; units are in cm and height differences over 30 cm were eliminated.

Considering Table 3.2 and Table 3.3, which represent the statistics of the comparison of the original SSH data sets and the new SSH data sets with DNSC08, the new SSH data sets for each satellite became much better adjusted into the referencing surface, the Jason-1 mean SSH, and more homogeneous and consistent with each other. Therefore, this analysis indicates that the mean SSH profiles and SSH profiles computed with the new SSH datasets through the integrating method are more accurate profiles.

In order to show the distribution, the height differences between mean profiles or SSH profiles of the new SSH for each satellite and DNSC08 are plotted with 40 minute resolution. For the height variation with respect to the mean value of height differences with respect to DNSC08, the value of 17.2 cm, which is the systematic bias between Jason-1 mean and DNSC08, is subtracted.

In the map for Geosat ERM in Figure 3.6, significant differences are evident along the tracks in the vicinity of the Indian Ocean. This is because the new SSH for Geosat ERM are obtained by integrating and editing bin-by-bin, and the change before and after the adjustment are the largest among the satellites. The lower panel of the figure shows results for T/P, which also indicates prominent trackiness along the east coastal area of the South American continent.

All of the maps show that high differences are evident in the regions of large ocean variability signals and enclosed small seas, near multiple islands of Southeast Asia and coastal areas. In general, for accurate MSS determination, more sophisticated processes are performed in the vicinity of small seas, multiple islands and coasts, where denser and more accurate SSH data are necessary. Thus, the results of the comparison with mean profiles of new SSH and DNSC08 show the dominant differences around those areas.

In fact, considering the differences range between -7.5 cm to +7.5 cm in the maps, the degrees of high differences are at an acceptable level. Moreover, considering the remaining ocean variability signals in each satellite, and inter-annual variability signals between the 7-year Jason-1 mean profile and DNSC08, the results of this comparison indicate that the SSH data of each satellite are adjusted to a reasonable level. The maps of the height variations between each satellite and DNSC08 are provided in Figures 3.6 to 3.8; the offset due to systematic bias between Jason-1 and DNSC08, 17.2 cm, is excluded.

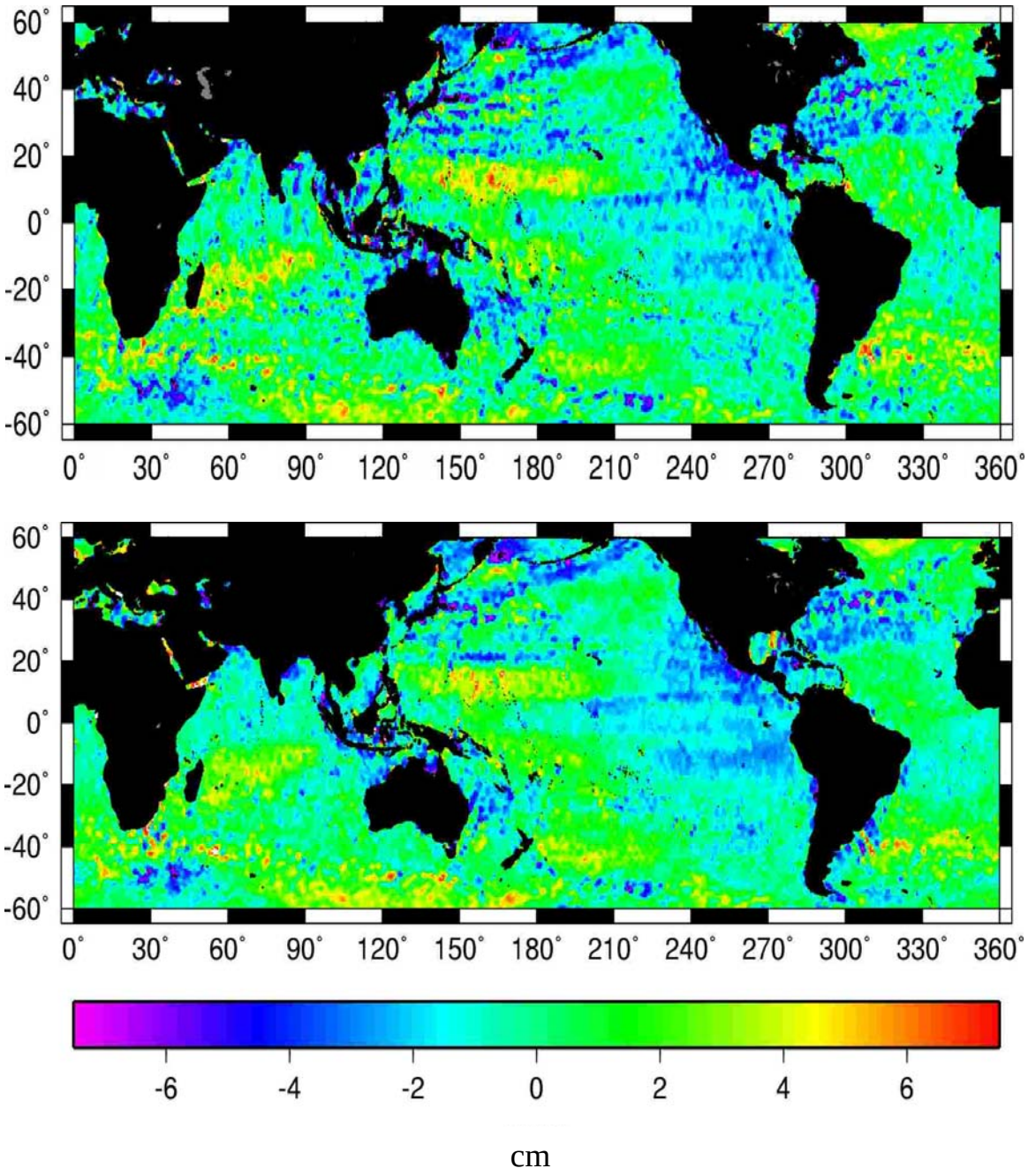

Figure 3.6: Height variations of Geosat ERM(Top) and T/P mean profiles (Bottom) computed with new SSH data with respect to DNSC08, after subtracting 17.2 cm.

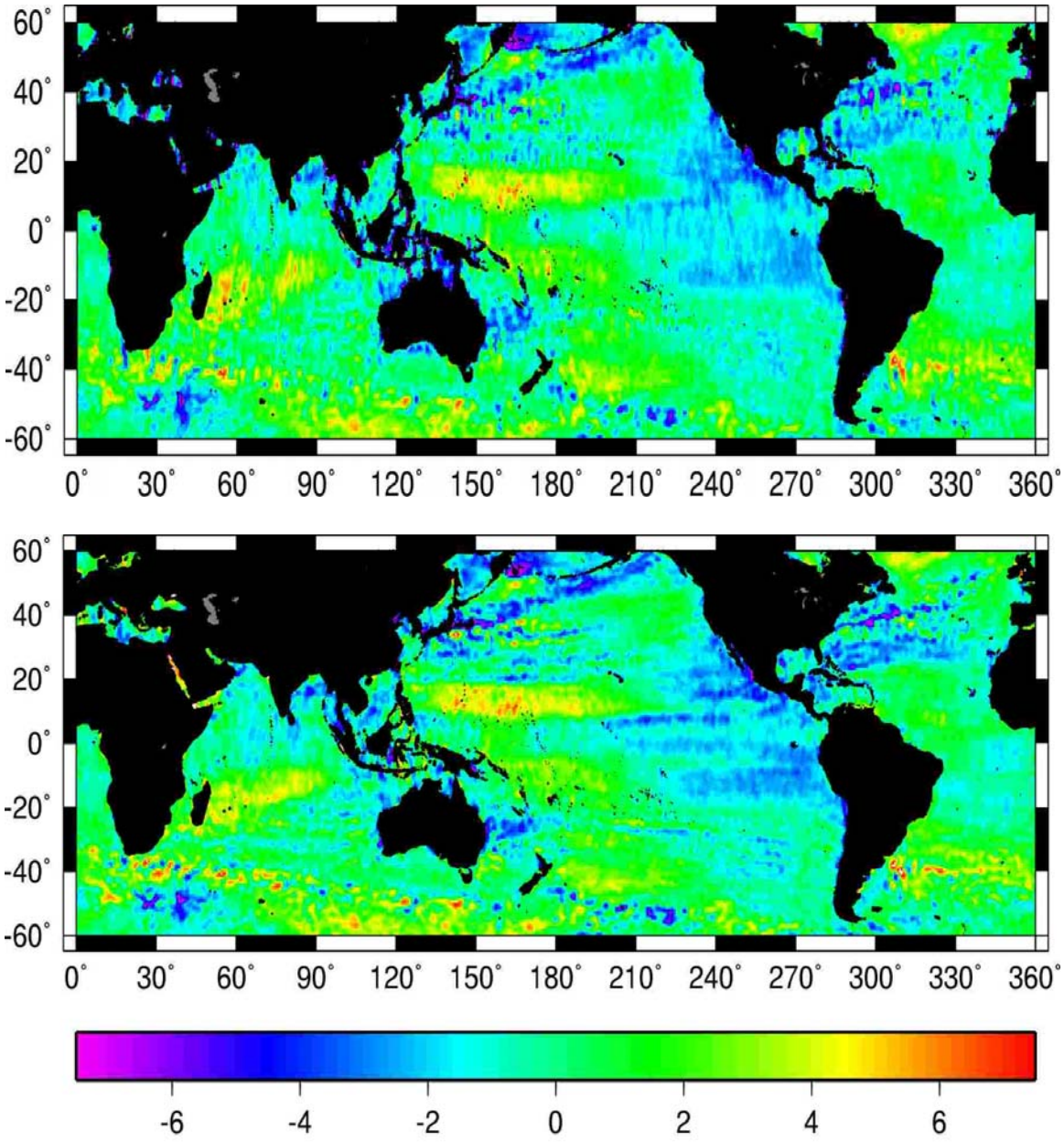

Figure 3.7: Height variations of ERS-2 (Top) and Envisat mean profiles (Bottom) computed with new SSH data with respect to DNSC08, after subtracting 17.2 cm.

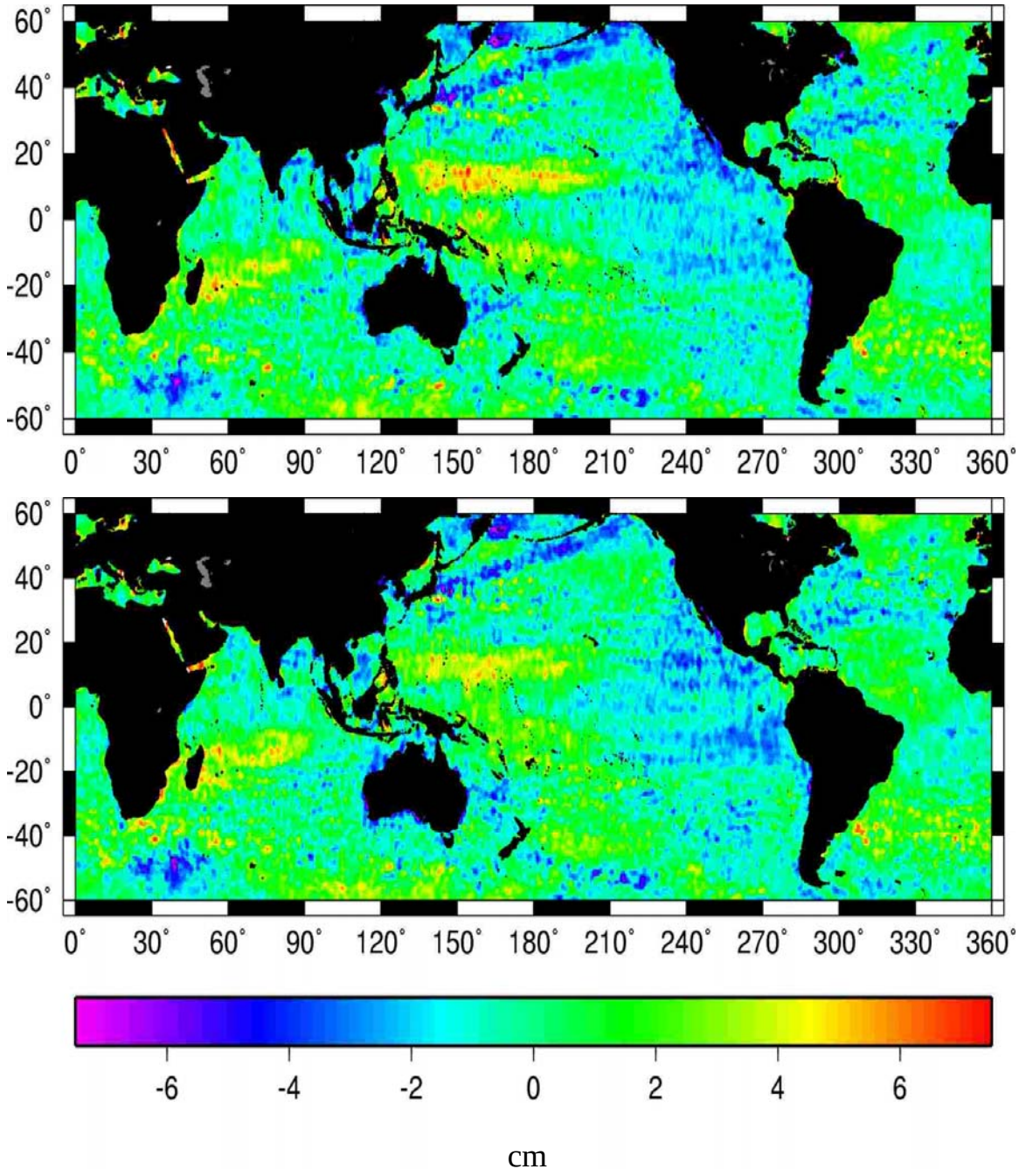

Figure 3.8: Height variations of the SSH profile of ERS-1 Phase E (Top) and ERS-1 Phase F (Bottom) computed with the new SSH data with respect to DNSC08, after subtracting 17.2 cm.

3-4-2. Comparison with DTU10 MSS

In this sub-section, the new mean profiles are evaluated by comparing them with the DTU10 MSS. The test is the same as that for DNSC08. The height differences between the mean or SSH profiles of each satellite and DTU10 are computed, and the mean and standard deviation of the differences are calculated. Table 3.4 summarizes the statistics of the comparison for the ERM and GM data with DTU10; units are in cm.

	Mean or SSH profiles of new SSH – DTU10		
Satellite	Numbers of compared points	Mean	STD
Geosat ERM	793339	12.1	3.6
ERS-2	1535883	12.0	3.7
Envisat	1299842	12.2	2.4
T/P	456383	12.2	2.5
ERS-1 Phase E	6351468	12.2	4.5
ERS-1 Phase F	6325254	12.2	4.4

Table 3.4: Statistics of height differences between mean or SSH profiles of new SSH and DTU10; units are in cm and height differences over 30 cm were eliminated.

In all cases, the mean value of height differences for each satellite is very close to 12.2 cm, which is the systematic bias between the 7-year Jason-1 mean profile and DTU10. The standard deviation of height differences ranges from 2.4 cm to 3.7 cm for ERM satellite, while the values are slightly higher (4.4 cm and 4.5 cm), for GM datasets. The results indicate that the all mean profiles or SSH profiles of the new SSH datasets are very

consistent and homogeneous with respect to DTU10 and the Jason-1 mean profile, as well as with DNSC08. The maps of the height differences with respect to DTU10 after subtracting 12.2 cm, which is the value of the systematic bias between Jason-1 mean SSH and the DTU10 surface, are given in the following figures.

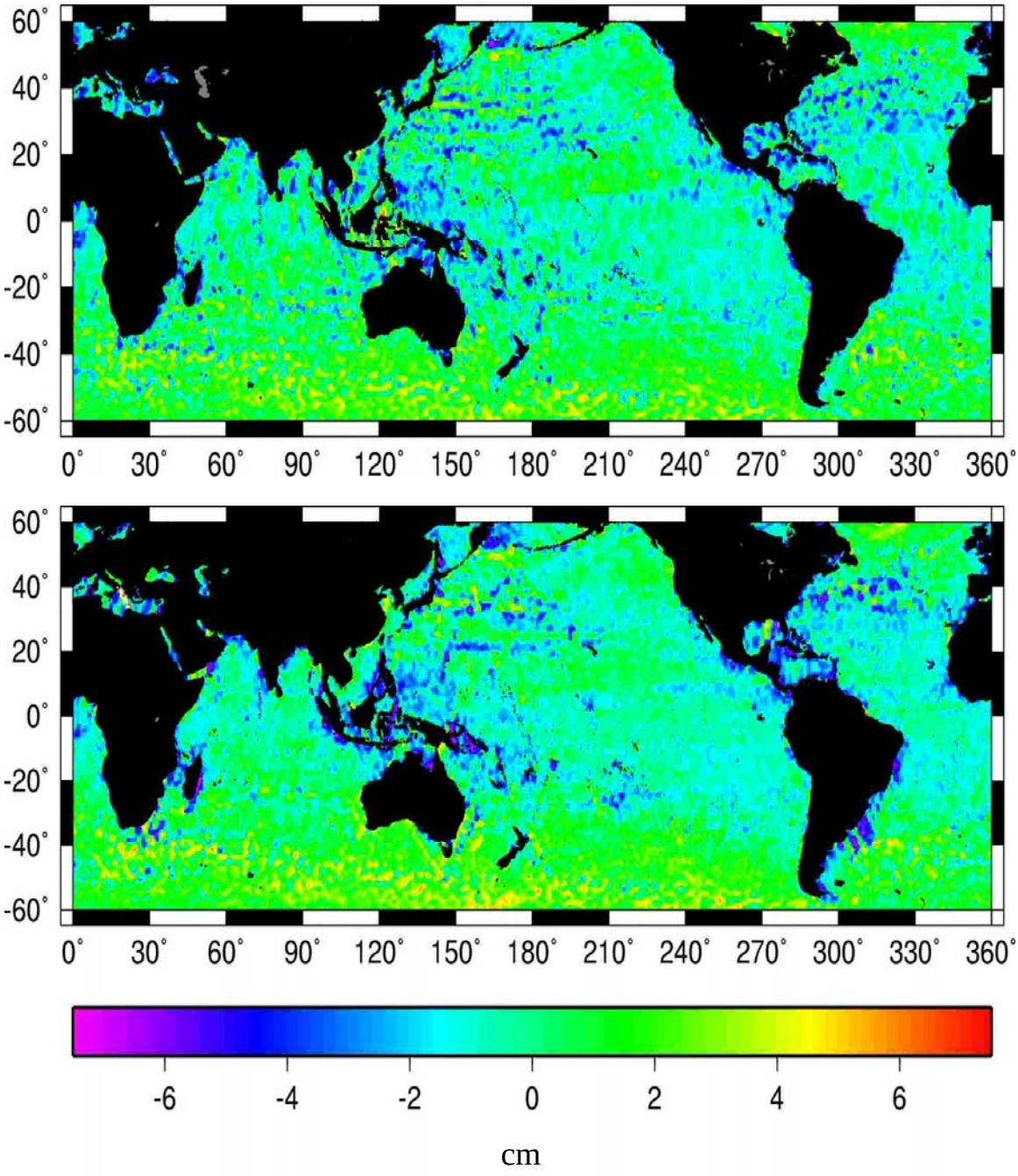

Figure 3.9: Height variations of Geosat ERM(Top) and T/P(Bottom) mean profiles computed with new SSH data with respect to DTU10, after subtracting 12.2 cm.

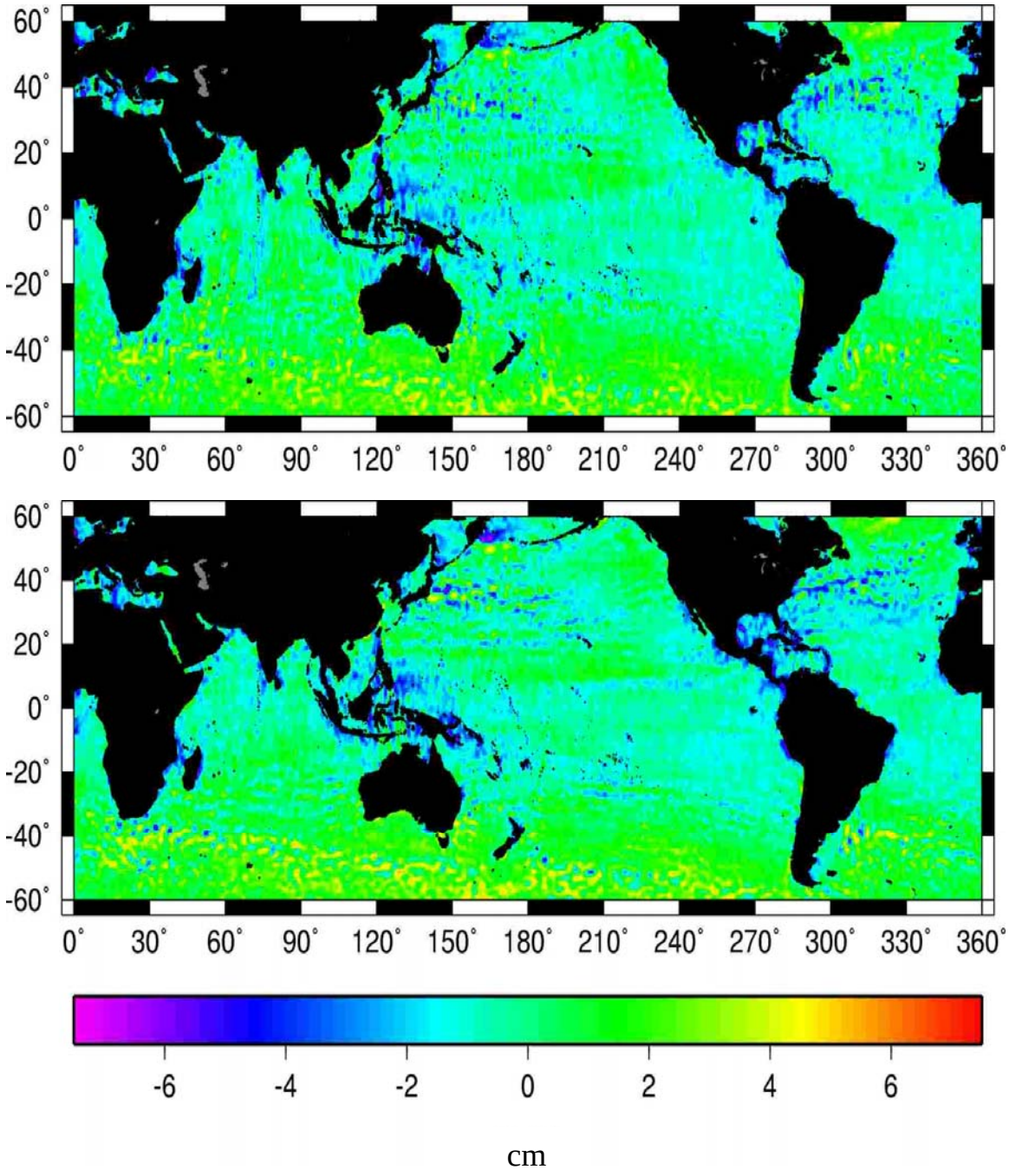

Figure 3.10: Height variations of ERS-2 (Top) and Envisat (Bottom) mean profiles computed with new SSH data with respect to DTU10, after subtracting 12.2 cm.

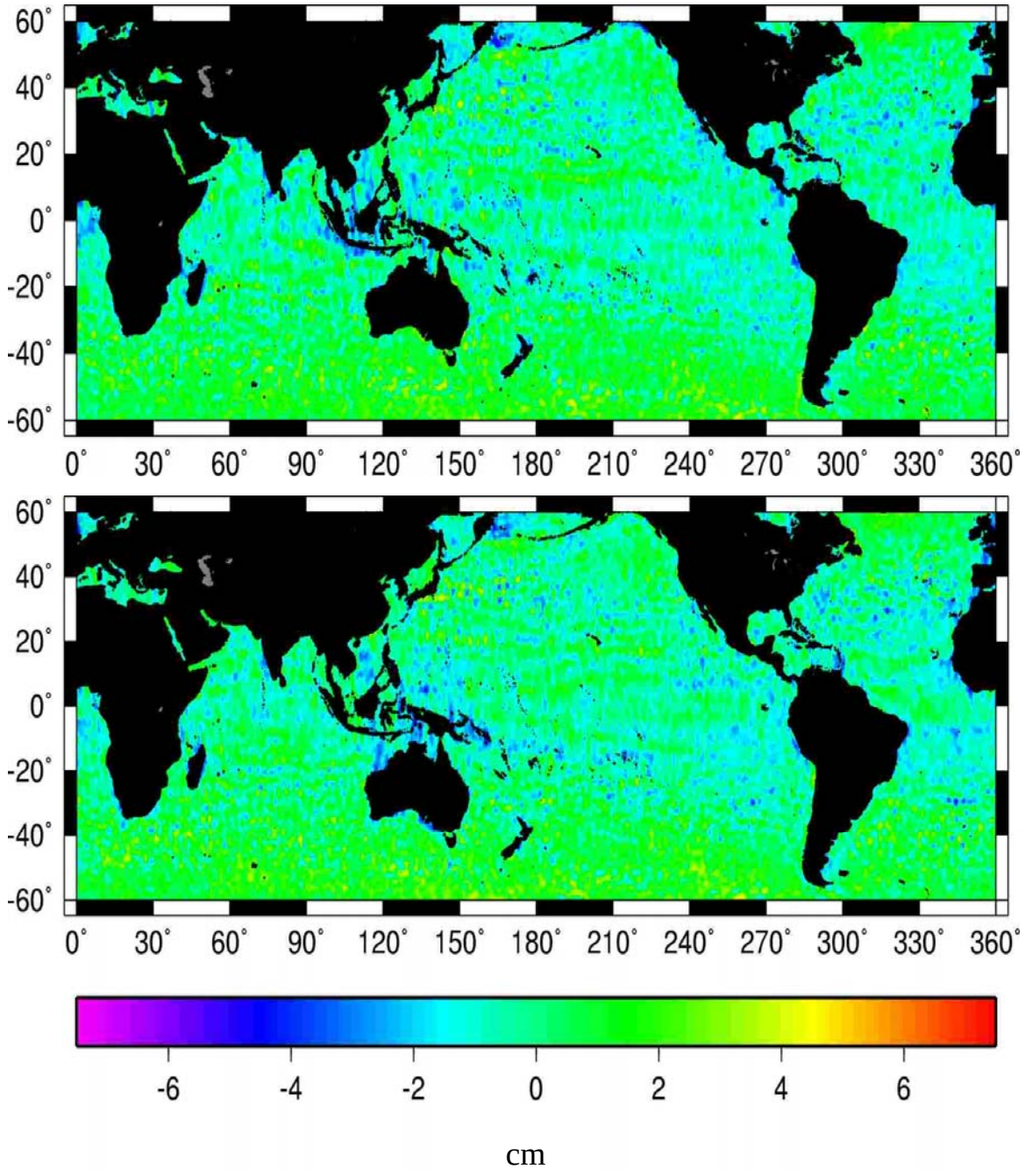

Figure 3.11: Height variations of ERS-1 Phase E (Top) and ERS-1 Phase F (Bottom) SSH profiles computed with new SSH data with respect to DTU10, after subtracting 12.2 cm.

The maps for Geosat ERM and T/P show that relatively high negative differences (about -5 cm) have noticeable satellite track patterns in Figure 3.9. In addition, large differences are found in the regions of enclosed seas and the vicinity of coastal areas. As explained previously, the data for those areas in the MSS are treated very carefully, so the differences are likely a reflection of more uniform and homogeneous MSS, DNSC08 or DTU10. However, mostly, the large differences due to high oceanic variability signals are not found in all maps of comparison with DTU10. This is consistent with the differences between the 7-year Jason-1 mean SSH and DNSC08, and between the 7-year Jason-1 mean SSH and DTU10, featured in Figures 3.4 and 3.5, respectively. It also demonstrates that the surface from the adjusted SSH datasets in each satellite is smoother and closer to DTU10 than DNSC08, because the 7-year Jason-1 mean SSH is closer to the reference surface used for DTU10. Therefore, the mean profiles or SSH profiles of enhanced datasets in each satellite are within the desired accuracy level of approximately 5 cm.

In conclusion, from comparing the mean profiles or SSH profiles of the new SSH with DNSC08 and DTU10, they showed small variations of relative height differences overall. The figures show that relatively high positive or negative differences are evident in the regions of enclosed small seas, vicinity of coastal area and high oceanic variability. Thus, more accurate data is needed in those areas for gridding into an accurate mean sea surface determination.

Chapter 4: Gridding into New Mean Sea Surface

4-1. INTRODUCTION

The mean or SSH profiles of the new SSH datasets, which were improved through the integrating process, were derived for both multiple ERM and ERS-1 GM satellites: Geosat, ERS-2, Envisat, T/P, and ERS-1 phase E and F. They were processed in order to make them homogeneous datasets using the accurate Jason-1 mean SSH data as a reference. Therefore, their accuracies are enhanced as their data were made similar to that of Jason-1. They are ready to be used as inputs of gridding as the final step of the mean sea surface determination.

Gridding is a 2-dimensional technique used to obtain the results of regular geographic locations from scattered positioned data. For MSS derivation, gridding provides the interpolated results on a uniform grid, given multiple satellite SSH datasets. Most of the recent MSS models have used least squares collocation as a gridding technique, whose method uses a second-order Gauss-Markov covariance function with a certain correlation length.

In this research, assuming that inputs for gridding are very homogeneous and consistent with respect to the reference surface, Jason-1 mean SSH, the algorithm for gridding uses a 2-D spline interpolation in tension with a Green's function. Section 4-2 derives the 2-D interpolation using Green's function in tension mathematically and conceptually, and the computation algorithm for gridding into the new MSS, named

CSRMSS14 is explained in Section 4-3. In Section 4-4, the determination method of the tension term for the research is described.

4-2. GRIDDING USING GREEN'S FUNCTION TECHNIQUE

Green's function is not only commonly used for solving differential equation, but also for deriving mathematical techniques for finite difference methods. It is also called the inverse matrix of the Laplace operator and treated as a data kernel for minimum curvature interpolation. Sandwell [1987] presented a gridding technique with bi-harmonic spline interpolation using Green's function and applied it to sea surface topography mapping using GEOS-3 and Seasat satellite altimeter data. He demonstrated that the gridding technique using a Green's function is very flexible and easy to apply to more dimensional results, while there is a limitation of input data and stability of computation.

The mapping surface is the result of the linear combinations of Green's functions computed at given individual datum. Wessel and Bercovici [1998] presented a more efficient and general method, adding a tension factor to 2-D interpolation with Splines using Green's function. Splines are very commonly used to provide data constraints smoothly, but they can produce unwanted large oscillations between two constraints. By adding tension on the curve, these phenomena can be significantly suppressed. The derivation of the two-dimensional (2-D) gridding method using Green's function for splines in tension, based on Wessel and Bercovici [1998], is described in the following.

Let's consider a set of irregularly scattered N sea surface heights, $\boldsymbol{h_i}$, at position, $\boldsymbol{x_i}$. The general equation of a point force for a Green's function, $g(\mathbf{x})$, for a spline in tension

is composed of the bi-harmonic operator (∇^4) and Laplacian (∇^2), and it should satisfy the following equation:

$$F\nabla^4 \mathrm{g}(\mathbf{x}) - T\nabla^2 \mathrm{g}(\mathbf{x}) = \delta(\mathbf{x}) \tag{4.1}$$

Here, *T* is the tension factor, *F* is the rigidity factor, and $\delta(\mathbf{x})$ is a dirac delta function. By applying this equation to the SSH dataset, the gridded sea surface heights at position vector **x** in terms of Green's function is written as:

$$\boldsymbol{H}(\boldsymbol{x}) = \sum_{\boldsymbol{i=1}}^{\boldsymbol{N}} \boldsymbol{A_i}\, \boldsymbol{G}(\boldsymbol{x} - \boldsymbol{x_i}) \tag{4.2}$$

where, $\boldsymbol{x}$ represents an expected position vector of outputs, and $\boldsymbol{x_i}$ is a given position vector of constraints (or input data). Applied to the real data, $\boldsymbol{x}$ is the vector of gridded positions in 5-minute (1/12°) spatial resolution, and $\boldsymbol{x_i}$ is the SSH datasets in mean or SSH profiles of 6 different satellites. $\boldsymbol{H}(\boldsymbol{x})$ indicates a matrix of gridded sea surface heights at $\boldsymbol{x}$, which means the results of the MSS. The $\boldsymbol{G}$ matrix is a matrix of Green's functions and the $\boldsymbol{A}$ matrix is the coefficient matrix. Therefore, the multiple SSH datasets are gridded into the MSS through the linear combination of the $\boldsymbol{A}$ matrix and the $\boldsymbol{G}$ matrix.

The $\boldsymbol{A}$ matrix is determined with input data by computing the linear system given by:

$$h_j = \sum_{j=1}^{N} \sum_{i=1}^{N} A_i G(\boldsymbol{x_j} - \boldsymbol{x_i}) \tag{4.3}$$

where, h_j is the data constraint or, in this research, the given SSH for the gridding method. $G(\boldsymbol{x_j} - \boldsymbol{x_i})$ is the Green's function of given input datasets. If the Green's function between input datasets, $G(\boldsymbol{x_j} - \boldsymbol{x_i})$, is determined, A_i is obtained by inverting equation (4.3).

For the numerical solution, twice integration and more steps are derived. The final solution of the Green's function, $\boldsymbol{G}(\boldsymbol{x})$ in order to derive 2-D spline interpolation in tension, is written as:

$$\boldsymbol{G}(\boldsymbol{x}) = \mathbf{K}_0(\mathrm{Q}|\mathbf{x}|) + \log(\mathrm{Q}|\mathbf{x}|) \tag{4.4}$$

Here, $\boldsymbol{K_0}$ is the modified Bessel function of the second kind and order zero (refer to numerical recipes in FORTRAN [page 229 ~ 231]). Q is a normalized tension term, and T, the tension factor, is less than one and greater or equal to 0.

$$\mathrm{Q} = \sqrt{\frac{\mathrm{T}}{1-\mathrm{T}}} \tag{4.5}$$

Finally, once the $\boldsymbol{A}$ and $\boldsymbol{G}$ matrices are determined, the interpolated sea surface heights at the desired positions, i.e., the MSS, are solved by the linear system (4.2).

4-3. ALGORITHM DESIGN FOR GRIDDING

The computing algorithm for gridding into mean sea surface is designed here to be implemented with Fortran 90 in the unix environment, using 2-D spline interpolation in tension with Green's function. This gridding process requires that input data be quite homogeneous with respect to the reference data for accurate results. For the input data, the mean SSH profiles for ERM satellites such as Geosat, ERS-2, Envisat, and T/P, and SSH profiles of ERS-1 GM satellite are used, which have been made more consistent with the Jason-1 SSH data. Jason-1 mean profiles of both ascending and descending passes are included as input data as well.

There are some considerations and pre-determinants for this gridding method. First, the grid size, input, and output window size should be resolved, because a program is repeated by small assigned locations due to computation storage and time. The grid size for output determines the spatial resolution of a gridded mean sea surface. For this research, the resolution of the gridded mean sea surface is determined to be a $\frac{1}{12}°\,(5minutes)$ resolution, and a window size of the output data for one time processing is assigned as $1°$ longitude by $1°$ latitude. Therefore, 144 outputs at 144 grid points are produced in one time computation.

The window size for input data is expanded by 0.3 degrees in longitude and latitude from the output window size. For outputs at boundaries and neighboring boundaries, input data outside of the input window should be considered to determine the accurate results, since the gridded outputs are resolved by only input data inside the input window. Thus, the input window size is 1.3º in longitude by 1.3º in latitude for one time computation. Figure 4.1 shows the input window and grids of output in a one-time process of the gridding computation. It is an example area of longitude from 300º to 301º, and latitude from 23ºN to 24ºN. Blue stars represent the real SSH data within an input window, and red circles show grids resulting in output positions.

Second, the tension factor, T should be determined and included in the algorithm. Tension ranges from 0 to 1 ($0 \leq T < 1$). If T is equal to 0, it means that the curves are able to pass freely like the standard cubic splines interpolation, while T = 1 means a linear interpolation. The following section will describe a test done using the sampled SSH data in order to determine an appropriate tension value for this research.

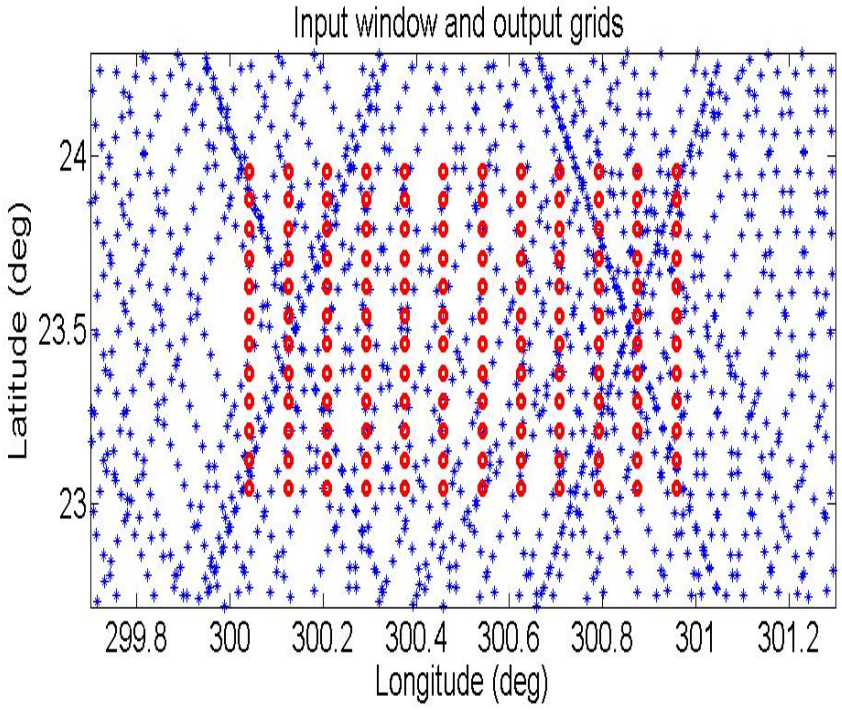

Figure 4.1: Input window and grids for output in one time process of gridding; blue stars show the real SSH datasets and red circles represent the output grids.

Finally, the programs for gridding into the MSS are implemented in FORTRAN 90, using 2-D spline interpolation in tension with Green's function. Due to limitations of computation storage and time, MPI (Message Passing Interface) parallel coded environment is included in the serial coded programs for the global results. The numerical steps for gridding method are described in Figure 4.2. Through the process, the newly gridded mean sea surface, CSRMSS14, is produced.

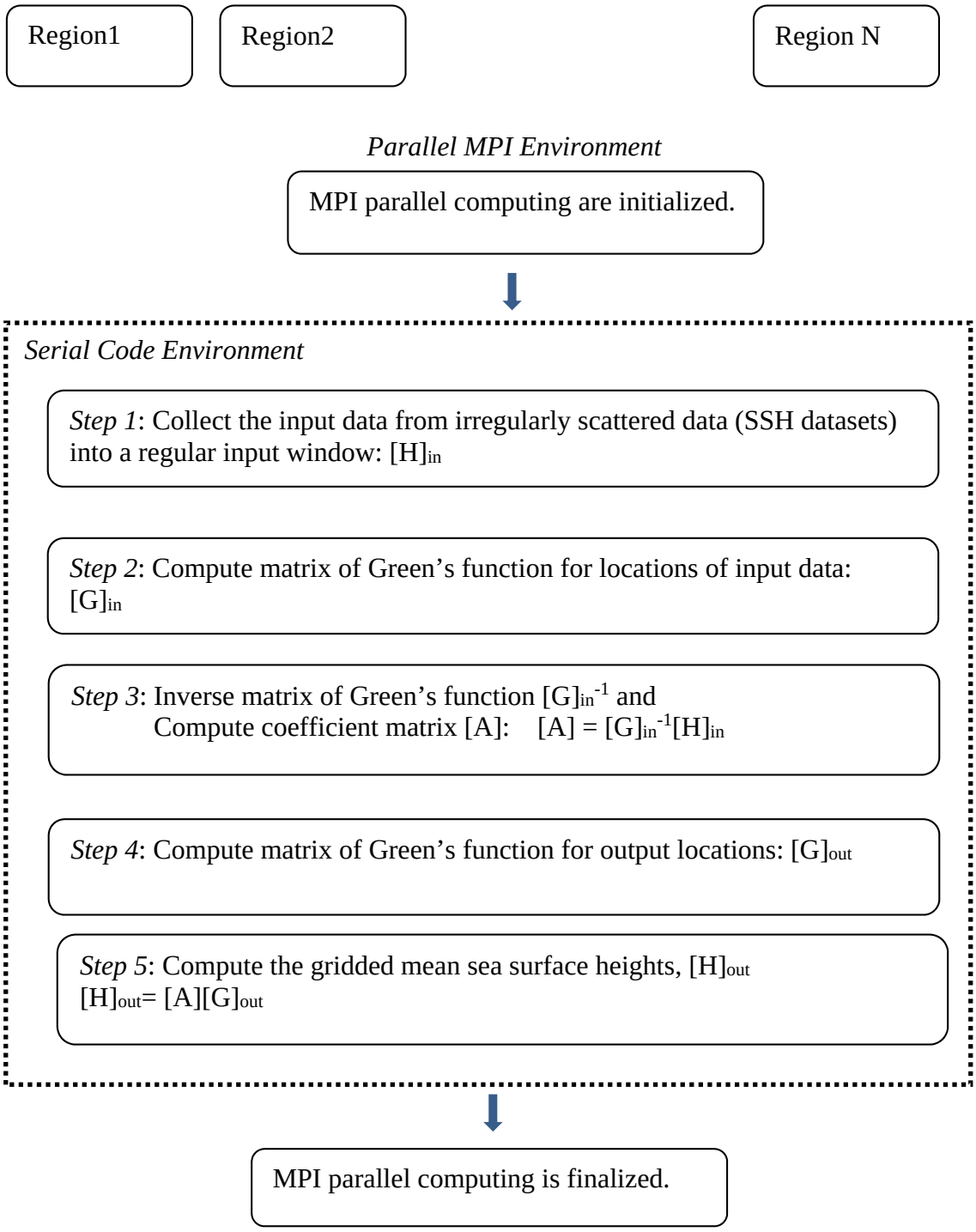

Figure 4.2: Flow chart of Gridding Algorithm.

4-4. EFFECT OF TENSION TERM, *T*

In this section, the effects of the tension term in the gridding method using Green's function are demonstrated. Since the cubic spline interpolation is not appropriate for noisy data, and a linear interpolation is too weak to represent the scattered data on sphere, the reasonable tension term should be between zero and one. To determine an appropriate tension factor for this research, a test by trial and error is performed by selecting a sample area using real SSH data.

The input window area was selected between the longitudes 181º to 182 º and the latitudes -21 º to -20 º. Then, the real SSH data from mean or SSH profiles of 6 different satellites are used as input datasets, and the outputs of the area are produced through a gridding program using Green's function in tension and varying the tension terms. Tension terms, *T*, are inserted with values of 0.1, 0.3, 0.5, 0.7 and 0.9. Then, the outputs are compared with the reference field, DNSC08, in the same area. The standard deviation of the differences between the two MSS models are evaluated. It is assumed that the smaller the standard deviation of the differences, the more appropriate the tension term is.

Figure 4.3 demonstrates the standard deviations of the differences between outputs gridded by various tension terms and DNSC08, tested in the sample area. The horizontal axis, indicates the tension terms, and the vertical axis represents the standard deviations of the differences (in cm). Since it shows the least value of the standard deviation when tension is 0.5 in this test, the tension term, $T = 0.5$ is chosen for the gridding method for this research. Ideally, the investigation should be done globally, not just for a sample

region. However, the sample test demonstrated that the simple cubic spline interpolation is not adequate for gridding with different satellite datasets, and thus the tension term should be between 0.3 and 0.7 for this research. As seen in Figure 4.3, the results are not especially sensitive to the tension term in this range.

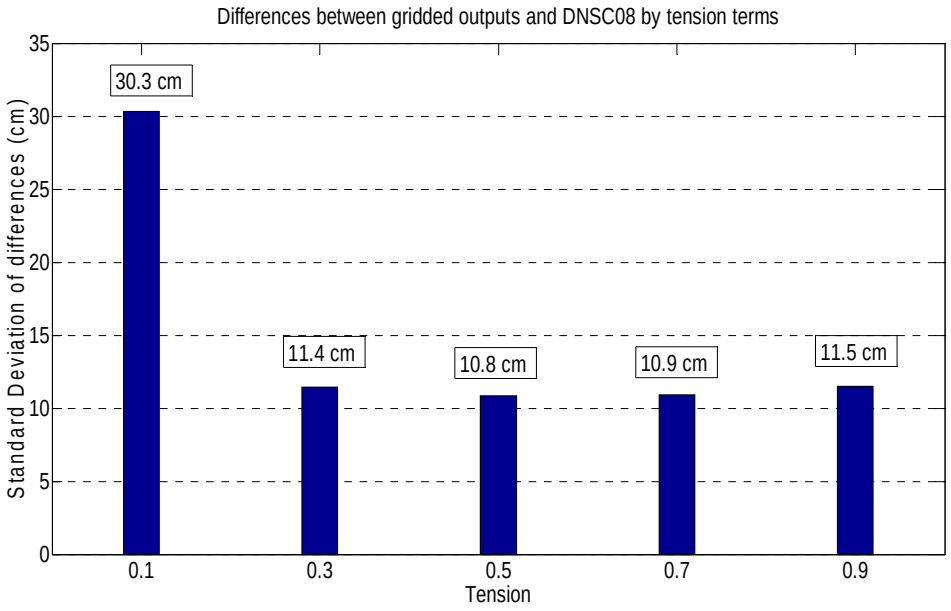

Figure 4.3: Standard deviations of SSH differences between new gridded SSH and DSNC08 by various tension terms.

4-5. SUMMARY

This chapter described the gridding method using 2-D spline interpolations in tension with Green's function based on Wessel and Bercovici [1998]. 1º interval for the input window and a 5-minute uniform grid for the output was adopted. Moreover, by a sample test, the tension term of T=0.5 was chosen for this research. For global results, an

MPI parallel program was added to the serial computational algorithm to save computation time. Therefore, through this gridding technique, the new mean sea surface, CSRMSS14, is obtained using SSH data from 7-years of Jason-1 data, and adjusted 2-year Geosat ERM, 6-year ERS-2, 8-year Envisat, 10-year T/P, and ERS-1 GM data. The global gravity model, EGM2008 geoid data, was used over land. The evaluations for CSRMSS14 are discussed in the next chapter.

Chapter 5: Evaluation of New Mean Sea Surface

5-1. INTRODUCTION

The mean or SSH profiles of the adjusted SSH datasets from 5 different satellite missions, including the Jason-1 mean profile, were gridded into a new mean sea surface, CSRMSS14, using 2-D spline interpolation in tension with Green's function. CSRMSS14 was computed on a 5-minute (1/12º) grid between latitude ± 60 º oceanwide. To be consistent with the comparison models DNSC08 and DTU10, the EGM2008 geoid was used to fill in over land. The CSRMSS14 is shown in Figure 5.1. In this chapter, the accuracy of CSRMSS14 as a representative of the mean sea surface is validated through three comparisons.

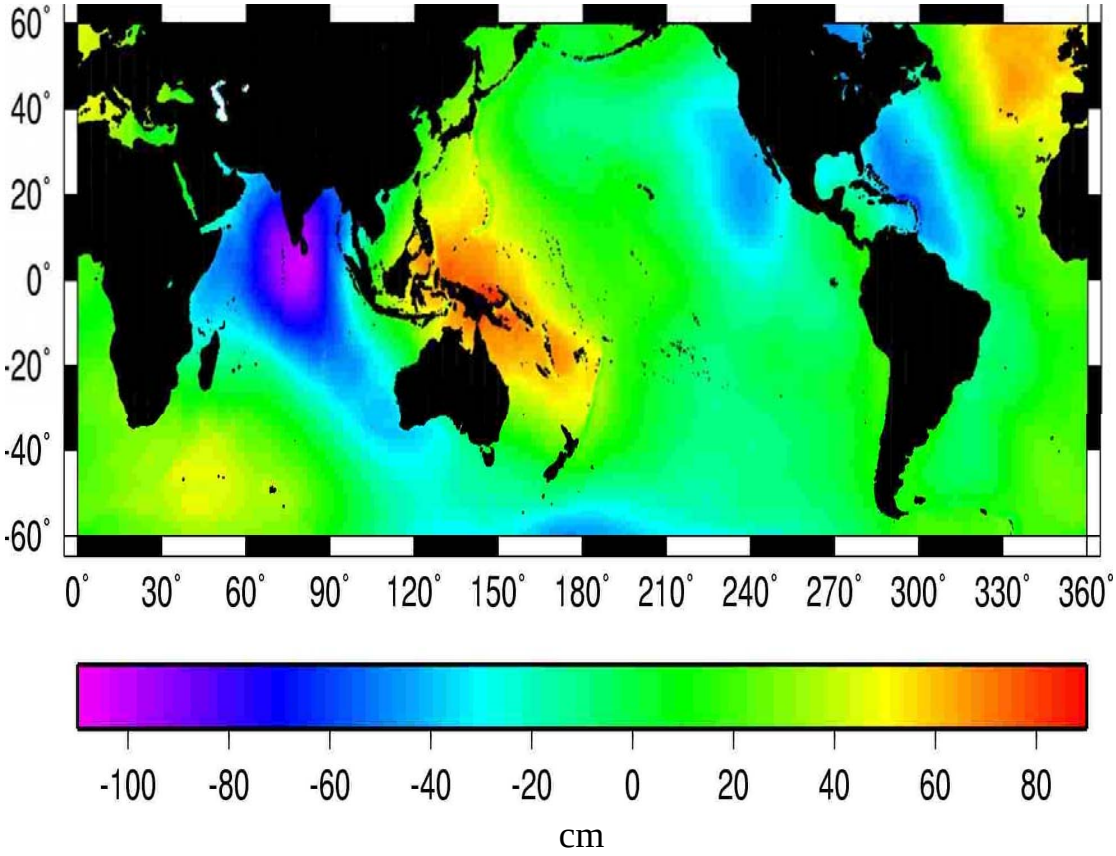

Figure 5.1: CSRMSS14 Mean Sea Surface

First, CSRMSS14 is compared with two accurate altimetric mean profiles, which were used as inputs for deriving CSRMSS14. These mean profiles are the 7-year Jason-1 mean profiles, which are used to reference other satellite datasets, and the 8-year Envisat mean profile, an accurate mean profile of adjusted SSH data from the original data in the RADS database. This validation is not an independent assessment of the accuracy of the MSS, since Jason-1 and Envisat data are already included in CSRMSS14. However, it would infer the reliability level of the gridding method used in this research, assuming that

the mean profiles used for inputs are very accurate. Section 5-2 will present the results of comparison of outputs versus inputs through the gridding method.

Second, as a grid-to-grid comparison, CSRMSS14 is validated by comparing it with two existing accurate mean sea surface models, DNSC08 and DTU10. This comparison concentrates on the height differences between three MSS, and focuses on the results of similarities among them. As described previously, there are systematic differences between the three MSS, due to different orbit and correction models, different gridding technique, and the use of different satellite data and time spans of the reference surface, so they should be taken into account when analyzing the results. In particular, note the inter-annual ocean variability witnessed between DNSC08 and DTU10 in Figure 3.3. The results of this direct grid comparison will be described in Section 5-3.

Finally, Jason-2 mean profiles are used for the evaluation of CSRMSS14. Jason-2 SSH data are not used for CSRMSS14, DNSC08 or DTU10, so this assessment will be an independent comparison. This assessment allows us to see CSRMSS14 as an accurate representation of a reference surface, comparable to DNSC08 and DTU10. Section 5-4 will describe the analysis.

5-2. COMPARISON WITH ALTIMETRIC MEAN SSH PROFILES

An assessment is performed by comparing CSRMSS14 with the 7-year Jason-1 mean profiles and the 8-year Envisat mean profiles, which are used for gridding into CSRMSS14. The idea of the test is that the outputs, processed through the gridding method, are compared with inputs in order to assess the precision of the gridding process. For this

evaluation, height differences between the mean profile and CSRMSS14 are computed by interpolating the grids to the mean profile. Then, the mean and root mean squares (RMS) of height differences along the mean profiles are computed, and the results represent the change quantitatively. Table 5.1 shows the statistics of the height differences between CSRMSS14 and two altimetric mean profiles in terms of the mean and RMS.

Statistics (in cm)	**7-year Jason-1 mean profile vs. CSRMSS14**	**8-year Envisat mean profile vs. CSRMSS14**
Mean	-0.002	-0.02
RMS	2.5	2.8

Table 5.1: Statistics of results by comparison between CSRMSS14 and mean profiles of Jason-1 or Envisat used for CSRMSS14 determination.

Statistics of the along-track height differences show that the mean is almost zero, and RMS ranges from 2.5 to 2.8 cm for Jason-1 and Envisat mean profiles, respectively. The fact that the mean is zero proves that the outputs through the gridding method faithfully represent the input data, globally. Regarding the RMS, it is not expected to be almost zero for the accuracy of the gridding method, because the MSS was determined to be a more homogenized surface, using multiple satellite datasets. The point of analysis from RMS, with respect to mean profiles, is to see a reasonable difference. Note that the standard deviations between the 7-year Jason-1 mean profile and DNSC08, and between the 7-year Jason-1 mean profile and DTU10 are 2.7 cm and 2.5 cm, respectively, as mentioned earlier. Thus, the values of 2.5 cm or 2.8 cm in the table above shows a comparable level of

accuracy in terms of RMS, considering ocean variability contained in these two altimeter satellite data.

Figure 5.1 shows geographically the height differences between the 7-year Jason-1 mean profile and CSRMSS14, while Figure 5.2 represents the results between the 8-year Envisat mean profile and CSRMSS14.

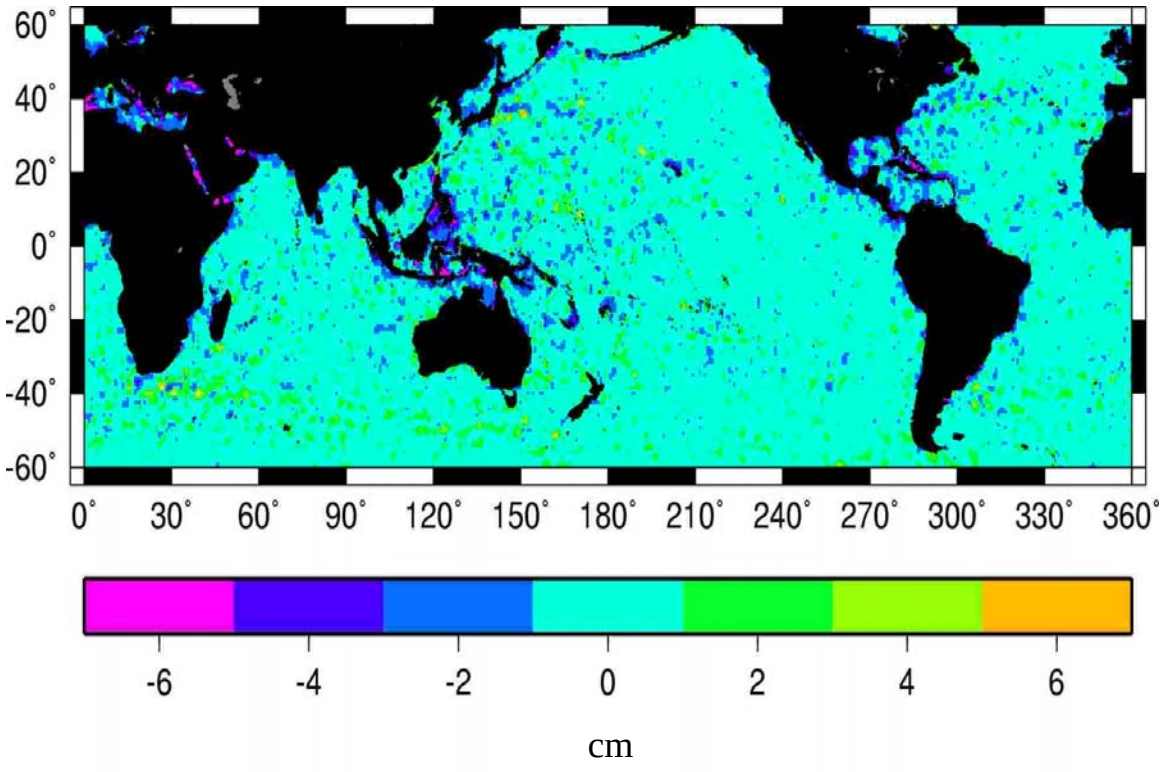

Figure 5.2: Height difference between the 7-year Jason-1 mean profile and CSRMSS14.

In Figures 5.1 and 5.2, the results for most of the open oceans show that height differences are between ±2 cm, except in isolated seas between the European and African continents and Southeast Asia seas. Moreover, high differences are shown mostly in coastal areas. The high differences result from comparison of mean profiles to more uniform and homogeneous surface, CSRMSS14, which was determined with the combination of EGM2008 geoid data on lands, and denser data, in particular, geodetic data, ERS-1 phase E and F.

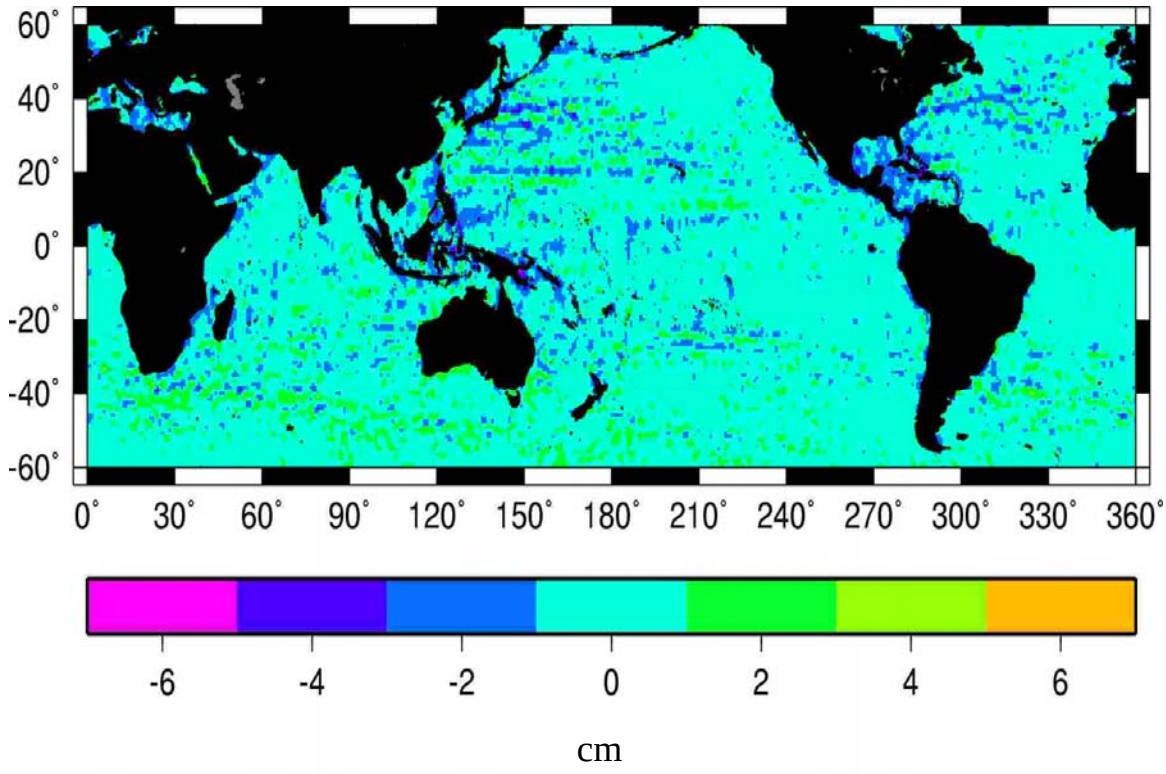

Figure 5.3: Height differences between the 8-year Envisat mean profile and CSRMSS14.

Figure 5.2 indicates smaller differences oceanwide, because Envisat SSH data are denser with high accuracy, so they contribute to these small seas, isolated seas and seas near the coasts, during the mean profile process. Through this analysis, the gridding technique is evaluated to be reliable and accurate with respect to two main input data used for this research.

5-3. COMPARISON WITH DNSC08 AND DTU10

In this section, CSRMSS14 is validated with the most accurate mean sea surfaces, DNSC08 and DTU10. CSRMSS14 is directly compared to the DNSC08 and DTU10 5-minute grid MSS, and the mean and standard deviation of height differences are computed within ±60 º of latitudes. The differences exceeding 30 cm were excluded in this plot. Originally, DNSC08 and DTU10 were determined at 1-minute (1/60 º) resolution, so they are extracted to 5-min resolution by sampling data at 5-min grids from 1-min resolution for comparison with the 5-min resolution of CSRMSS14. Table 5.2 shows the statistics of the results for this comparison (in cm).

	CSRMSS14 - DNSC08	**CSRMSS14 - DTU10**
Number of compared points	6187421	6192978
Mean	16.3	11.3
Standard Deviation	6.1	6.1

Table 5.2: Statistics of three MSS differences: CSRMSS14, DNSC08 and DTU10.

The mean values of height differences between two MSS (CSRMSS14 vs. DNSC08 or CSRMSS14 vs. DTU10) are 16.3 cm and 11.3 cm, which are very similar to the mean of differences between the 7-year Jason-1 mean profiles used as the reference surface for determining CSRMSS14 and DNSC08 or DTU10, respectively. The standard deviations of differences represent the similarity between new MSS, CSRMSS14, and two existing MSS, DNSC08 or DTU10. In addition, the statistics infer the respective accuracy of CSRMSS14. According to Hernandez and Schaeffer [2000], comparison between two different MSS within ± 66º latitudes showed that the standard deviations of height differences ranged from 6 cm to 10 cm [Hernandez and Schaeffer, 2000; Hernandez and Schaeffer, 2001]. In Table 5.2, the standard deviations of differences between CSRMSS14 and DNSC08 or DTU10 is only 6.1 cm for both. This result indicates that CSRMSS14 is at the same level of accuracy as DNSC08 and DTU10.

For the maps of height differences between the two MSS, SSH differences were subtracted from the mean of the height differences between Jason-1 mean profile and DNSC08 or DTU10: 17.2 cm or 12.2 cm, respectively. These values correspond to the initial systematic biases between the two MSS. The figures are plotted in a resolution of 20 minutes since details at 5-minute resolution would be too small to see.

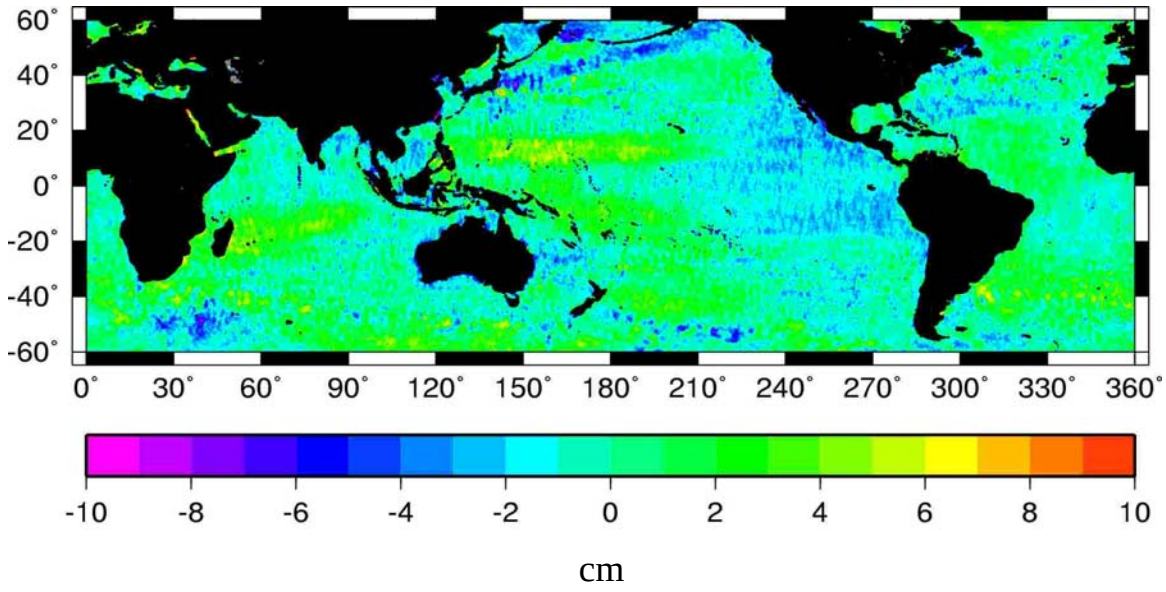

Figure 5.4**:** Map of height differences between CSRMSS14 and DNSC08, after subtracting the initial systematic bias, 17.2 cm.

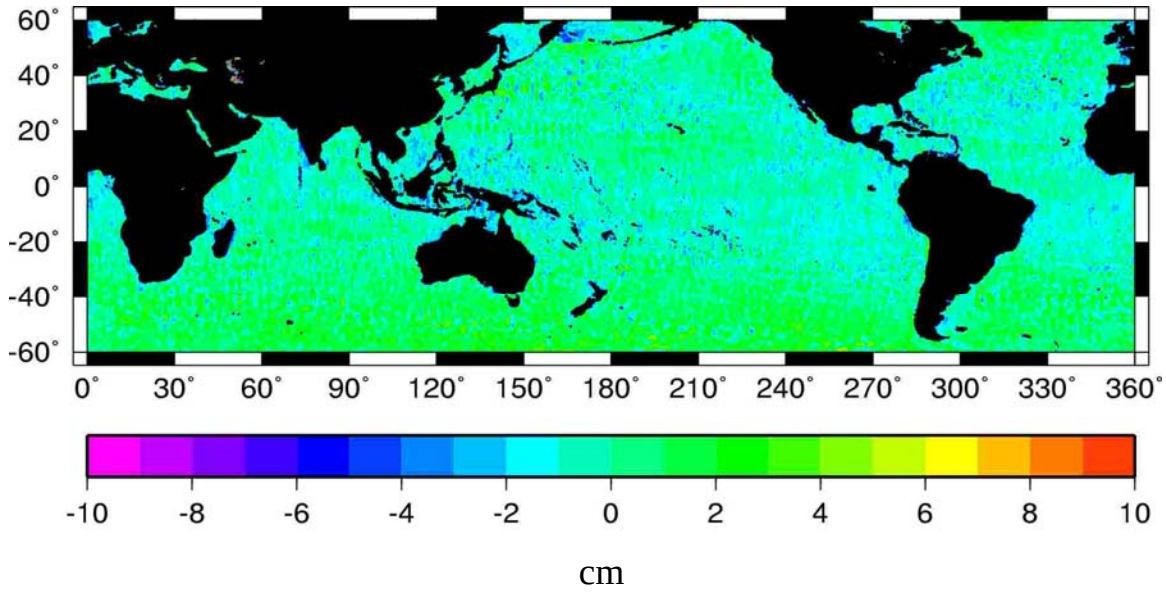

Figure 5.5: Map of height differences between CSRMSS14 and DTU10, after subtracting the initial systematic bias, 12.2 cm.

In Figure 5.3, high positive or negative difference areas, larger than 5cm or less than -5cm, correspond to the same high difference areas shown in Figure 3.3. The differences between CSRMSS14 and DTU10 are more uniform overall because the ending periods of the two reference surfaces are relatively closer than that of DNSC08. Since DNSC08 and DTU10 have similar accuracies, and the main differences shown in two figures (Figure 5.3 and Figure 5.4) are likely representations of the inter-annual variability of the ocean observed in Figure 3.3. The SSH errors from the input datasets and the different gridding processes will also contribute to the differences.

In summary, primary differences between CSRMSS14 and DNSC08 or DTU10 occur because of two factors: systematic differences resulted from different data and different models of MSS determination from different institutions, and inter-annual variability of the ocean due to the different time periods of reference surfaces for the two MSS. In conclusion, this grid-to-grid comparison indicates that CSRMSS14 is a generally an accurate referencing surface comparable to DNSC08 and DTU10.

5-4. COMPARISON WITH JASON-2 MEAN PROFILE

An analysis for CSRMSS14 is carried out using 2-year Jason-2 mean profiles computed from the SSH data in the CSR-Stackfile. Currently, Jason-2 altimeter data for cycles 1 to 62 (July 2008 to March 2010), are available in the database, so data for these time frames are used. Jason-2 data are chosen for the independent analysis of CSRMSS14, because it is not used for DNSC08, DTU10 or CSRMSS14 determination. In fact, the time span of 2-year Jason-2 data overlaps somewhat with two MSS periods, DTU10 (1993-

2009) and CSRMSS14 (2002-December 2008). Thus, considering time spans of the reference surface used for three MSS and 2-year Jason-2 mean profile, this test is not completely independent validation. However, this analysis is still useful to test the accuracy of CSRMSS14 as a representative surface for a new satellite.

For this comparison, height differences between each MSS and Jason-2 mean profiles are first computed. Then, the mean and standard deviation of height differences are computed and plotted within ±60º latitudes. Since there are initial systematic biases between the three MSS, offset terms are added for computation. Equation 5.1 shows the height differences in a mathematical way:

$$\text{Height differences} = [\text{Jason-2} - \text{offset} - \text{MSS}] \tag{5.1}$$

Here, each MSS is interpolated to the mean sea surface on the Jason-2 mean profile.

The systematic biases between the 7-year Jason-1 mean profile and the two MSS, which were computed previously and already used for several comparisons, are used as offsets for this analysis. Thus, the offset for CSRMSS14 is set to 0.0 cm, and offsets for DNSC08 and DTU10 are 17.2 cm and 12.2 cm, respectively. Table 5.3 shows the offset of three mean sea surface models used for this assessment.

MSS models	Offset (in cm)
DNSC08	17.2
DTU10	12.2
CSRMSS14	0.0

Table 5.3: Used relative biases (offset) between the Jason-2 Mean profiles and three MSS: DNSC08, DTU10 and CSRMSS14.

For statistics, the mean and standard deviation of height differences between the 2-year Jason-2 mean profile and the three MSS are computed after applying offset factors. The mean corresponds to the average differences globally, and the results show a similar mean value for the height differences, 5.1 or 5.2 cm. The standard deviation indicates that DTU10 has the least value, at 3.8 cm, while DNSC08 and CSRMSS14 are at a comparable level of accuracy, at 4.1 and 4.2 cm, respectively.

	Jason-2-DNSC08	Jason-2-DTU10	Jason-2-CSRMSS14
Number of compared points	437123	437123	437123
Mean	5.1	5.2	5.2
Standard Deviation	4.1	3.8	4.2

Table 5.4: Statistics of DNSC08, DTU10 and CSRMSS14 for comparison with Jason-2 Mean profile; offset was applied, and units are in cm.

Maps of the height differences between the 2-year Jason-2 mean profile and the three MSS models are plotted geographically in the following figures. The three figures

are quite similar, except for the areas of high inter-annual variability, which is expected due to the different time spans for the MSS models and Jason-2.

A closer analysis is carried out in Southeast Asia seas, where high positive difference areas appear in the all three figures. Since DTU10 contains Jason-1 SSH data that overlaps with a certain time period of the Jason-2 mean profile used in this analysis, the differences in those areas are the smallest (Figure 5.7), while the results for DNSC08, which does not have any overlaps, are the largest (Figure 5.5). CSRMSS14 has a small amount of difference in that area, because the model also incorporated a certain time period of Jason-2 mean profile (from July 2008 to December 2008), but DTU10 still displays smaller differences because it contains a greater period of overlap. This analysis indicates that CSRMSS14 represents well as a reference surface for the other satellite mission, as well as DNSC08 and DTU10 within ±60 º of latitudes.

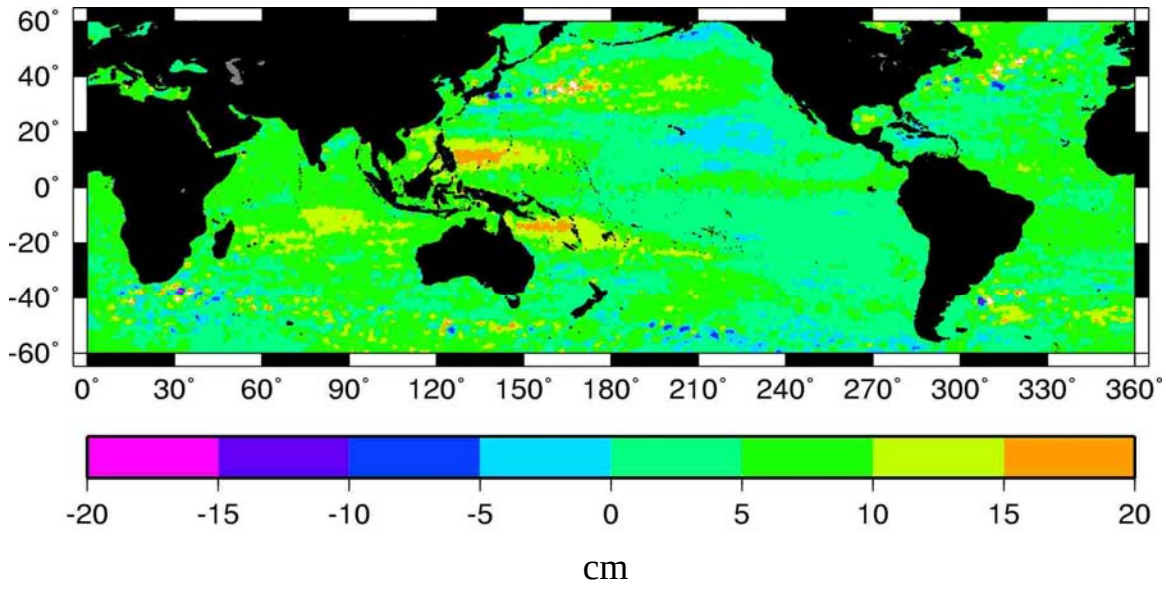

Figure 5.6: Map of height differences between Jason-2 Mean profile and DNSC08.

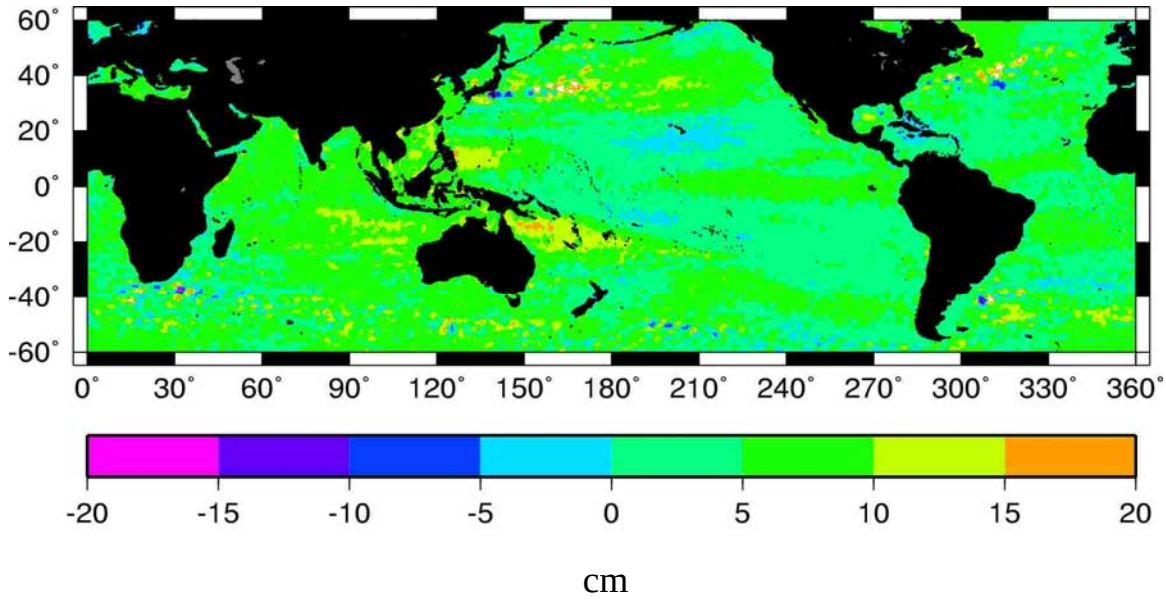

Figure 5.7: Map of height differences between Jason-2 Mean profile and DTU10.

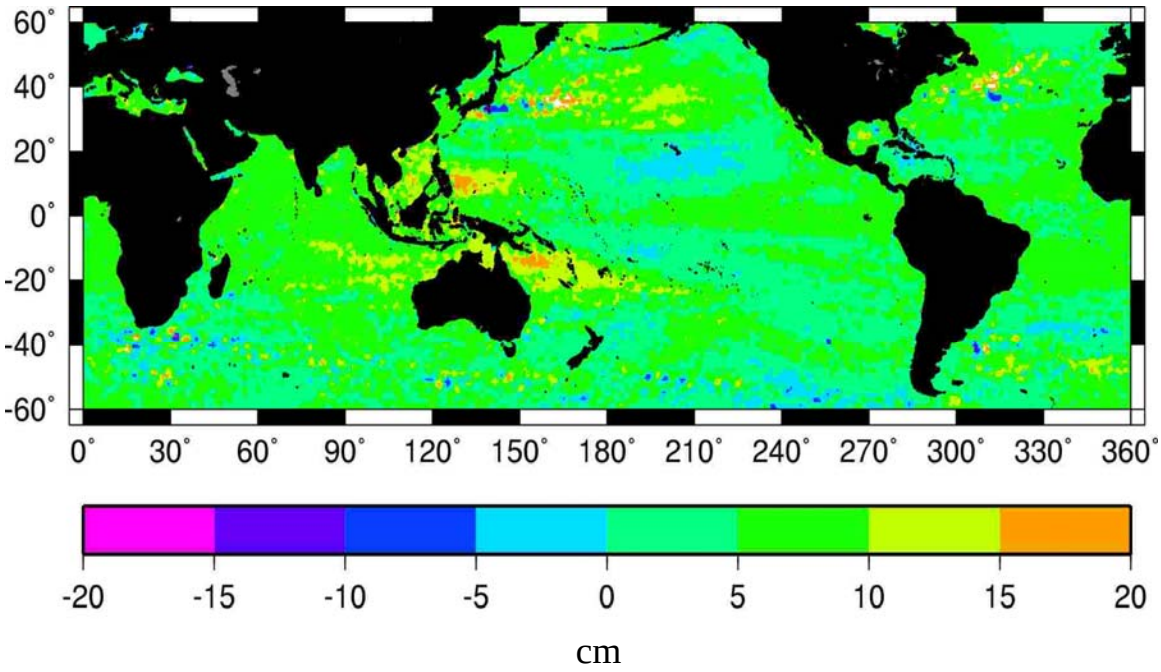

Figure 5.8: Map of height differences between Jason-2 Mean profile and CSRMSS14.

5-5. SUMMARY

5-minute resolution mean sea surface model, CSRMSS14 was validated by three comparisons. First, it was compared with the 7-year Jason-1 mean profile and 8-year Envisat mean profile. Second, grid-to-grid comparison was analyzed by comparing with two recent MSS models, DNSC08 and DTU10. Third, the three MSS models (DNSC08, DTU10 and CSRMSS14) were evaluated using the 2-year Jason-2 mean profile as an independent comparison since none of these MSS have yet used Jason-2 data. Except for the differences expected from inter-annual ocean variability (and ignoring the systematic bias between the various MSS models), CSRMSS14 demonstrates a level of accuracy comparable to the DNSC08 and DTU10 models.

Chapter 6: Summary and Future Work

6-1. SUMMARY AND CONCLUSIONS

The data adjustment method based on the integrating approach has been derived and carried out in order to make consistent datasets for the purpose of constructing a mean sea surface. The primary process for the adjustments is composed of three steps. First, the along-track SSH gradients of each satellite using three SSH points (ahead, current and behind data) are computed. Second, dual crossover computation between Jason-1 and the other satellite is performed in order to obtain the initial values (or constraints) for integrating process. In this step, the Jason-1 mean SSH values were used as a fixed reference surface due to their high accuracy. Finally, the new SSH values of each satellite are obtained by integrating the SSH gradients bin-by-bin with the Jason-1 mean values at dual crossovers as initial values or constraints. Through this process, a total of 5 different satellite data from Geosat ERM, ERS-2, Envisat, T/P and ERS-1 GM were adjusted to the 7-year Jason-1 mean profile.

The analysis of dual crossover computation between the Jason-1 and the other satellite was performed in terms of mean and standard deviations of SSH differences for each satellite. The statistics represent the approximate level of correction from the original SSH datasets to the new SSH datasets of each satellite after the adjustment process. In addition, the statistics of the dual crossovers between Jason-1 and the other satellites

showed regular sinusoidal waves, indicating the annual ocean variability signals of each satellites (Figures 2.8 to 2.10).

The adjusted SSH data for each satellite were averaged into mean profiles with additional computations: (1) removing annual, semi-annual and secular trend terms in the new SSH, (2) performing 3-sigma editing, and (3) removing large differences by comparison with the Jason-1 grid file. The mean profiles were validated by comparison with two recent mean sea surfaces, DNSC08 and DTU10. The statistics for the mean and standard deviation of the height differences indicate that the quality of the new SSH datasets was improved to a level of accuracy comparable to the Jason-1 mean profile, and ultimately, they became more homogeneous and consistent with each other.

Prior to the analysis, the systematic differences (or biases) between DNSC08 and DTU10 models were investigated, and the mean of the height differences between them is 5.7 cm, and the standard deviation of height difference is 3.5 cm (computation limited to ± 60^{o} latitude). The biases are likely due to inter-annual ocean variability resulted from the different time periods of the reference surface (T/P+Jason-1) used for the two MSS models: 1993-2004 vs. 1993-2009. In addition, the 7-year Jason-1 mean profile, which is the main reference surface for new MSS in this research, CSRMSS14 model, was examined by comparing it with DNSC08 and DTU10. The mean of differences with respect to DNSC08 and DTU10 are 17.2 cm and 12.2 cm, respectively, which are taken into account as initial systematic biases between CSRMSS14 and DNSC08 or DTU10 models, respectively.

A 2-D spline interpolation in tension with Green's function based on Wessel and Bercovici [1998] was applied to derive the gridding method. For the gridding computation, the proper tension terms were simulated locally with real SSH datasets, and the results demonstrated that a tension value of 0.5 appeared to produce the best result, though the results were not particularly sensitive to the exact value. Finally, CSRMSS14 was gridded on a 5-minute (1/12º) resolution within the latitudes of ±60 º, using SSH data from the 7-years Jason-1, and the adjusted 2-years Geosat ERM, 6-years ERS-2, 8-years Envisat, 10-years T/P, and ERS-1 GM data.

CSRMSS14 was evaluated by three comparisons. First, it was compared with the more accurate 7-year Jason-1 and 8-year Envisat mean profiles, which were already used for the CSRMSS14 model: inputs vs. outputs. The statistics of the differences were computed, and the results showed that the mean is zero, and RMS is 2.5 cm and 2.8 cm, respectively, for the Jason-1 and Envisat mean profiles. This comparison showed that the output (CSRMSS14) is accurate with respect to the inputs, and the gridding method is reliable.

Second, CSRMSS14 was compared directly with DNSC08 and DTU10. The mean of the height differences with respect to the DNSC08 and DTU10 are 16.3 cm and 11.3 cm, respectively, and the standard deviation of the differences is 6.1 cm for both. The results of this comparison showed that the CSRMSS14 is an accurate reference surface comparable to the DTU10 and DNSC08. In particular, CSRMSS14 is closer to DTU10 than DNSC08. This may reflect a similar level of accuracy comparable to DTU10

(presumably more accurate than DNSC08) or the fact that the time spans used for CSRMSS14 (ending in 2008) and DTU10 (ending in 2009) are closer than that of DNSC08 (ending in 2004).

Finally, DNSC08, DTU10 and CSRMSS14 were analyzed by comparing with the altimeter data of Jason-2 satellite, which were not used for any of the three MSS models. Applying the systematic biases between the Jason-1 mean profile and the two MSS as offsets, the mean and standard deviation of the height differences between the 2-year Jason-2 mean profile (07/2008-03/2010) and the three MSS were computed. Although DTU10 compared most favorably with a standard deviation of 3.8 cm, DNSC08 and CSRMSS14 were quite close at 4.1 and 4.2 cm, respectively. Bearing in mind that DTU10 has 17 years of total altimeter data, including 15 years of ERS-1 and Envisat ERM data, this level of comparison indicates that the approach used here to construct CSRMSS14 has provided an accurate representative mean sea surface model.

In conclusion, the new mean sea surface model (CSRMSS14) was developed using a new data adjustments method based on integrating process, and using 2-D spline interpolation in tension with Green's function as a gridding method in this research. The results indicate that this approach was successful and efficient in making datasets from different satellites more homogeneous and consistent with each other. For this method, it is important to choose the most accurate reference surface. Consequently, Jason-1, whose orbit is estimated to be accurate at the 1 cm level, was adopted as the reference surface for

the data adjustments. As a result, CSRMSS14 was created from multi-satellite radar data and demonstrated to be comparable in accuracy as other recent mean sea surfaces.

6-2. RECOMMENDATIONS FOR FUTURE WORK

Several future works are recommended for a higher-accuracy and higher-resolution global mean sea surface model. First, a better integrating method may be possible, which is the last step of the data adjustment in this research. Instead of using only two new SSH data computed from the nearest two dual crossovers, a more robust method to minimize the errors of several new SSH data sets effectively could be investigated. In addition, the process for adjustments should be investigated for the higher latitudes area (over ± 66 º), where no crossovers with Jason-1 exist.

Additionally, more recent and accurate radar datasets are recommended for a more accurate reference surface. For example, instead of 1980's Geosat satellite data, more recent and accurate data, GFO (Geosat follow on) satellite data (spanning from 2000 to 2008), will provide a better result. This data can be obtained from DEOS-RADS database. They can be pre-processed into the bin-by-bin format used by the CSR-Stackfile described in sub-section 2-2-2 and computed through new adjustments procedure for error and bias reduction.

Finally, the use of ICESat ocean data is strongly recommended for inclusion in the MSS determination. The Geoscience Laser Altimeter System (GLAS) on ICESat uses a laser altimeter to measure the range to the surface [Urban and Schutz, 2005]. The DNSC08

and DTU10 MSS did incorporate some ICESat laser altimeter data at high latitudes only. It is recommended to utilize ICESat data ranging across the entire global oceans, including near coastal areas, and spanning the entire ICESat mission time (2003~2009). By including ICESat data, we are able to reach global coverage from -86º to +87º latitude and better results in vicinity of isolated and small seas.

These recommendations will improve and expand CSRMSS14 to a more accurate and higher spatial resolution of a mean sea surface. The improved MSS can be used to study the ocean mass change component of the global water cycle and its interactions between atmosphere, land, and cryosphere components. A direct consequence is that the improved MSS will better reflect the geoid and ocean bottom topography, leading to a more accurate gravitational field. These and many other investigations will benefit from the improved MSS, which will enhance the understanding of the Earth's oceans and climate.

References

Anderson, O. B., and P. Knudsen, Global marine gravity field from ERS-1 and Geosat geodetic mission altimetry, *J. Geophys. Res*., 103, 8129-8137, 1998.

Anderson, O. B., and P. Knudsen, The DNSC08 mean sea surface and mean dynamic topography from multi-mission radar altimetry, EGU2008-A-08267, OS6-1WE1O-003, Vienna, Austria, 2008.

Andersen O. B., and P. Knudsen, The DNSC08 mean sea surface and mean dynamic topography, *J. Geophys. Res.*, 114, C11001, doi:10.1029/2008JC005179, 2009.

Andersen, O. B., and R. Scharroo, Range and geophysical corrections in coastal regions—Implications for mean sea surface determination, *Coastal Altimetry*, Springer, Berlin, 2011.

Andersen, O. B., The DTU10 Gravity field and Mean sea surface, Second international symposium of the gravity field of the Earth (IGFS2), Fairbanks, Alaska, 2010.

Anzenhofer, M. and T. Gruber, MSS93A: A new stationary sea surface combining one year upgraded ERS-1 fast delivery data and 1987 Geosat altimeter data, *Bull. Geod*., 69, 157-163, 1995.

AVISO and PODAAC, AVISO and PODAAC User Handbook: IGDR and GDR Jason Products, 2008.

Beckley, B. D., F. G. Lemoine, S. B. Luthcke, R. D. Ray, and N. R. Zelenka, A reassessment of global and regional mean sea level trends from TOPEX and Jason-1 altimetry based on revised reference frame and orbits, *Geophys. Res. Lett*., 34, L14608, doi:10.1029/2007GL030002, 2007.

Benada, R., TOPEX/Poseidon merged GDR generation B user's handbook, JPL Rep. D-11007, Jet Propul. Lab., Pasadena, Calif., 1997.

Brachet, S., P. Y. Le Traon, and C. Le Provost, Mesoscale variability from a high-resolution model and from altimeter data in the North Atlantic Ocean, *J. Geophys. Res.*, 109, C12025, doi:10.1029/2004JC002360, 2004.

Bretherton, F., R. Davis, and C. Fandry, A technique for objective analysis and design of oceanographic experiments applied to MODE-73, *Deep-Sea Res.*, 23, 559–582, 1976.

Carrère, L., and F. Lyard, Modeling the barotropic response of the global ocean to atmospheric wind and pressure forcing-comparisons with observations, *Geophys. Res. Lett*, 30 (6), 1275, doi:10.1029/2002GL016473, 2003.

Cazenave, A. and J. Y. Royer, Applications to Marine Geophysics, *Satellite Altimetry and Earth Sciences: A Handbook of Techniques and Applications*, Academic Press, 407-439, 2001.

Chambers, D., Time-varying sea surface topography from satellite altimetry, *CSR-96-4*, Center for Space Research, University of Texas, Austin, TX, 1996.

Chelton, D. B., and M. G. Schlax, The resolution capability of an irregularly sampled dataset with application to GEOSAT altimeter data, *J. Atmos. Oceanic Technol.*, 11, 534–550, 1994.

Chelton, D. B., J. C. Ries, B. J. Haines, L.-L. Fu, and P. S. Callahan, Satellite Altimetry, *Satellite Altimetry and Earth Sciences: A Handbook of Techniques and Applications*, Academic Press, 1-131, 2001.

Chelton, D. B., and M. G. Schlax, The accuracies of smoothed sea surface height fields constructed from tandem satellite altimeter datasets, *J. Atmos. Oceanic Technol.*, 20, 1276–1302, 2003.

Dibarboure, G., M. I. Pujol, F. Briol, P.Y. Le Traon, G. Larnicol, N. Picot, F. Mertz, and M. Ablain, Jason-2 in DUACS: Updated system description, first tandem results and impact on processing and products, *Marine Geodesy*, 34(3-4), 214-241, 2011.

Dorandeu, J., M. Ablain, Y. Faug`ere, F. Mertz, B. Soussi, and P. Vincent., Jason-1 global statistical evaluation and performance assessment: Calibration and cross-calibration results, *Marine Geodesy*, 27, 345–372, 2004.

Ducet, N., P.Y. Le Traon, and G. Reverdin, Global high-resolution mapping of ocean circulation from TOPEX/Poseidon and ERS-1 and -2, *J. Geophys. Res*., 105 (C8), 19477-19498, 2000.

Francis, C. R., G. Graf, P. G. Edwards, M. McCaig, C. McCarthy, A. Lefebvre, B. Pieper, et al., The ERS-2 Spacecraft and its Payload, *ESA Bulletin*, 83, 13-31, 1995.

Fu, L.-L., E. J. Christensen, C. A. Yamarone, M. Lefebvre, Y. Menard, M. Dorrer, and P. Escudier, TOPEX/POSEIDON mission overview, *J. Geophys. Res*., 99, 24369–24381, 1994.

Gardini, B., G. Graf, and G. Ratier, The instruments on Envisat, *Acta Astronautica,* 37, 301-311, 1995.

Gaspar, P., and J.-P. Florens, Estimation of the sea state bias in radar altimeter measurements of sea level: Results from a new nonparametric method, *J. Geophys. Res*., 103, 15803– 15814, doi:10.1029/98JC01194, 1998.

Guman, M., Determination of global mean sea level variations using multi-satellite altimetry, *CSR-97-3*, Center for Space Research, University of Texas, Austin, TX, 1997.

Hernandez, F., P. Y. Le Traon, and R. Morrow, Mapping mesoscale variability of the Azores current using TOPEX/POSEIDON and ERS-1 altimetry, together with hydrographic and Lagrangian measurements, *J. Geophys. Res.*, 100, 24995–25006, 1995.

Hernandez, F., and P. Schaeffer, Altimetric mean sea surfaces and gravity anomaly maps inter-comparisons, *AVISO Tech. Rep AVI-NT-011-5242-CLS*, Cent. Natl. d'Etudes Spatiales, Toulouse, France, 2000.

Hernandez, F., and P. Schaeffer, The CLS01 Mean Sea Surface: A validation with the GSFC00.1 surface, *CLS Technical Note*, 2001.

Hwang, C., H. Hsu, and R. Jang, Global mean sea surface and marine gravity anomaly from multi-satellite altimetry: applications of deflection-geoid and inverse Vening Meinesz formulae, *J. Geod.*, 76(8), 407– 418, doi:10.1007/s00190-002-0265-6, 2002.

Kim, H., Design and assessment of along-track mean sea surface models from topex altimeter data, *master thesis*, Center for space research, University of Texas at Austin, 2002.

Kim, M. C., Determination of high resolution mean sea surface and marine gravity field, *CSR-93-2*, Center for Space Research, University of Texas, Austin, TX, 1993.

Knudson, P. and O. B. Andersen, Global high resolution mean sea surface from multi-mission satellite altimetry, *Bull. Geofis et Teorica ed Applicata*, 40(3-4), 439-443, 1999.

Kozel, B., Dual satellite altimeter crossover measurements for precise orbit determination, *CSR-95-4*, Center for Space Research, University of Texas, Austin, TX, 1995.

Kruizinga, G., Validation and applications of satellite radar altimetry, *CSR-97-6*, Center for Space Research, University of Texas, Austin, TX, 1997.

Le Traon, P.-Y., J. Stum, J. Dorandeu, P. Gaspar, and P. Vincent., Global statistical analysis of TOPEX and POSEIDON data, *J. Geophys. Res.*, 99, 24619–24631, 1994.

Le Traon, P.-Y. and F. Ogor, ERS-1/2 orbit improvement using TOPEX/POSEIDON: The 2 cm challenge, *J. Geophys. Res.*, 103, 8045-8057, 1998.

Le Traon, P.-Y., F. Nadal, and L Ducet, An improved mapping method of multi-satellite altimeter data, *J. Atmos. Oceanic Technol.*, 15, 522-534, 1998.

Le Traon, P.-Y., and G. Dibarboure, An illustration of the contribution of the TOPEX/Poseidon-Jason-1 tandem mission to mesoscale variability studies, *Marine Geodesy*, 27, 3–13, 2004.

Louis, G., M. –F. Lequentrec-Lalancette, J. –Y. Royer, D. Rouxel, L. Géli, M. Maïa, and M. Faillot, Ocean gravity models from future satellite missions, *EOS Trans*. AGU, 91(3), 21-22, 2010.

Marsh, J. G., and R. G. Williamson, Precision orbit analysis in support of the Seasat altimeter experiment, *J. Astronaut. Sci*., 28(141), 345-369, 1980.

Marsh, J. G., T. V. Martin, J. J. McCarthy, and P.S. Chovity, Mean sea surface computation using GEOS 3 altimeter data, *Marine Geodesy*, 3, 359-378, 1980.

Marsh, J. G., and T. V. Martin, The Seasat altimeter mean sea surface model, *J. Geophys. Res.*, 87, 3269-3280, 1982.

Marsh, J. G., T. V. Martin, and J. J. McCarthy, Global mean sea surface computation using GEOS 3 altimeter data, *J. Geophys. Res*., 87(B13), 10955-10964, 1982.

Marsh, J. G., A. C. Brenner, B. D. Beckley, and T. V. Martin, Global mean sea surface based upon the Seasat altimeter data, *J. Geophys. Res*., 91(B3), 3501-3506, 1986.

Marsh, J. G., C. J. Koblinsky, H. J. Zwally, A. C. Brenner, and B. D. Beckley, A global mean sea surface based upon Geos3 and Seasat altimeter data, *J. Geophys. Res.*, 97(B4), 4915-4921, 1992.

Mesia, J. M, and P. T. Strub, An inversion method to determine ocean surface currents using irregularly sampled satellite altimetry data, *J. Atmos. Oceanic. Technol*., 12, 830-849, 1995.

Moritz, H., Least-squares collocation, *Reviews of Geophysics and Space Physics*, 16(3), 421-430, 1978.

Moritz, H., *Advanced physical Geodesy*, 2nd ed. Wichmann Karlsruhe, Germany, 1989.

Naeije, M. C., E. J. O. Schrama and R. Scharroo, The Radar Altimeter Database System project RADS, *Proceedings of the International Geoscience and Remote Sensing Symposium IGARSS 2000*, 2000.

Pavlis, N. K., S. A. Holmes, S. C. Kenyon, and J. K. Factor, An Earth gravitational model to degree 2160 : EGM2008, *Geophys. Res. Abstr.*, 10, EGU2008-A-01891, 2008.

Rapp, R. H., Y. Yi, and Y. M. Wang, Mean sea surface and geoid gradient comparisons with TOPEX altimeter data, *J. Geophys. Res*., 99, 24657-24667, 1994.

Rapp, R. H., and Y. Yi, Role of ocean variability and dynamic ocean topography in the recovery of the mean sea surface and gravity anomalies from satellite altimeter data, *J. geod.*, 71, 617-629, 1997.

Ray, R., A global ocean tide model from TOPEX/Poseidon altimetry, GOT99.2, NASA/TM-1999–209478, GSFC/NASA, Greenbelt, Md, 58, 1999.

Rio, M.-H., and F. Hernandez, A mean dynamic topography computed over the world ocean from altimetry, in situ measurements and a geoid model, *J. Geophys. Res*., 109, C12032, doi:10.1029/2003JC002226, 2004.

Robinson, I., Measuring the Oceans from Space: The principles and methods of satellite oceanography, Springer-Verlag, Chichester, UK, 2004.

Sandwell, D. T., Biharmonic spline interpolation of Geos-3 and Seasat altimeter data, *Geophys. Res. Lett.*, 14(2), 139-142, 1987.

Sandwell, D. T., and W. H. F. Smith, Bathymetric Estimation, *Satellite Altimetry and Earth Sciences: A Handbook of Techniques and Applications*, Academic Press, 441-456, 2001.

Scharroo, R. and P.N.A.M. Visser, Precise orbit determination and gravity field improvement for the ERS Satellites, *J. Geophys. Res*., 103 (C4), 8113-8127, 1998.

Scharroo, R. and W. H. F. Smith, A global positioning system-based climatology for the total electron content in the ionosphere, *J. Geophys. Res*., 15, A10318, doi:10.1029/2009JA014719, 2010.

Scharroo, R., RADS v 3.1 user manual and format specification, TU delft, Delft Aerospace, 2012.

Scharroo, R., E. W. Leuliette, J. L. Lillibridge, D. Byrne, M. C. Naeije, and G. T. Mitchum, RADS: Consistent multi-mission products, in *Proc. of the Symposium on 20 Years of Progress in Radar Altimetry, Venice, 20-28 September 2012*, ESA SP-710, 2013.

Schutz, B. E., H. J. Zwally, C. A. Shuman, D. Hancock, and J. P. DiMarzio, Overview of the ICESat Mission, *J. Geophys. Res.*, 32, L21S01, 2005.
Shaffer, P., Y. Faugere, J. F. Legeais, A. Ollivier, T. Guinle, and N. Picot, The CNES_CLS11 global mean sea surface computed from 16 years of satellite altimeter data, *Marine Geodesy*, 24(S1), 3-19, 2012.

Smith, W. H. F., and P. Wessel, Gridding with a continuous curvature surface in tension, *Geophysics*, 55, 293-305, 1990.

Smith, W. F. H., and R. Scharroo, Mesoscale ocean dynamics observed by satellite altimeters in non-repeat orbits, *Geophys. Res. Lett*., 36, doi:10.1029/2008GL036530, 2009.

Stammer, D. and C. Wunsch, Preliminary assessment of the accuracy and precision of TOPEX/POSEIDON altimeter data with respect to the large scale ocean circulation, *J. Geophys. Res.*, 99(C12), 24584-24604, 1994.

Stammer, D., Global characteristics of ocean variability estimated from regional TOPEX/POSEIDON altimeter measurements, *J. Phys. Oceanogr.*, 27, 1743–1769, 1997.

Swain, C. J., 1976, A FORTRAN IV program for interpolating irregularly spaced data using the difference equations for minimum curvature: Computers & Geosciences, v. 1, no. 4, 231-240, 1976.

Tai, C. K., and Fu L. L., On crossover adjustment in satellite altimetry and its oceanography implications, *J. Geophys. Res*., 91(C2), 2549-2554, 1986.

Tapley, B., and D. Kim, Applications to geodesy, *Satellite Altimetry and Earth Sciences: A Handbook of Techniques and Applications*, Academic Press, 371-406, 2001.

Tapley, B., J. Ries, S. Bettadpur, D. Chambers, M. Cheng, F. Condi and S. Poole, The GGM03 mean earth gravity model from GRACE, *EOS Trans*. AGU, 88 (52), Fall Meet. Suppl., Abstract, G42A-03, 2007.

Tran, N., S. Labroue, S. Philipps, E. Bronner, and N. Picot., Overview and update of the sea-state bias corrections for the Jason-2, Jason-1, and TOPEX missions, *Marine Geodesy*, 33(S1), 348–362, 2010.

Urban, T., The integration and application of multi-satellite radar altimetry, *CSR-00-01*, Center for Space Research, University of Texas, Austin, TX, 2000.

Urban, T. and B. E. Schutz, ICESat sea level comparisons, *Geophys. Res. Lett.*, 32, L23S10, doi:10.1029/2005GL024306, 2005.
Vincent, P., S. D. Desai, J. Dorandeu, M. Ablain, B. Soussi, P. S., Callahan, and B. J. Haines, Jason-1 geophysical performance evaluation, *Mar. Geod*., 26, 167–186, doi:10.1080/714044517, 2003.

Wang, Y. M, The satellite altimeter data derived mean sea surface GSFC98, *Geophys. Res. Lett.*, 27, 701-704, 2000.

Wang, Y. M, GSFC00 mean sea surface, gravity anomaly and vertical gravity gradient from satellite altimeter data., *J. Geophys. Res.*, 106(C12), 31167-31174, 2001.

Wessel, P., and W. H. F. Smith, New version of the generic mapping tools released, *EOS Trans*. AGU, 76(33), 329, 1995.

Wessel, P., and W. H. F. Smith, New improved version of generic mapping tools released, *EOS Trans*. AGU, 79, 579, 1998.

Wessel, P., and D. Bercovici, Interpolation with splines in tension: A Green's function approach, *Math. Geol.*, 30(1), 77-93, 1998.

Wessel, P., and W.H.F. Smith, The generic mapping tools version 4.5: a map-making tutorial, laboratory for satellite altimetry NOAA/NESDIS, 2009.

Zlotnicki, V., Correlated environmental corrections in TOPEX/POSEIDON, with a note on ionospheric accuracy. *J. Geophys. Res.*, 99, 24907–24914, 1994.

Zwally, J., et al., ICESat's laser measurements of polar ice, atmosphere, ocean, and land, *J. Geodyn*., 34(3– 4), 405– 445, doi:10.1016/S0264-3707(02)00042-X, 2002.